UNIV OF MICHIGAN
MAY 19 1953
ENGINEERING LIBRARY

JOURNAL OF THE AERONAUTICAL SCIENCES

VOLUME 20 MAY, 1953 NUMBER 5

CONTENTS

Stability Derivatives for a Slender Missile with Application to a Wing-Body-Vertical-Tail Configuration.....ARTHUR E. BRYSON, JR. 297

Calculation Method for Three-Dimensional Rotationally Symmetrical Laminar Boundary Layers with Arbitrary Free-Stream Velocity and Arbitrary Wall-Temperature Variation.....ROBERT M. DRAKE, JR. 309

Statistical Aspects of Dynamic Loads.....Y. C. FUNG 317

An Experimental Study of Natural Vibrations of Cantilevered Triangular Plates.....P. N. GUSTAFSON, W. F. STOKEY, AND C. F. ZOROWSKI 331

Some Effects of Surface Curvature on Laminar Boundary-Layer Flow.....JAMES S. MURPHY 338

Shock-Wave Effects on the Laminar Skin Friction of an Insulated Flat Plate at Hypersonic Speeds.....TING-YI LI AND H. T. NAGAMATSU 345

Readers' Forum: "Further Note on the 'Dynamic Stability of a Missile in Rolling Flight,'" by R. E. Bolz; "Turbulent Channel Flow from a Variational Principle," by Stanley Corrsin; "The Gas Bending Stress on a Blade in an Axial-Flow Compressor," by John Mitchell Stephenson; "Additional Comments on 'A Study of Transonic Gas Dynamics by the Hydraulic Analogy,'" by J. R. Bruman; "Location of Detached Shock Waves Ahead of Plane Bodies," by W. R. Moeckel; "Comments on a Method for Location of Detached Shock Waves Ahead of Plane Bodies," by E. V. Laitone; "Note on Effects of Density Fluctuations on the Turbulent Skin Friction of an Insulated Flat Plate at High Supersonic Speeds," by E. R. Van Driest; "Further Comments on 'Aerodynamic Coefficients of an Oscillating Airfoil in Two-Dimensional Subsonic Flow,'" by P. F. Jordan; "Remarks on Thermal Characteristics of Boundary Layers," by Martin Bloom; "Effect of Flapping Hinge Offset on Rotor-Blade Stall," by J. P. Chawla; "Actuator Disc Theory for Compressible Flow and a Subsonic Correction for Propellers," by E. V. Laitone; "Theory of Heat Transfer Through a Laminar Boundary Layer," by Myron Tribus; "Errata—'Diffuser Efficiency of Free-Jet Supersonic Wind Tunnels at Variable Test Chamber Pressure'" by Rudolf Hermann.....356–366

Published by the
INSTITUTE OF THE AERONAUTICAL SCIENCES, INC.

JOURNAL OF THE AERONAUTICAL SCIENCES

Editor: HUGH L. DRYDEN, *Director, N.A.C.A.*

Associate Editor: ROBERT R. DEXTER *Managing Editor:* BERNEICE H. JARCK

Editorial Committee

Aerodynamics

Francis Clauser
Howard Emmons
Antonio Ferri
Alexander Flax
R. Paul Harrington
R. T. Jones
Carl Kaplan
H. W. Liepmann
C. C. Lin
H. F. Ludloff
Harold Luskin
John R. Markham
Carl B. Millikan
Shatswell Ober
W. Bailey Oswald
Allen E. Puckett
Elliott G. Reid
H. J. E. Reid
Russell Robinson
G. B. Schubauer
W. R. Sears
John Stack
Theodore von Kármán
Richard von Mises

Air Transport

Charles Froesch
J. A. Herlihy
R. D. Kelly
Otto E. Kirchner
Jerome Lederer
John C. Leslie
R. Dixon Speas

Flight Testing

W. K. Ebel
R. R. Gilruth
Melvin N. Gough
E. G. Stout

Structures and Materials

W. B. Bleakney
E. W. Conlon
L. H. Donnell
E. C. Hartmann
N. J. Hoff
Samuel Levy
E. E. Lundquist
Alfred S. Niles
W. Ramberg
E. Reissner
F. R. Shanley
H. W. Sibert
C. R. Strang
S. Timoshenko
H. S. Tsien
Chi-Teh Wang

Rotating Wing Aircraft

F. B. Gustafson
K. H. Hohenemser
Bartram Kelley
R. B. Maloy
Ralph McClarren
R. H. Miller
R. H. Prewitt
Igor I. Sikorsky

Vibration and Flutter

Lee Arnold
M. A. Biot
R. L. Bisplinghoff
William Bollay
Chieh-Chien Chang
I. E. Garrick
Martin Goland
J. P. Den Hartog

Aircraft Design

W. E. Beall
W. K. Ebel
Hall L. Hibbard
Richard Hutton
C. L. Johnson
A. A. Kartveli
C. J. McCarthy
Fred E. Weick
Robert J. Woods

Electronics in Aviation

K. C. Black
E. F. Herzog
David S. Little
D. K. Martin
George Rappaport
Paul Rosenberg
L. M. Sherer

Physiologic Problems

H. G. Armstrong
Louis H. Bauer
Robert J. Benford
Eugene Du Bois
W. Randolph Lovelace, II
Ross A. MacFarland

Fuels and Oils

D. P. Barnard
J. H. Doolittle
Graham Edgar
R. T. Goodwin
S. D. Heron
A. M. Rothrock

Flight Propulsion

George W. Brady
Frank W. Caldwell
L. S. Hobbs
E. R. Johnson
Joseph Keenan
R. P. Kroon
Hans Reissner
Abe Silverstein
C. Fayette Taylor
E. S. Taylor
P. Taylor
E. S. Thompson
H. S. Tsien

Instruments

Allan G. Binnie
J. R. Bradburn
Charles H. Colvin
C. S. Draper
S. G. Eskin
O. E. Esval
H. W. Holzapfel
W. L. Howland
George H. Purcell
C. F. Savage
O. Hugo Schuck
C. L. Seward, Jr.
L. D. Statham
R. C. Sylvander
D. K. Warner

Meteorology

C. F. Brooks
D. M. Little
E. J. Minser
F. W. Reichelderfer
H. C. Willett

SUBSCRIPTION RATES

JOURNAL OF THE AERONAUTICAL SCIENCES, Published Monthly.—United States and Possessions: 1 Year, $12.00; Single Copies, $1.50. Foreign Countries Including Canada (American Currency Rates): 1 Year, $13.00; Single Copies, $1.50.

AERONAUTICAL ENGINEERING REVIEW, Published Monthly.—United States and Possessions: 1 Year, $3.00; Single Copies, $0.50. Foreign Countries Including Canada (American Currency Rates): 1 Year, $3.50; Single Copies, $0.50.

Notices of change of address should be sent to the Institute at least 30 days prior to actual change of address.

Manuscripts for publication, proofs, and all correspondence should be addressed to the Editorial Office of the JOURNAL.

Correspondence regarding subscriptions may be addressed to Publication Office, 20th and Northampton Sts., Easton, Pa., or to the Editorial Office of the JOURNAL OF THE AERONAUTICAL SCIENCES, 2 East 64th Street, New York 21, New York.

Copyright, 1953, by the Institute of the Aeronautical Sciences, Inc.

Entered as Second Class Matter at the Post Office, Easton, Pa., May 1, 1937. Acceptance for mailing at a special rate of Postage provided for in the Act of August 24, 1912. Authorized April 29, 1937.

JOURNAL OF THE AERONAUTICAL SCIENCES

VOLUME 20 MAY, 1953 NUMBER 5

Stability Derivatives for a Slender Missile with Application to a Wing-Body-Vertical-Tail Configuration

ARTHUR E. BRYSON, JR.*

Hughes Research and Development Laboratories

ABSTRACT

Theoretical stability derivatives are determined for a slender missile through use of the concept of inertia coefficients of its cross section. The inertia coefficients are determined by the velocity potentials for two-dimensional motion of the cross section in two mutually perpendicular directions and for rotation about an axis perpendicular to the cross section. The inertia coefficients are derived for the cross section of a configuration consisting of a slender body of revolution with low aspect ratio wings and unequal vertical tails.

INTRODUCTION

MUNK,[1] JONES,[2] AND SPREITER[3] have shown how to estimate the aerodynamic forces on slender fuselages, wings, and wing-fuselage combinations by considering the flow in planes perpendicular to the wing or fuselage axis to be uninfluenced by the change in the component of fluid velocity parallel to this axis. Munk and Jones made use of the concept of the apparent additional mass of the cross section in a two-dimensional flow to find the lift and moment due to angle of attack. This concept is enlarged upon here to include all six of the inertia coefficients of the cross section, utilizing them to find all the stability derivatives (except the axial force derivatives) of the three-dimensional configuration.

Consideration is limited here to configurations where the aft end of the fuselage and all wing trailing edges lie in a plane perpendicular to the long axis of the configuration. Extension to cases where trailing edges occur ahead of this base plane can be made by considering the effect of the vorticity shed from these edges as shown by Jones.

Received November 18, 1952.

* Research Engineer, Guided Missile Laboratories.

INERTIA COEFFICIENTS OF THE CROSS SECTION

Consider a slender body† moving through an infinite fluid medium. By "slender" we shall mean that the maximum dimension of any cross section of the body is small compared to the length of the body and that the dimensions of the cross section change slowly with distance along the length of the body. Let x,y,z be axes fixed relative to the body with origin at the center of gravity of the body and with the x-axis in the direction of the length of the body (see Fig. 1). We consider only those motions of the body where the instantaneous velocity vector of any point in the body makes a small angle with the body x-axis. Let ξ,η,ζ be axes such that

† We shall use the term "body," henceforth, to mean a general aerodynamic shape that includes wings, fuselages, wing-fuselage combinations, etc.

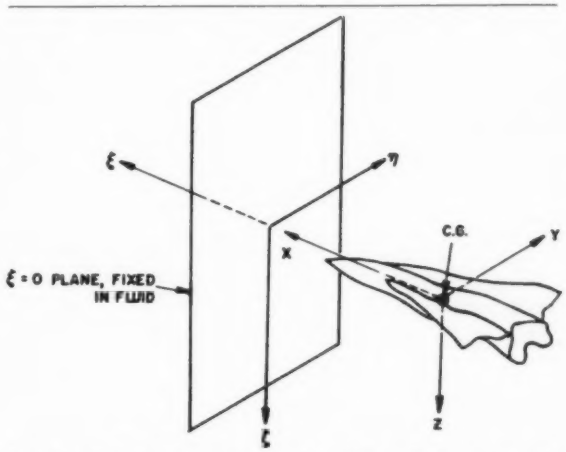

FIG. 1. Coordinate systems used in the analysis. x,y,z axes fixed in body.

the $\xi = 0$ plane is a plane at rest with respect to the fluid far away from the body and such that the ξ-axis is parallel to the x-axis at the instant under consideration. Let the η,ζ-axes be the projections of the y,z-axes onto the $\xi = 0$ plane.

We approximate the three-dimensional fluid flow around the body by considering the fluid in the η-ζ plane to be incompressible and the fluid motion to be two-dimensional—i.e., uninfluenced by any part of the body or fluid which does not lie in the η-ζ plane. The motion in the η-ζ plane is thus a nonstationary motion induced by a two-dimensional body (the three-dimensional body's cross section) whose velocities and shape change with time.

The kinetic energy of the fluid in the η-ζ plane (actually a kinetic energy per unit distance normal to the η-ζ plane) is given by[4]

$$T' = \frac{1}{2}\rho S[v,\ w,\ pD][A]\begin{bmatrix} v \\ w \\ pD \end{bmatrix} \tag{1}$$

where the symmetric matrix $[A]$ is given by

$$[A] = \begin{bmatrix} A_{11}, & A_{12}, & A_{13} \\ A_{12}, & A_{22}, & A_{23} \\ A_{13}, & A_{23}, & A_{33} \end{bmatrix} = -\frac{1}{S}\begin{bmatrix} \oint \varphi_1 \frac{\partial \varphi_1}{\partial n}\,ds, & \oint \varphi_1 \frac{\partial \varphi_2}{\partial n}\,ds, & \frac{1}{D}\oint \varphi_1 \frac{\partial \varphi_3}{\partial n}\,ds \\ \oint \varphi_1 \frac{\partial \varphi_2}{\partial n}\,ds, & \oint \varphi_2 \frac{\partial \varphi_2}{\partial n}\,ds, & \frac{1}{D}\oint \varphi_2 \frac{\partial \varphi_3}{\partial n}\,ds \\ \frac{1}{D}\oint \varphi_1 \frac{\partial \varphi_3}{\partial n}\,ds, & \frac{1}{D}\oint \varphi_2 \frac{\partial \varphi_3}{\partial n}\,ds, & \frac{1}{D_2}\oint \varphi_3 \frac{\partial \varphi_3}{\partial n}\,ds \end{bmatrix} \tag{2}$$

and

S = a reference area

D = a reference length

ρ = fluid density

φ_1 = potential due to a unit velocity of the cross section in the η direction

φ_2 = potential due to a unit velocity of the cross section in the ζ direction

φ_3 = potential due to a unit angular velocity of the cross section about the ξ-axis

v = velocity of the cross section in the η direction

w = velocity of the cross section in the ζ direction

p = angular velocity of the cross section about the ξ-axis

$\oint (\ )ds$ = the line integral around the boundary of the cross section

The dimensionless quantities A_{ij} we shall call the inertia coefficients of the cross section.

The Forces Acting on the Body Cross Section

The aerodynamic sideforce, downforce, and rolling moment per unit length on the body at any given cross section are given by[4]

$$\begin{bmatrix} Y' \\ Z' \\ l' \end{bmatrix} = -\frac{d}{dt}\begin{bmatrix} \frac{\partial T'}{\partial v} \\ \frac{\partial T'}{\partial w} \\ \frac{\partial T'}{\partial p} \end{bmatrix} + p\begin{bmatrix} -\frac{\partial T'}{\partial w} \\ \frac{\partial T'}{\partial v} \\ 0 \end{bmatrix} + w\begin{bmatrix} 0 \\ 0 \\ \frac{\partial T'}{\partial v} \end{bmatrix} - v\begin{bmatrix} 0 \\ 0 \\ \frac{\partial T'}{\partial w} \end{bmatrix} \tag{3}$$

The yawing moment and pitching moment per unit length are given by

$$\begin{bmatrix} n' \\ -m' \end{bmatrix} = \begin{bmatrix} xY' \\ xZ' \end{bmatrix} \tag{4}$$

Now T' is a function of v, w, p and the six inertia coefficients. Thus T' can change with time in two ways: (1) by a change in the motion of the cross section and (2) by a change in the shape of the cross section. Furthermore, the motion of the cross section can change in two ways: (1) by a change in the linear velocity of the c.g. of the body and (2) by a change in the angular velocity of the body. Thus,

$$\left.\begin{aligned} v &= \beta U + rx \\ w &= \alpha U - qx \end{aligned}\right\} \tag{5}$$

where

α = angle of attack of the body
β = angle of sideslip of the body
} linear velocities

q = pitching angular velocity of the body
r = yawing angular velocity of the body
} angular velocities

U = forward velocity of the body

All five of these quantities are functions of the time alone.

The inertia coefficients are functions of x, since the shape of the cross section changes with x. Therefore,

$$(d/dt) = (\partial/\partial t) - U(\partial/\partial x) \tag{6}$$

Since $[A]$ is a symmetric matrix,

$$\frac{d}{dt}\begin{bmatrix} \dfrac{\partial T'}{\partial v} \\ \dfrac{\partial T'}{\partial w} \\ \dfrac{1}{D}\dfrac{\partial T'}{\partial p} \end{bmatrix} = \rho S\left[\frac{dA}{dt}\right]\begin{bmatrix} v \\ w \\ pD \end{bmatrix} + \rho S[A]\begin{bmatrix} \dfrac{dv}{dt} \\ \dfrac{dw}{dt} \\ D\dfrac{dp}{dt} \end{bmatrix} \tag{7}$$

From Eqs. (5) and (6) we see that

$$\begin{bmatrix} \dfrac{dv}{dt} \\ \dfrac{dw}{dt} \\ D\dfrac{dp}{dt} \end{bmatrix} \quad \begin{bmatrix} \dot\beta U + \beta\dot U + \dot r x - Ur \\ \dot\alpha U + \alpha\dot U - \dot q x + Uq \\ D\dot p \end{bmatrix} \tag{8}$$

Substituting Eqs. (5), (6), (7), and (8) into Eq. (3), we have, finally,

$$\frac{D}{\rho U^2 S}\begin{bmatrix} Y' \\ Z' \\ \dfrac{l'}{D} \end{bmatrix} = -[A]\begin{bmatrix} \dfrac{\dot\beta D}{U} + \beta\dfrac{UD}{U^2} + \dfrac{\dot r D^2}{U^2}\dfrac{x}{D} \\ \dfrac{\dot\alpha D}{U} + \alpha\dfrac{\dot U D}{U^2} - \dfrac{\dot q D^2}{U_2}\dfrac{x}{D} \\ \dfrac{\dot p D^2}{U^2} \end{bmatrix} + \frac{\partial}{\partial\left(\dfrac{x}{D}\right)}\left\{[A]\begin{bmatrix} \beta + \dfrac{rD}{U}\dfrac{x}{D} \\ \alpha - \dfrac{qD}{U}\dfrac{x}{D} \\ \dfrac{pD}{U} \end{bmatrix}\right\} -$$

$$\left\{\left(\beta + \frac{rD}{U}\frac{x}{D}\right)[E] + \left(\alpha - \frac{qD}{U}\frac{x}{D}\right)[F] + \frac{pD}{U}[G]\right\}\begin{bmatrix} \beta + \dfrac{rD}{U}\dfrac{x}{D} \\ \alpha - \dfrac{qD}{U}\dfrac{x}{D} \\ \dfrac{pD}{U} \end{bmatrix} \tag{9}$$

$$[E] = \begin{bmatrix} 0, & 0, & 0 \\ 0, & 0, & 0 \\ A_{12}, & A_{22}, & A_{23} \end{bmatrix}$$

$$[F] = -\begin{bmatrix} 0, & 0, & 0 \\ 0, & 0, & 0 \\ A_{11}, & A_{12}, & A_{13} \end{bmatrix} \tag{10}$$

$$[G] = \begin{bmatrix} -A_{12}, & -A_{22}, & -A_{23} \\ A_{11}, & A_{12}, & A_{13} \\ 0, & 0, & 0 \end{bmatrix}$$

The Total Forces and Moments on the Body

By integrating Eqs. (9) and (4) with respect to x over the length of the body, the sideforce Y, the downforce Z, the rolling moment l, the pitching moment m, and the yawing moment n can be found to second order in terms of α, β, p, q, r, $\dot\alpha$, $\dot\beta$, $\dot p$, $\dot q$, $\dot r$, and $\dot U$.

We shall define force and moment coefficients as follows:

$$[C_Y, C_Z, C_l, C_m, C_n] = \frac{D}{(1/2)\rho U^2 S}\int_{-x_b/D}^{x_n/D}\left[Y', Z', \frac{l'}{D}, \frac{m'}{D}, \frac{n'}{D}\right]d\left(\frac{x}{D}\right) \tag{11}$$

where x_n = distance from the c.g. to the nose of the body and x_b = distance from the c.g. to the base plane of the body.

Integrating Eqs. (9) and (4) and using the definitions of Eq. (11), we have, finally,

$$\begin{bmatrix} C_y \\ C_z \\ C_l \end{bmatrix} = -2[\bar{A}] \begin{bmatrix} \beta - \frac{rD}{U}\frac{x_b}{D} \\ \alpha + \frac{qD}{U}\frac{x_b}{D} \\ \frac{pD}{U} \end{bmatrix} - 2\int_{-x_b/D}^{x_n/D} [A]\, d\left(\frac{x}{D}\right) \begin{bmatrix} \frac{\dot{\beta}D}{U} + \beta\frac{\dot{U}D}{U^2} \\ \frac{\dot{\alpha}D}{U} + \alpha\frac{\dot{U}D}{U^2} \\ \frac{\dot{p}D^2}{U^2} \end{bmatrix} - 2\int_{-x_b/D}^{x_n/D} [A]\frac{x}{D}\, d\left(\frac{x}{D}\right) \begin{bmatrix} \frac{\dot{r}D^2}{U^2} \\ -\frac{\dot{q}D^2}{U^2} \\ 0 \end{bmatrix} -$$

$$2\int_{-x_b/D}^{x_n/D} \left\{\left(\beta + \frac{rD}{U}\frac{x}{D}\right)[E] + \left(\alpha - \frac{qD}{U}\frac{x}{D}\right)[F] + \frac{pD}{U}[G]\right\} d\left(\frac{x}{D}\right) \begin{bmatrix} \beta \\ \alpha \\ \frac{pD}{U} \end{bmatrix} - 2\int_{-x_b/D}^{x_n/D} \left\{\left(\beta + \frac{rD}{U}\frac{x}{D}\right)[E] + \right.$$

$$\left.\left(\alpha - \frac{qD}{U}\frac{x}{D}\right)[F] + \frac{pD}{U}[G]\right\} \frac{x}{D}\, d\left(\frac{x}{D}\right) \begin{bmatrix} \frac{rD}{U} \\ -\frac{qD}{U} \\ 0 \end{bmatrix} \quad (12)$$

$$\begin{bmatrix} C_n \\ -C_m \\ C_0 \end{bmatrix} = 2\frac{x_b}{D}[\bar{A}] \begin{bmatrix} \beta - \frac{rD}{U}\frac{x_b}{D} \\ \alpha + \frac{qD}{U}\frac{x_b}{D} \\ \frac{pD}{U} \end{bmatrix} - 2\int_{-x_b/D}^{x_n/D} [A]\, d\left(\frac{x}{D}\right) \begin{bmatrix} \beta \\ \alpha \\ \frac{pD}{U} \end{bmatrix} -$$

$$2\int_{-x_b/D}^{x_n/D} [A]\left(\frac{x}{D}\right) d\left(\frac{x}{D}\right) \begin{bmatrix} \frac{\dot{\beta}D}{U} + \frac{rD}{U} + \beta\frac{\dot{U}D}{U^2} \\ \frac{\dot{\alpha}D}{U} - \frac{qD}{U} + \alpha\frac{\dot{U}D}{U^2} \\ \frac{\dot{p}D^2}{U^2} \end{bmatrix} - 2\int_{-x_b/D}^{x_n/D} [A]\left(\frac{x}{D}\right)^2 d\left(\frac{x}{D}\right) \begin{bmatrix} -\frac{\dot{r}D^2}{U^2} \\ -\frac{\dot{q}D^2}{U^2} \\ 0 \end{bmatrix} -$$

$$2\int_{-x_b/D}^{x_n/D} [G]\left(\frac{x}{D}\right) d\left(\frac{x}{D}\right) \begin{bmatrix} \frac{pD}{U}\beta \\ \frac{pD}{U}\alpha \\ \left(\frac{pD}{U}\right)^2 \end{bmatrix} - 2\int_{-x_b/D}^{x_n/D} [G]\left(\frac{x}{D}\right)^2 d\left(\frac{x}{D}\right) \begin{bmatrix} \frac{pD}{U}\frac{rD}{U} \\ -\frac{pD}{U}\frac{qD}{U} \\ 0 \end{bmatrix} \quad (13)$$

where $(^-)$ indicates the value in the base plane and the quantity C_0 has no physical significance.

Example: Consider the flat delta wing of span $\bar{b}$ and chord c. Here,

$$[A] = \begin{bmatrix} 0, & 0, & 0 \\ 0, & \frac{\pi}{4}\frac{b^2}{S}, & 0 \\ 0, & 0, & \frac{\pi}{64}\frac{b^4}{SD^2} \end{bmatrix} \quad \text{where} \quad \begin{cases} b = \bar{b}[(x_n - x)/c] \\ c = x_n + x_b \end{cases} \quad (14)$$

For simplicity we let $S = (\pi/4)\bar{b}^2$ and $D = \bar{b}$; then,

$$[A] = \begin{bmatrix} 0, & 0, & 0 \\ 0, & \left(\frac{b}{\bar{b}}\right)^2, & 0 \\ 0, & 0, & \left(\frac{b}{2\bar{b}}\right)^4 \end{bmatrix}, \quad [E] = \begin{bmatrix} 0, & 0, & 0 \\ 0, & 0, & 0 \\ 0, & \left(\frac{b}{\bar{b}}\right)^2, & 0 \end{bmatrix} \quad [G] = \begin{bmatrix} 0, & -\left(\frac{b}{\bar{b}}\right)^2, & 0 \\ 0, & 0, & 0 \\ 0, & 0, & 0 \end{bmatrix} \tag{15}$$

and $[F]$ vanishes.

Carrying out the integrations indicated, we find, from Eqs. (12) and (13),

$$\left.\begin{aligned} C_y &= \frac{2}{3}\frac{c}{D}\frac{pD}{U}\alpha - K_1\frac{pD}{U}\frac{qD}{U} \\ C_z &= -2\alpha - 2\frac{x_b}{D}\frac{qD}{U} - \frac{2}{3}\frac{c}{D}\frac{\dot{\alpha}D}{U} - \frac{2}{3}\frac{c}{D}\alpha\frac{\dot{U}D}{U^2} + K_1\frac{\dot{q}D^2}{U^2} \\ C_l &= -\frac{1}{8}\frac{pD}{U} - \frac{1}{40}\frac{c}{D}\frac{\dot{p}D^2}{U^2} - \frac{2}{3}\frac{c}{D}\alpha\beta - K_1\left(\alpha\frac{rD}{U} - \beta\frac{qD}{U}\right) - K_2\frac{qD}{U}\frac{rD}{U} \\ C_m &= -2\left(\frac{x_b}{D} - \frac{1}{3}\frac{c}{D}\right)\alpha - 2\left(\frac{x_b}{D}\right)^2\frac{qD}{U} - K_1\left(\frac{qD}{U} - \frac{\dot{\alpha}D}{U}\right) + K_1\alpha\frac{\dot{U}D}{U^2} - K_2\frac{\dot{q}D^2}{U^2} \\ C_n &= K_1(pD/U)\alpha - K_2(pD/U)(qD/U) \end{aligned}\right\} \tag{16}$$

where

$$\left.\begin{aligned} K_1 &= \frac{1}{6}\left(\frac{c}{D}\right)^2 - \frac{2}{3}\frac{c}{D}\frac{x_b}{D} \\ K_2 &= \frac{1}{15}\left(\frac{c}{D}\right)^3 - \frac{1}{3}\left(\frac{c}{D}\right)^2\frac{x_b}{D} + \frac{2}{3}\frac{c}{D}\left(\frac{x_b}{D}\right)^2 \end{aligned}\right.$$

These expressions contain all the terms of reference 5 and a few more. It is interesting to note that the sideforce and yawing moment terms that arise due to leading-edge suction are taken care of very simply in this method of analysis.

The Stability Derivatives

Let us denote derivatives in the following manner:

$$[(\ )_\alpha, (\ )_\beta, (\ )_p, (\ )_q, (\ )_r, (\ )_{\dot{\alpha}}, (\ )_{\dot{\beta}}, (\ )_{\dot{p}}, (\ )_{\dot{q}}, (\ )_{\dot{r}}, (\ )_{\dot{U}}] =$$
$$\left[\frac{\partial}{\partial\alpha}, \frac{\partial}{\partial\beta}, \frac{\partial}{\partial\left(\frac{pD}{U}\right)}, \frac{\partial}{\partial\left(\frac{qD}{U}\right)}, \frac{\partial}{\partial\left(\frac{rD}{U}\right)}, \frac{\partial}{\partial\left(\frac{\dot{\alpha}D}{U}\right)}, \frac{\partial}{\partial\left(\frac{\dot{\beta}D}{U}\right)}, \frac{\partial}{\partial\left(\frac{\dot{p}D^2}{U^2}\right)}, \frac{\partial}{\partial\left(\frac{\dot{q}D^2}{U^2}\right)}, \frac{\partial}{\partial\left(\frac{\dot{r}D^2}{U^2}\right)}, \frac{\partial}{\partial\left(\frac{\dot{U}D}{U^2}\right)}\right] \tag{17}$$

All of the derivatives are evaluated at $\alpha = \alpha$, $\beta = p = q = r = \dot{p} = \dot{q} = \dot{r} = \dot{U} = \dot{\alpha} = \dot{\beta} = 0$ (although some other equilibrium condition could, of course, have been specified).

From Eqs. (12), (13), and (17) we see that we can obtain 55 stability derivatives. They are given as follows:

$$\begin{bmatrix} C_{Y_\beta}, & C_{Y_\alpha}, & C_{Y_p} \\ C_{Z_\beta}, & C_{Z_\alpha}, & C_{Z_p} \\ C_{l_\beta}, & C_{l_\alpha}, & C_{l_p} \end{bmatrix} = -2\begin{bmatrix} \bar{A}_{11}, & \bar{A}_{12}, & \bar{A}_{13} \\ \bar{A}_{12}, & \bar{A}_{22}, & \bar{A}_{23} \\ \bar{A}_{13}, & \bar{A}_{23}, & \bar{A}_{33} \end{bmatrix} + 2\alpha\int_{-x_b/D}^{x_n/D}\begin{bmatrix} 0, & 0, & A_{22} \\ 0, & 0, & -A_{12} \\ A_{11}-A_{22}, & 2A_{12}, & A_{13} \end{bmatrix} d\left(\frac{x}{D}\right) \tag{18}$$

$$\begin{bmatrix} -C_{Y_r}, & C_{Y_q} \\ -C_{Z_r}, & C_{Z_q} \\ -C_{l_r}, & C_{l_q} \end{bmatrix} = -2\frac{x_b}{D}\begin{bmatrix} \bar{A}_{11}, & \bar{A}_{12} \\ \bar{A}_{12}, & \bar{A}_{22} \\ \bar{A}_{13}, & \bar{A}_{23} \end{bmatrix} - 2\alpha\int_{-x_b/D}^{x_n/D}\begin{bmatrix} 0, & 0 \\ 0, & 0 \\ A_{11}-A_{22}, & 2A_{12} \end{bmatrix}\frac{x}{D}\,d\left(\frac{x}{D}\right) \tag{19}$$

$$\begin{bmatrix} C_{n_\beta}, & C_{n_\alpha}, & C_{n_p} \\ -C_{m_\beta}, & -C_{m_\alpha}, & -C_{m_p} \end{bmatrix} = 2\frac{x_b}{D}\begin{bmatrix} \bar{A}_{11}, & \bar{A}_{12}, & \bar{A}_{13} \\ \bar{A}_{12}, & \bar{A}_{22}, & \bar{A}_{23} \end{bmatrix} - 2\int_{-x_b/D}^{x_n/D}\begin{bmatrix} A_{11}, & A_{12}, & A_{13} \\ A_{12}, & A_{22}, & A_{23} \end{bmatrix} d\left(\frac{x}{D}\right) -$$
$$2\alpha\int_{-x_b/D}^{x_n/D}\begin{bmatrix} 0, & 0, & -A_{22} \\ 0, & 0, & A_{12} \end{bmatrix}\frac{x}{D}\,d\left(\frac{x}{D}\right) \tag{20}$$

$$\begin{bmatrix} -C_{n_r}, & C_{n_q} \\ C_{m_r}, & -C_{m_q} \end{bmatrix} = 2\left(\frac{x_b}{D}\right)^2 \begin{bmatrix} \bar{A}_{11}, & \bar{A}_{12} \\ \bar{A}_{12}, & \bar{A}_{22} \end{bmatrix} + 2\int_{-x_b/D}^{x_n/D} \begin{bmatrix} A_{11}, & A_{12} \\ A_{12}, & A_{22} \end{bmatrix} \frac{x}{D}\, d\left(\frac{x}{D}\right) \tag{21}$$

$$\begin{bmatrix} C_{Y_{\dot\beta}}, & C_{Y_{\dot\alpha}}, & C_{Y_{\dot p}} \\ C_{Z_{\dot\beta}}, & C_{Z_{\dot\alpha}}, & C_{Z_{\dot p}} \\ C_{l_{\dot\beta}}, & C_{l_{\dot\alpha}}, & C_{l_{\dot p}} \end{bmatrix} = -2\int_{-x_b/D}^{x_n/D} \begin{bmatrix} A_{11}, & A_{12}, & A_{13} \\ A_{12}, & A_{22}, & A_{23} \\ A_{13}, & A_{23}, & A_{33} \end{bmatrix} d\left(\frac{x}{D}\right) \tag{22}$$

$$\begin{bmatrix} C_{Y_{\dot r}}, & -C_{Y_{\dot q}} \\ C_{Z_{\dot r}}, & -C_{Z_{\dot q}} \\ C_{l_{\dot r}}, & -C_{l_{\dot q}} \end{bmatrix} = -2\int_{-x_b/D}^{x_n/D} \begin{bmatrix} A_{11}, & A_{12} \\ A_{12}, & A_{22} \\ A_{13}, & A_{23} \end{bmatrix} \frac{x}{D}\, d\left(\frac{x}{D}\right) \tag{23}$$

$$\begin{bmatrix} C_{n_{\dot\beta}}, & C_{n_{\dot\alpha}}, & C_{n_{\dot p}} \\ -C_{m_{\dot\beta}}, & -C_{m_{\dot\alpha}}, & -C_{m_{\dot p}} \end{bmatrix} = -2\int_{-x_b/D}^{x_n/D} \begin{bmatrix} A_{11}, & A_{12}, & A_{13} \\ A_{12}, & A_{22}, & A_{23} \end{bmatrix} \frac{x}{D}\, d\left(\frac{x}{D}\right) \tag{24}$$

$$\begin{bmatrix} C_{n_{\dot r}}, & C_{n_{\dot q}} \\ C_{m_{\dot r}}, & C_{m_{\dot q}} \end{bmatrix} = -2\int_{-x_b/D}^{x_n/D} \begin{bmatrix} A_{11}, & A_{12} \\ A_{12}, & A_{22} \end{bmatrix} \left(\frac{x}{D}\right)^2 d\left(\frac{x}{D}\right) \tag{25}$$

$$\begin{bmatrix} C_{Y_{\dot v}} \\ C_{Z_{\dot v}} \\ C_{l_{\dot v}} \end{bmatrix} = -2\alpha\int_{-x_b/D}^{x_n/D} \begin{bmatrix} A_{12} \\ A_{22} \\ A_{23} \end{bmatrix} d\left(\frac{x}{D}\right) \tag{26}$$

$$\begin{bmatrix} C_{n_{\dot v}} \\ -C_{m_{\dot v}} \end{bmatrix} = -2\alpha\int_{-x_b/D}^{x_n/D} \begin{bmatrix} A_{12} \\ A_{22} \end{bmatrix} \frac{x}{D}\, d\left(\frac{x}{D}\right) \tag{27}$$

Thus, in general, for a body with a cross section with no symmetries, 14 integrals must be evaluated,

$$\int_{-x_b/D}^{x_n/D} \begin{bmatrix} A_{11}, & A_{12}, & A_{13} \\ 0, & A_{22}, & A_{23} \\ 0, & 0, & A_{33} \end{bmatrix} d\left(\frac{x}{D}\right), \quad \int_{-x_b/D}^{x_n/D} \begin{bmatrix} A_{11}, & A_{12}, & A_{13} \\ 0, & A_{22}, & A_{23} \end{bmatrix} \frac{x}{D}\, d\left(\frac{x}{D}\right), \quad \int_{-x_b/D}^{x_n/D} \begin{bmatrix} A_{11}, & A_{12} \\ 0, & A_{22} \end{bmatrix} \left(\frac{x}{D}\right)^2 d\left(\frac{x}{D}\right)$$

For a cross section with one plane of symmetry (such as almost all present-day airplane and missile configurations), $A_{12} = A_{23} = 0$, and, hence, only nine integrals must be evaluated. For a cross section with two perpendicular planes of symmetry, A_{13} also vanishes and only seven integrals must be evaluated. If the cross section is the same when rotated 90° (such as a cruciform missile configuration), then, also, $A_{11} = A_{22}$ and only four integrals must be evaluated.

It is interesting that the only stability derivatives that require a knowledge of φ_3, the potential due to rolling, are C_{l_p} and $C_{l_{\dot p}}$. Also, because of the symmetry of $[A]$, we find that

$$\begin{aligned} C_{Z_\beta} &= C_{Y_\alpha}, \quad C_{m_r} = C_{n_\alpha}, & C_{m_{\dot r}} &= C_{n_{\dot q}}, \quad C_{Y_{\dot r}} = C_{n_{\dot\beta}} \\ C_{m_\beta} &= -C_{n_\alpha}, \quad C_{Z_{\dot\beta}} = C_{Y_{\dot\alpha}}, & C_{l_{\dot\beta}} &= C_{Y_{\dot p}}, \quad C_{m_{\dot\alpha}} = C_{Z_{\dot q}} \\ C_{Z_r} &= -C_{Y_q}, \quad C_{m_{\dot\beta}} = -C_{n_{\dot\alpha}} = -C_{Z_{\dot r}} = C_{Y_{\dot q}}; & C_{l_{\dot\alpha}} &= C_{Z_{\dot p}} \end{aligned}$$

and, in addition, when $\alpha = 0$, $C_{l_\beta} = C_{Y_p}$ and $C_{l_\alpha} = C_{Z_p}$.

Application to a Slender Wing-Body-Vertical-Tail Configuration

The method described above is applied here to finding the longitudinal and lateral stability derivatives of a configuration consisting of a slender body of revolution with low aspect ratio wings and unequal low aspect ratio vertical tails (see Fig. 2). The cross section of the configuration is mapped conformally onto a circle in order to determine the velocity potentials for the low-speed two-dimensional motion of the cross section. The inertia coefficients of the cross section are then determined, leading finally to the stability derivatives of the three-dimensional configuration.

Conformal Mapping of the Wing-Body-Vertical-Tail Cross Section onto a Circle†

The cross section of the body is shown in Fig. 3. It consists of a circle with two equal opposing fins and two unequal opposing fins at right angles to the equal fins. The plane of the cross section will be called the w plane. The conformal mapping of the exterior of the finned circle onto a circle is most easily seen in terms of three consecutive simpler mappings:

(1) First the w plane is mapped onto the ξ plane by a Joukowsky transformation that "flattens" the circle,

† The author is indebted to R. H. Edwards for pointing out this transformation to him.

$$\xi = w + (a^2/w) \tag{21}$$

(2) Next the "slit" ξ plane is mapped onto the Z plane by the transformation

$$\xi^2 = Z^2 - c^2 \tag{22}$$

(3) Finally, the "flat plate" along the real axis in the Z plane is mapped onto a circle in the ζ plane by a translation and another Joukowsky transformation,

$$Z - \frac{h-f}{2} = \zeta + \frac{(h+f)^2}{16\zeta} \tag{23}$$

Combining these three transformations, the mapping of the finned circle onto a circle is

$$c^2 + \left(w + \frac{a^2}{w}\right)^2 = \left[\frac{h-f}{2} + \zeta + \frac{(h+f)^2}{16\zeta}\right]^2 \tag{24}$$

On the boundary of the contour,

$$\left.\begin{aligned} \zeta &= [(h+f)/4]e^{i\theta} \\ w &= \pm\frac{1}{2}\left[\sqrt{\left(\frac{h-f}{2} + \frac{h+f}{2}\cos\theta\right)^2 - c^2} + \right. \\ &\qquad \left.\sqrt{\left(\frac{h-f}{2} + \frac{h+f}{2}\cos\theta\right)^2 - c^2 - 4a^2}\right] \end{aligned}\right\} \tag{25}$$

where the plus sign holds for the right half of the w plane and the minus sign holds for the left half of the w plane.

The angles in the ζ plane are given by

$$\left.\begin{aligned} \cos\theta_0 &= 1 - \frac{2(h - \sqrt{c^2 + 4a^2})}{h+f} \\ \cos\theta_1 &= 1 - [2(h-c)/(h+f)] \\ \cos\theta_2 &= 1 - [2f/(h+f)] \\ \cos\theta_3 &= 1 - [2(f-c)/(h+f)] \\ \cos\theta_4 &= 1 - \frac{2(f - \sqrt{c^2 + 4a^2})}{h+f} \end{aligned}\right\} \tag{26}$$

The expressions for c, h, and f in terms of a, s, t_1, and t_2 are

$$\left.\begin{aligned} c &= s[1 - (a^2/s^2)] \\ h &= \sqrt{s^2\left(1 - \frac{a^2}{s^2}\right)^2 + t_1^2\left(1 + \frac{a^2}{t_1^2}\right)^2} \\ f &= \sqrt{s^2\left(1 - \frac{a^2}{s^2}\right)^2 + t_2^2\left(1 + \frac{a^2}{t_2^2}\right)^2} \end{aligned}\right\} \tag{27}$$

It is easily seen that the cross section of the configuration considered can be specialized to twelve particular cases; these are shown in Fig. 4. The mapping can be easily extended to the case of a fuselage with elliptical cross section by first mapping the ellipse onto a circle by a Joukowsky transformation and then proceeding as above.

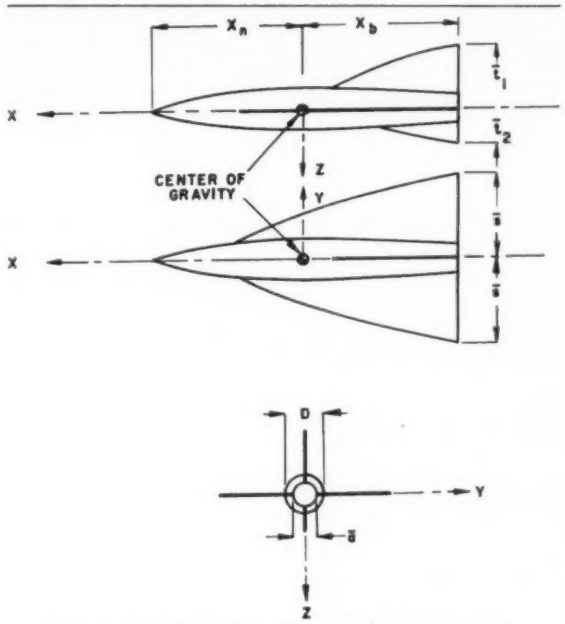

FIG. 2. Slender wing-body-vertical-tail configuration.

THE INERTIA COEFFICIENTS OF THE WING-BODY-VERTICAL-TAIL CROSS SECTION

The expressions for the inertia coefficients of the cross section are given in Eq. (2).

Because of the plane of symmetry of the cross section under consideration here, we see that

$$A_{12} = A_{23} = 0 \tag{28}$$

The vertical fins do not affect the inertia coefficient A_{22}, since they lie along stream lines of the flow. Hence, the case of no vertical fins suffices to find A_{22}. This has already been done by Spreiter.[3] The result is

$$A_{22} = \left(\frac{2S}{D}\right)^2\left(1 - \frac{a^2}{s^2} + \frac{a^4}{s^4}\right) \tag{29}$$

The expression for A_{11} is worked out in Appendix (1). The result is

$$A_{11} = \frac{1}{2}\left(\frac{h+f}{D}\right)^2[G(\theta_0, \theta_4) + G(\theta_1, \theta_3)] - \left(\frac{2a}{D}\right)^2 \tag{30}$$

where

$$\begin{aligned} G(\lambda, \mu) = {} & \frac{2}{\pi}\left[1 - \left(\frac{\cos\lambda + \cos\mu}{2}\right)^2\right] \times \\ & \left\{K(k)\left[E\left(\frac{\pi-\lambda}{2}, k'\right) + E\left(\frac{\pi-\mu}{2}, k'\right) - \right.\right. \\ & \left.\frac{\cos\lambda + \cos\mu}{2\cos\frac{\lambda}{2}\cos\frac{\mu}{2}}\right] - [K(k) - E_0(k)] \times \\ & \left.\left[F\left(\frac{\pi-\lambda}{2}, k'\right) + F\left(\frac{\pi-\mu}{2}, k'\right)\right]\right\} \end{aligned} \tag{31}$$

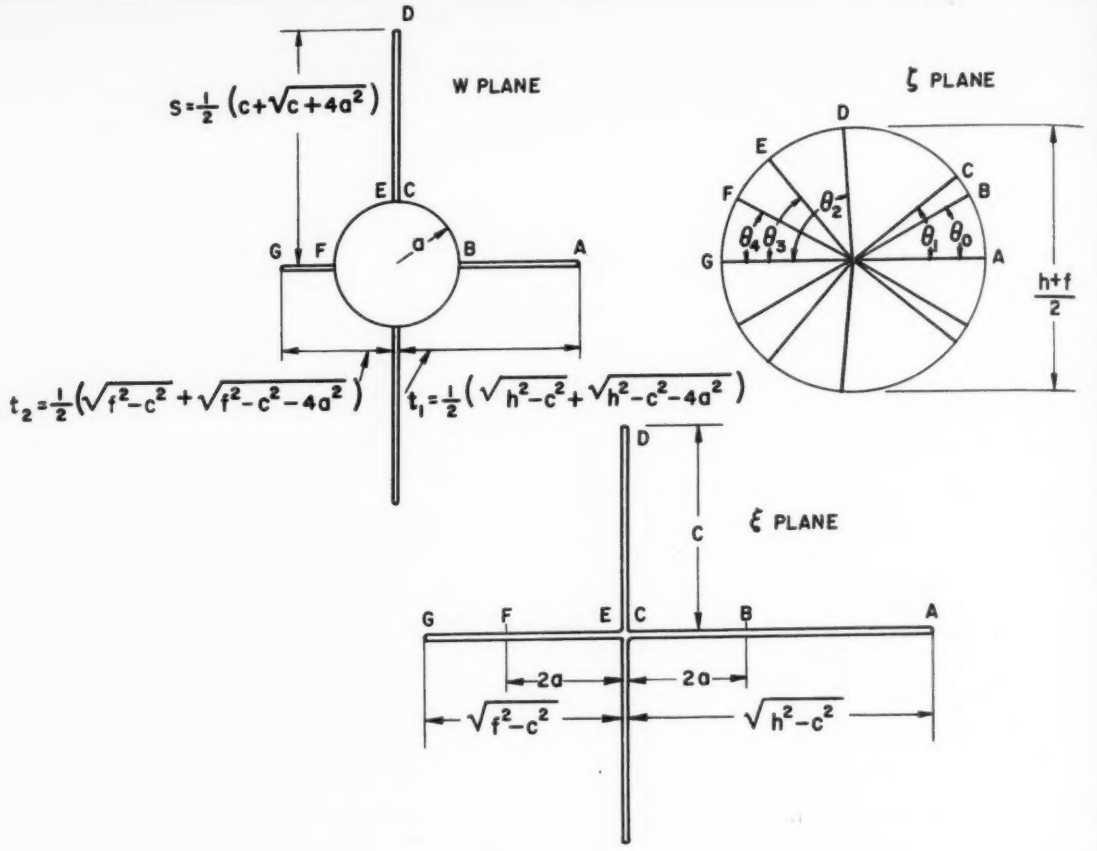

FIG. 3. Conformal mapping of cross section onto a circle.

and

k $= \tan\frac{\lambda}{2}\tan\frac{\mu}{2}$ (note $0 \leq k \leq 1$, since $0 \leq \lambda \leq \pi$, $0 \leq \mu \leq \pi - \lambda$)

k' $= \sqrt{1-k^2}$

$E(\varphi, k) = \int_0^{\varphi} \sqrt{1-k^2\sin^2\varphi}\,(d\varphi$ = incomplete elliptic integral of second kind)

$E_0(k) = E\left(\frac{\pi}{2}, k\right)$ = complete elliptic integral of second kind

$F(\varphi, k) = \int_0^{\varphi} \frac{d\varphi}{\sqrt{1-k^2\sin^2\varphi}}$ = incomplete elliptic integral of first kind

$K(k) = F\left(\frac{\pi}{2}, k\right)$ = complete elliptic integral of first kind

A graph of the function $G(\lambda,\mu)$ is shown in Fig. 5, and a table of values of the function is given in Table 1. A discussion of the function is given in Appendix (1).

The expressions for A_{13} and A_{33} cannot be given in terms of tabulated functions. The expression for A_{33} will not be given here, but A_{13} is worked out in Appendix (2) The result is

$$A_{13} = \frac{1}{\pi}\left(\frac{2a}{D}\right)^2 \frac{h+f}{2D}(\sin\theta_0 + \sin\theta_1 - \sin\theta_3 - \sin\theta_4) - \frac{1}{\pi}\left(\frac{h+f}{2D}\right)^3 \Big\{ 2(\sin\theta_0 - \sin\theta_1 + \sin\theta_3 - \sin\theta_4) - \frac{2}{3}(\sin^3\theta_0 - \sin^3\theta_1 + \sin^3\theta_3 - \sin^3\theta_4) - (\cos\theta_0 + \cos\theta_1 - \cos\theta_3 - \cos\theta_4) \times \left[\frac{1}{2}(\theta_0 - \theta_1 - \theta_3 + \theta_4) + \frac{1}{4}(\sin 2\theta_0 - \sin 2\theta_1 - \sin 2\theta_3 + \sin 2\theta_4)\right] + \frac{\pi}{8}(\cos\theta_0 + \cos\theta_1 + \cos\theta_3 + \cos\theta_4)(\cos\theta_0 - \cos\theta_1 + \cos\theta_3 - \cos\theta_4) \times (\cos\theta_0 - \cos\theta_1 - \cos\theta_3 + \cos\theta_4) + 2H(\theta_0, \theta_1, \theta_3, \theta_4) + 2H(\theta_1, \theta_0, \theta_4, \theta_3)\Big\} \quad (36)$$

where

$$\left.\begin{aligned} H(\alpha, \beta, \gamma, \delta) &= H^*(\alpha, \beta, \gamma, \delta) + H^*(\delta, \gamma, \beta, \alpha) \\ H^*(\alpha, \beta, \gamma, \delta) &= \int_0^\alpha \sqrt{(\cos\theta - \cos\alpha)(\cos\theta - \cos\beta)(\cos\theta + \cos\gamma)(\cos\theta + \cos\delta)}\,\cos\theta\, d\theta \end{aligned}\right\} \quad (37)$$

The value of H^* can easily be determined numerically for any particular cross section, since the integrand has no singularities.

The Stability Derivatives for a Wing-Body-Vertical-Tail Configuration

The stability derivatives for the equilibrium condition $\alpha = \alpha, \beta = p = q = r = \dot{\alpha} = \dot{\beta} = \dot{p} = \dot{q} = \dot{r} = \dot{U} = 0$ can be obtained by substituting the expressions for the inertia coefficients into Eqs. (13) through (27).

In general, the integrals involving A_{11} and A_{13} will have to be integrated numerically. The integrals involving A_{22} can often be integrated in simple forms because of the simplicity of the analytic expression for A_{22}.

It is interesting that for $\alpha = 0$ the only stability derivatives that depend upon the distribution of the inertia coefficients with x are C_{m_α}, C_{n_β}, $C_{n_{\dot{\beta}}}$, C_{n_r}, C_{m_q}, and all derivatives with respect to $\dot{\alpha}$, $\dot{\beta}$, $\dot{p}$, $\dot{q}$, $\dot{r}$, and $\dot{U}$. All the other stability derivatives depend only on the values of the inertia coefficients in the base plane. Furthermore, the important quantities $C_{n_r} - C_{n_{\dot{\beta}}}$ and $C_{m_q} + C_{m_{\dot{\alpha}}}$ depend only on the values of A_{11} and A_{22} in the base plane; in fact,

$$C_{n_r} - C_{n_{\dot{\beta}}} = -2\left(\frac{x_b}{D}\right)^2 \bar{A}_{11} = \left(\frac{x_b}{D}\right)^2 C_{Y_\beta}$$

$$C_{m_q} + C_{m_{\dot{\alpha}}} = -2\left(\frac{x_b}{D}\right)^2 \bar{A}_{22} = \left(\frac{x_b}{D}\right)^2 C_{Z_\alpha}$$

This means, for example, that the damping of the short-period longitudinal oscillation depends only on the geometry of the base plane. If τ is the time to damp to $1/e$ times the undamped amplitude, then

$$\tau = \frac{4W}{g\rho U \dfrac{\pi D^2}{4}\left[-C_Z{}^\alpha - \left(\dfrac{D}{r}\right)^2 (C_{m_q} + C_{m_{\dot{\alpha}}})\right]}$$

$$\tau = \frac{2W}{g\rho U \pi \bar{s}^2 \left(1 - \dfrac{\bar{a}^2}{\bar{S}^2} + \dfrac{\bar{a}^4}{\bar{S}^4}\right)\left(1 + \dfrac{x_b{}^2}{r^2}\right)}$$

where W = weight of the missile, r = radius of gyration of the missile about the y-axis, and g = acceleration due to gravity.

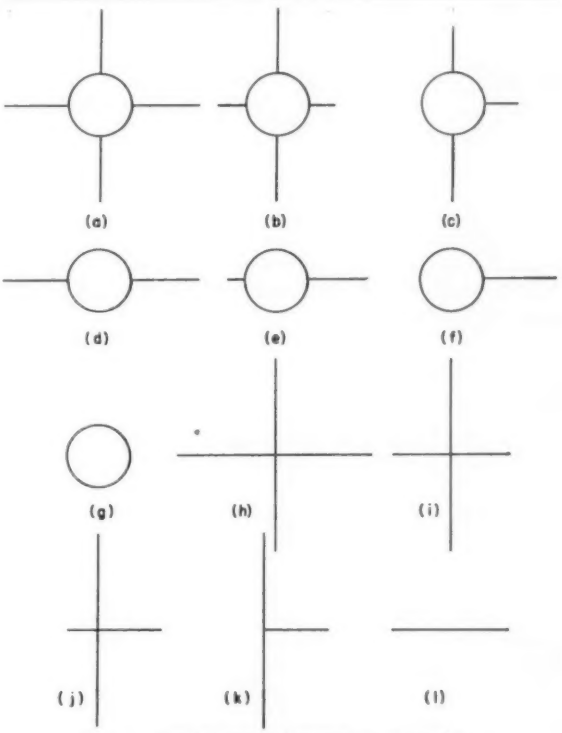

Fig. 4. Special cases of general cross section.

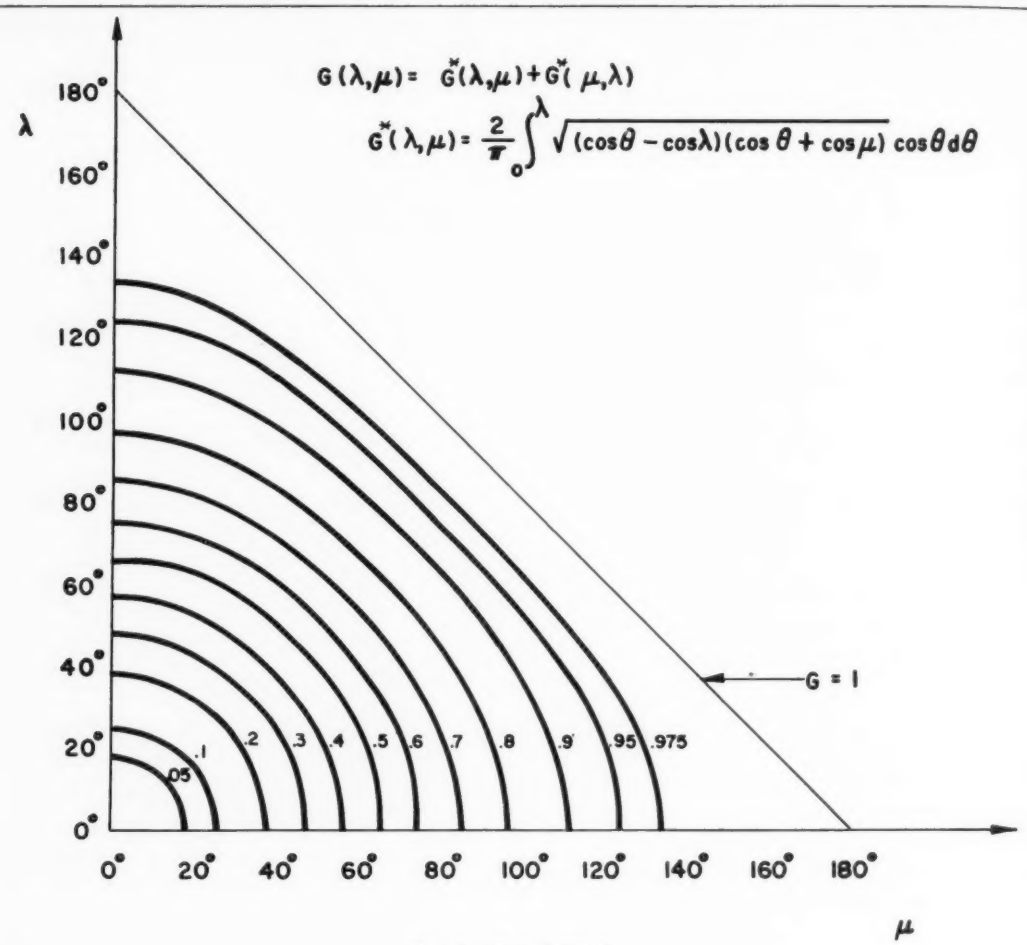

FIG. 5. Plot of $G(\lambda,\mu)$.

Appendix (1)

INERTIA COEFFICIENT A_{11}

Referring to Fig. 3, we wish to find the inertia coefficient (apparent additional mass coefficient) for motion of the cross section in the w_2 direction where $w = w_1 + iw_2$. The velocity potential for unit velocity in this direction is

$$\varphi_1 = Rl\{-i(\zeta - w) + i[(h+f)^2/16\zeta]\} \tag{1}$$

where

$$\left[\frac{h^* - f}{2} + \zeta + \frac{(h+f)^2}{16\zeta}\right]^2 = c^2 + \left(w + \frac{a^2}{w}\right)^2$$

On the boundary of the cross section $\zeta = [(h+f)/4]e^{i\theta}$, so the potential there is

$$\varphi_1 = [(h+f)/2]\sin\theta - w_2$$

$$w_1 + iw_2 = \pm\frac{h+f}{4}\left[\sqrt{(\cos\theta - \cos\theta_0)(\cos\theta + \cos\theta_4)} + \sqrt{(\cos\theta - \cos\theta_1)(\cos\theta + \cos\theta_3)}\right] \tag{2}$$

The inertia coefficient is given by

$$A_{11} = -\frac{1}{S}\oint \varphi_1 \frac{\partial\varphi_1}{\partial n}\,ds = -\frac{4}{\pi D^2}\oint \varphi_1 dw_1 \tag{3}$$

TABLE 1

The Function $G(\lambda,\mu) = G(\mu,\lambda)$

λ/μ	0°	10°	20°	30°	40°	50°	60°	70°	80°	90°
0°	0									
10	0.015	0.030								
20	0.059	0.074	0.117							
30	0.129	0.143	0.185	0.250						
40	0.220	0.234	0.273	0.334	0.413					
50	0.325	0.338	0.374	0.431	0.503	0.586				
60	0.437	0.449	0.482	0.534	0.599	0.673	0.750			
70	0.549	0.560	0.590	0.635	0.693	0.757	0.823	0.883		
80	0.655	0.665	0.690	0.730	0.779	0.833	0.886	0.933	0.969	
90	0.750	0.757	0.779	0.812	0.853	0.897	0.937	0.970	0.992	1.0
100	0.829	0.836	0.853	0.880	0.912	0.945	0.973	0.992	1.0	
110	0.891	0.897	0.910	0.931	0.955	0.977	0.993	1.0		
120	0.937	0.942	0.951	0.966	0.982	0.994	1.0			
130	0.968	0.971	0.978	0.987	0.995	1.0				
140	0.986	0.988	0.992	0.996	1.0					
150	0.995	0.996	0.998	1.0						
160	0.999	0.999	1.0							
170	0.999	1.0								
180	1.0									

From Eq. (2) we see that

$$w_1 = \pm\frac{h+f}{4}\begin{cases}\sqrt{(\cos\theta-\cos\theta_0)(\cos\theta+\cos\theta_4)}+\sqrt{(\cos\theta-\cos\theta_1)(\cos\theta+\cos\theta_3)}; & 0\le\theta\le\theta_0\\ & \pi-\theta_4\le\theta\le\pi\\ \sqrt{(\cos\theta-\cos\theta_1)(\cos\theta+\cos\theta_3)}; & \theta_0<\theta<\theta_1;\ \pi-\theta_3\le\theta\le\pi-\theta_4\\ 0; & \theta_1\le\theta\le\theta_3\end{cases} \tag{4}$$

Also, it is easily seen that

$$\oint w_2\,dw_1 = \pi a^2 \tag{5}$$

Substituting Eqs. (2) and (4) into Eq. (3), integrating by parts, and changing integration variables in the last two integrals, we have

$$A_{11} = \frac{1}{\pi}\left(\frac{h+f}{D}\right)^2\Bigg[\int_0^{\theta_0}\sqrt{(\cos\theta-\cos\theta_0)(\cos\theta+\cos\theta_4)}\cos\theta\,d\theta + \int_0^{\theta_1}\sqrt{(\cos\theta-\cos\theta_1)(\cos\theta+\cos\theta_3)}\cos\theta\,d\theta + \int_0^{\theta_3}\sqrt{(\cos\theta-\cos\theta_3)(\cos\theta+\cos\theta_1)}\cos\theta\,d\theta + \int_0^{\theta_4}\sqrt{(\cos\theta-\cos\theta_4)(\cos\theta+\cos\theta_0)}\cos\theta\,d\theta\Bigg] - 2\left(\frac{a}{D}\right)^2 \tag{6}$$

Hence,

$$A_{11} = \frac{1}{2}\left(\frac{h+f}{D}\right)^2[G(\theta_0,\theta_4)+G(\theta_1,\theta_3)] - 2\left(\frac{a}{D}\right)^2 \tag{7}$$

where

$$\left.\begin{aligned}G(\lambda,\mu) &= G^*(\lambda,\mu)+G^*(\mu,\lambda)\\ G^*(\lambda,\mu) &= \frac{2}{\pi}\int_0^{\lambda}\sqrt{(\cos\theta-\cos\lambda)(\cos\theta+\cos\mu)}\cos\theta\,d\theta\end{aligned}\right\} \tag{8}$$

where $0 \le \lambda \le \pi$ and $0 \le \mu \le \pi - \lambda$.

The function $G(\lambda,\mu)$ can be expressed in terms of complete and incomplete elliptic integrals by a lengthy manipulation, leading to Eq. (9) in the text.†

Note that $G(\lambda,\mu) = G(\mu,\lambda)$. If $\mu = 0$, then $k = 1$, $k' = 0$, and

$$G(\lambda,0) = 1 - \cos^4(\lambda/2) \tag{9}$$

If $\mu = \pi - \lambda$, then $k = 1$, $k' = 0$, and

$$G(\lambda, \pi - \lambda) = 1 \tag{10}$$

If $\lambda = \mu$, then

$$G(\lambda,\lambda) = \sin^2\lambda \tag{11}$$

It is easy to show that the contour lines of constant G have the following slopes (see Fig. 5):

$$d\lambda/d\mu = \left\{\begin{matrix} 0; & \mu = 0 \\ -1; & \lambda = \mu \\ \infty; & \lambda = 0 \end{matrix}\right\} \tag{12}$$

† The author is indebted to H. A. Linstone for working out this expression.

Two particular cases are easily worked out in elementary functions. (a) $t_1 = t_2 = t$, corresponding to Fig. 4b:

$$A_{11} = \left(\frac{2t}{D}\right)^2\left(1 - \frac{a^2}{t^2} + \frac{a^4}{t^4}\right) \tag{13}$$

which checks Spreiter's result of Eq. (7).

(b) $a = 0$, $t_2 = 0$, corresponding to Fig. 4k:

$$A_{11} = \left(\frac{t_1}{D}\right)^2\left(1 - 2\frac{s^2}{t_1^2} + 2\frac{s}{t_1}\sqrt{1 + \frac{s^2}{t_1^2}}\right) \tag{14}$$

$A_{11} = \left(\frac{t_1}{D}\right)^2$ as $\frac{t_1}{s} \to \infty$, corresponding to a flat plate

$A_{11} = 2\left(\frac{t_1}{D}\right)^2$ as $\frac{s}{t_1} \to \infty$, corresponding to a flat plate in presence of an infinite end plate on one end

Appendix (2)

Inertia Coefficient A_{13}

The expression for A_{13} is

$$\left.\begin{aligned} A_{13} &= -(1/SD)\oint \varphi_1(\partial\varphi_3/\partial n)\,ds \\ A_{13} &= -\frac{8}{\pi D^3}\left(-\int_{\theta=0}^{\theta_0}\varphi_1 w_1\,dw_1 + \int_{\theta=\theta_1}^{\pi-\theta_4}\varphi_1 w_2\,dw_2 - \int_{\theta=\pi-\theta_4}^{\pi}\varphi_1 w_1\,dw_1\right) \end{aligned}\right\} \tag{1}$$

where

$$\left.\begin{aligned} \varphi_1 &= [(h+f)/2]\sin\theta - w_2 \\ w_1^2 &= \frac{1}{4}\left(\frac{h+f}{2}\right)^2\left[\sqrt{(\cos\theta - \cos\theta_0)(\cos\theta + \cos\theta_4)} + \sqrt{(\cos\theta - \cos\theta_1)(\cos\theta + \cos\theta_3)}\right]^2 \\ &\text{for } 0 \le \theta \le \theta_0 \text{ and } \pi - \theta_4 \le \theta \le \pi; \\ w_2^2 &= \frac{1}{4}\left(\frac{h+f}{2}\right)^2\left[\sqrt{(\cos\theta - \cos\theta_0)(\cos\theta + \cos\theta_4)} + \sqrt{(\cos\theta_1 - \cos\theta)(\cos\theta + \cos\theta_3)}\right]^2 \\ &\text{for } \theta_1 \le \theta \le \pi - \theta_3. \end{aligned}\right\} \tag{2}$$

Substituting Eq. (2) into Eq. (1), integrating by parts, and manipulating, we finally arrive at Eq. (10) of the text.

For the special case of no body—i.e., $a = 0$—Eq. (10) simplifies greatly, since $\theta_0 = \theta_1$ and $\theta_3 = \theta_4$ for this case:

$$A_{13} = -\frac{1}{2\pi}\left(\frac{h+f}{D}\right)^3\left\{\sin\theta_0 + \sin\theta_4 - \frac{1}{3}\sin^3\theta_0 - \frac{1}{3}\sin^3\theta_4 + (\cos\theta_4 - \cos\theta_0)\left[\frac{1}{2}(\theta_0 - \theta_4) + \frac{1}{4}(\sin 2\theta_0 - \sin 2\theta_4)\right] - \cos\theta_0\cos\theta_4(\sin\theta_0 + \sin\theta_4)\right\} \tag{3}$$

References

[1] Munk, Max M., *The Aerodynamic Forces on Airship Hulls*, N.A.C.A. Report No. 184, 1924.

[2] Jones, Robert T., *Properties of Low Aspect Ratio Pointed Wings at Speeds Below and Above the Speed of Sound*, N.A.C.A. Report No. 835, 1946.

[3] Spreiter, John R., *The Aerodynamic Forces on Slender Plane- and Cruciform-Wing and Body Combinations*, N.A.C.A. Report No. 962, 1950.

[4] Lamb, Horace, *Hydrodynamics*, 6th Ed. pp. 160–168; Dover Publications, New York.

[5] Ribner, Herbert S., *The Stability Derivatives of Low-Aspect Ratio Triangular Wings at Subsonic and Supersonic Speeds*, N.A.C.A. T.N. No. 1423, September, 1947.

Calculation Method for Three-Dimensional Rotationally Symmetrical Laminar Boundary Layers with Arbitrary Free-Stream Velocity and Arbitrary Wall-Temperature Variation*

ROBERT M. DRAKE, JR.†

University of California at Berkeley

Abstract

A calculation method is presented enabling a rapid prediction of the distribution of the local skin-friction and heat-transfer coefficients to be made for rotationally symmetrical bodies having arbitrarily specified free-stream velocity distributions and surface-temperature variations for constant-property, incompressible, laminar boundary-layer flows. The method utilizes the Mangler transformation as a basis, thus enabling the results calculated by Hartree and Levy for the two-dimensional case to be used directly in the determination of boundary-layer quantities for the three-dimensional case.

Example results using the proposed method are presented in the form of the boundary-layer momentum and displacement thicknesses, the skin-friction coefficients, and the heat-transfer coefficients for a three-dimensional half-body with constant surface temperature. These results, utilizing the Hartree velocity profiles, are compared with similar results obtained by Scholkemeier utilizing the Pohlhausen P-4 velocity profiles. The skin-friction coefficient for stagnation-point flow as obtained by the approximate method is compared with the exact solution for this region given by Homann to show excellent agreement.

Nomenclature

A, B, C	=	constants
a	=	thermal diffusivity, $k/\rho c_p$ (ft.²/sec.)
c_p	=	specific heat at constant pressure (B.t.u./lb.-°F.)
C_f	=	skin-friction coefficient, $\tau_0/{}^1/_2\rho U_\infty{}^2$, dimensionless
D	=	maximum diameter of half-body (ft.)
$F(\bar{Z})$	=	solution of momentum equation, Eq. (5)
$g(\bar{Z})$	=	solution of energy equation, Eq. (28)
g	=	acceleration of gravity (ft./sec.²)
h	=	heat-transfer coefficient (B.t.u./hr.-ft.²-°F.)
k	=	thermal conductivity (B.t.u./hr.-ft.-°F.)
L	=	constant in Mangler transform (ft.)
m	=	exponent defining free-stream velocity variation
n	=	normal coordinate (ft.)
q_0	=	heat flux (B.t.u./hr.-ft.²)
r	=	thermal recovery factor, $T_{aw} - T_1/(U_1{}^2/2gJC_p)$
r_0	=	radius of body (ft.)
s	=	tangential coordinate (ft.)
S	=	distance from stagnation point along body surface (ft.)
T	=	temperature in boundary layer (°F.)
T_{aw}	=	adiabatic wall temperature, $T_{aw} = T_1 + r\,(U_1{}^2 \div 2gJC_p)$(°F.)
T_0	=	surface temperature of body (°F.)
T_1	=	state temperature at edge of boundary layer (°F.)
T_{s_1}	=	stagnation temperature at edge of boundary layer (°F.)
U_1	=	velocity of the free stream at edge of boundary layer (ft./sec.)
U_∞	=	velocity of the onstream flow (ft./sec.)
u	=	tangential velocity component (ft./sec.)
v	=	normal velocity component (ft./sec.)
Z	=	dimensionless normal coordinate
Z^*	=	dimensionless displacement thickness
Z_i	=	dimensionless momentum thickness
α	=	included angle of cone, deg.
β	=	parameter relating to the free-stream velocity variation, $2m/(m+1)$
γ	=	exponent defining temperature variation of surface
δ	=	boundary-layer thickness (ft.)
δ^*	=	boundary-layer displacement thickness (ft.)
μ	=	absolute viscosity (lb. sec./ft.²)
ν	=	kinematic viscosity (ft.²/sec.)
ψ	=	stream function in the boundary layer (ft.³/sec.)
θ	=	boundary-layer momentum thickness (ft.)
θ_t	=	boundary-layer thermal momentum thickness (ft.)
τ_0	=	shear stress at the surface (lb./ft.²)
ρ	=	density (lb. sec.²/ft.⁴)
σ	=	Prandtl Number, $\mu c_p/k = \nu/a$, dimensionless

Note: Barred symbols indicate two-dimensional values; unbarred symbols indicate three-dimensional values.

Introduction

Knowledge of the laminar boundary-layer characteristics on rotationally symmetrical, three-dimensional bodies is significant to the design of high-speed aircraft and missiles. This rotationally symmetrical flow has been investigated by Millikan,[1] Frössling,[2] Scholkemeier,[3] Tomotika,[4] Whitehead and Canetti,[5] and others, with the ultimate aim of specifying distribution of the local skin-friction and heat-transfer coefficients on the surface of any arbitrarily shaped body. The usefulness of any so devised specification lies in its utility, as well as the accuracy, of the results. In practical instances, a variation of the surface temperature generally occurs which has a marked effect

Received August 18, 1952.

* This work was conducted at the University of California, Berkeley, under the auspices of the Flight Research Laboratory, Air Research and Development Command, on U.S.A.F. Contract 33(038)-12941 dealing with research on heat transfer to boundary layers. The author acknowledges the contributions of S. Levy and J. T. Bevan in the calculation of the examples.

† Assistant Professor, Mechanical Engineering Division.

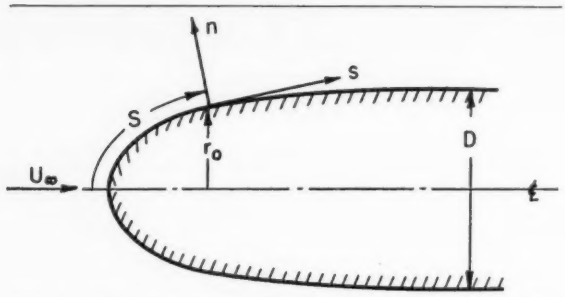

FIG. 1. Coordinate system for rotationally symmetrical body.

upon the heat-transfer rate, and, as a consequence, solutions of the momentum and energy equations accounting for the effect of variable wall temperature, as well as variable free-stream velocity, are necessary.

All boundary-layer solutions in which the variation of wall temperature can be accounted for relate to constant property, incompressible flows with a free-stream velocity distribution that is expressible as a power function of the meridional distance from the forward stagnation point ($U_1 = C_3 S^m$). Exact solutions of the corresponding energy equations are possible for a wall-temperature distribution of the same type ($T_0 = A_3 S^\gamma$). Such solutions for the momentum and energy equations for two-dimensional flows have been computed by Hartree[6] and Levy.[7]

Since for the specification of an arbitrary free-stream velocity and surface temperature distribution there is correspondence with exact solutions only at the stagnation point, approximate solutions are resorted to for the regions downstream of the stagnation point. Such approximate methods for two-dimensional flows have been discussed by Seban.[8]

Since rotationally symmetrical three-dimensional flows, wherein the boundary-layer thickness is much smaller than the body radius, may be represented by momentum and energy equations that are identical with the two-dimensional case (the three-dimensional character of the flow having its specification only in the continuity equation), the two-dimensional flow results are directly applicable to these particular three-dimensional flows. It is the purpose of this paper to present an approximate method for the calculation of laminar boundary-layer characteristics for rotationally symmetrical three-dimensional flows that will yield a specification of the local skin-friction and heat-transfer coefficients for an arbitrarily specified free-stream velocity and surface-temperature variation.

ANALYSIS

In the instance wherein the boundary-layer thickness is small when compared with the body radius the applicable equations for constant property, incompressible flow, are (Fig. 1)

$$u\frac{\partial u}{\partial s} + v\frac{\partial u}{\partial n} = U_1\frac{dU_1}{ds} + \nu\frac{\partial^2 u}{\partial n^2} \quad \text{(momentum)} \tag{1}$$

$$u\frac{\partial T}{\partial s} + v\frac{\partial T}{\partial n} = a\frac{\partial^2 T}{\partial n^2} + \frac{\nu}{c_p}\left(\frac{\partial u}{\partial n}\right)^2 \quad \text{(energy)} \tag{2}$$

$$[\partial(r_0 u)/\partial s] + [\partial(r_0 v)/\partial n] = 0 \quad \text{(continuity)} \tag{3}$$

with the general boundary conditions,

$$n = 0, \quad u = v = 0, \quad T = T_0(S)$$

$$n \to \infty, \quad u = U_1, \quad T = 0$$

Momentum Equations

Exact Solution.—The continuity equation may be satisfied by a stream function of the type,

$$u = \frac{1}{r_0}\frac{\partial \psi}{\partial n}, \qquad v = -\frac{1}{r_0}\frac{\partial \psi}{\partial s}$$

which statements when used in combination with the Mangler transformation,[9] where barred variables are two-dimensional quantities,

$$\bar{S} = \int_0^s \frac{C^2 r_0^2}{L^2}\,ds, \qquad \bar{n} = \frac{C r_0}{L}\,n$$

result in a statement of the momentum equation of the form

$$\left(\frac{C}{L}\right)^2 \frac{\partial \psi}{\partial \bar{n}}\cdot\frac{\partial^2 \psi}{\partial \bar{n}\partial s} - \left(\frac{C}{L}\right)^2 \frac{\partial \psi}{\partial \bar{s}}\cdot\frac{\partial^2 \psi}{\partial \bar{n}^2} = \nu\left(\frac{C}{L}\right)\frac{\partial^3 \psi}{\partial \bar{n}^3} + U_1\frac{dU_1}{d\bar{s}}$$

which yields, upon setting $\bar{\psi} = (C/L)\psi$, the following equation, which is identical in form with the corresponding two-dimensional case:

$$\frac{\partial \bar{\psi}}{\partial \bar{n}}\cdot\frac{\partial^2 \bar{\psi}}{\partial \bar{n}\partial \bar{s}} - \frac{\partial \bar{\psi}}{\partial \bar{s}}\cdot\frac{\partial^2 \bar{\psi}}{\partial \bar{n}^2} = \nu\frac{\partial^3 \bar{\psi}}{\partial \bar{n}^3} + U_1\frac{dU_1}{d\bar{s}} \tag{4}$$

Eq. (1) may be further transformed by virtue of the Hartree variables, wherein

$$U_1 = C_2 \bar{S}^m$$

$$\bar{Z} = \sqrt{\frac{\bar{m}+1}{2}}\sqrt{\frac{U_1}{\nu \bar{S}}}\,\bar{n} = \frac{\bar{n}}{\sqrt{2-\bar{\beta}}}\sqrt{\frac{U_1}{\nu \bar{S}}}$$

$$\bar{\psi} = \sqrt{2-\bar{\beta}}\,\sqrt{U_1 \nu \bar{S}}\,F(\bar{Z})$$

to yield the familiar equation for the "wedge flows" for which solutions are available.[6]

$$F'''(\bar{Z}) + F(\bar{Z})F''(\bar{Z}) + \bar{\beta}\left\{1 - F'^2(\bar{Z})\right\} = 0 \tag{5}$$

The relationship between the two- and three-dimensional cases may be shown by considering the three-dimensional body as a right circular cone in analogy with the two-dimensional wedge. The cone may be represented by $r_0 = S \sin \alpha$ and the velocity distribution as $U_1 = C_3 S^m$. Now relating S to $\bar{S}$, one obtains

$$S = \frac{C^2}{L^2}\int_0^s r_0^2\,dS = \frac{C^2}{L^2}\int_0^s S^2\sin^2\alpha\,dS = \left\{\frac{C^2}{L^2}\frac{\sin^2\alpha}{3}\right\}S^3$$

and for the velocity distribution,

$$U_1 = C_2\bar{S}^{\bar{m}} = C_2\left\{\frac{C^2}{L^2}\frac{\sin^2\alpha}{3}\right\}^{\bar{m}} S^{3\bar{m}} = C_3S^{\bar{m}}$$

Therefore, by comparison,

$$C_3 = C_2\left\{\frac{C^2}{L^2}\frac{\sin^2\alpha}{3}\right\}^{\bar{m}}; \qquad \bar{m} = \frac{m}{3} \tag{6}$$

Further, since $\bar{m} = \bar{\beta}/(2-\bar{\beta})$ and $m = \beta/(2-\beta)$, the following relationships exist:

$$\bar{\beta} = \beta/(3-\beta); \quad \beta = 3\bar{\beta}/(\bar{\beta}+1) \tag{7}$$

Thus, by virtue of the above transformation, exact solutions are available for three-dimensional axisymmetrical flows wherein the free-stream velocity distribution may be expressed as a power function of the distance from the stagnation point.

Approximate Solution.—It is possible in the three-dimensional axisymmetrical case to utilize the exact solutions for the "cone flows" to form approximate solutions for such bodies with arbitrary free-stream velocity distributions in a form that utilizes the computations already made for the "wedge flows."

The momentum equation may be integrated across the boundary layer to yield the expression

$$\frac{d}{ds}\int_0^\delta u^2\,dn - U_1\frac{d}{ds}\int_0^\delta u\,dn - \frac{1}{r_0}\frac{dr_0}{ds}\left\{U_1\int_0^\delta u\,dn - \int_0^\delta u^2\,dn\right\} = \delta\,U_1\frac{dU_1}{ds} - \nu\left(\frac{\partial u}{\partial n}\right)_0 \tag{8}$$

Eq. (8) may be written as

$$\frac{\tau_0}{\rho} = U_1^2\frac{d\theta}{ds} + (2\theta+\delta^*)\,U_1\frac{dU_1}{ds} + \frac{1}{r_0}\frac{dr_0}{ds}\theta U_1^2 \tag{9}$$

wherein

$$\theta = \int_0^\delta \frac{u}{U_1}\left(1-\frac{u}{U_1}\right)dn; \quad \delta^* = \int_0^\delta\left(1-\frac{u}{U_1}\right)dn$$

Eq. (9) for the rotationally symmetrical three-dimensional case differs from the corresponding statement for the two-dimensional case only in the third term on the right-hand side. Using the Holstein-Bohlen form parameter, $(\theta^2/\nu)\,(dU_1/dS)$, Eq. (9) may be written as

$$\frac{\tau_0}{\mu}\frac{\theta}{U_1} = \frac{U_1}{\nu}\theta\frac{d\theta}{dS} + \left(2+\frac{\delta^*}{\theta}\right)\frac{\theta^2}{\nu}\frac{dU_1}{dS} + \frac{1}{r_0}\frac{dr_0}{dS}\frac{\theta^2}{\nu}U_1 \tag{10}$$

Writing Eq. (10) in terms of the variable θ^2/ν gives

$$\frac{U_1}{2}\frac{d(\theta^2/\nu)}{dS} + \frac{U_1}{r_0}\frac{dr_0}{dS}\left(\frac{\theta^2}{\nu}\right) = \left\{\frac{\tau_0}{\mu}\frac{\theta}{U_1} - \left(2+\frac{\delta^*}{\theta}\right)\frac{\theta^2}{\nu}\frac{dU_1}{dS}\right\} \tag{11}$$

In the instance wherein the free-stream velocity distribution may be expressed as a power function of the distance along the body $U_1 = C_3S^m$ and the dimensionless momentum thickness is defined as

$$Z_i = (\theta/\sqrt{2-\beta})\,\sqrt{U_1/\nu S}$$

the right-hand side of Eq. (11) is a function of the form parameter, which in this case is

$$(\theta^2/\nu)\,(dU_1/dS) = \beta z_i^2$$

By means of the Mangler transformations, the left-hand side of Eq. (11) yields the relationship

$$\frac{U_1}{2}\frac{d(\theta^2/\nu)}{dS} + \frac{U_1}{r_0}\frac{dr_0}{dS}(\theta^2/\nu) = \frac{1}{2}\frac{U_1}{\nu}\frac{d\bar{\theta}^2}{d\bar{S}} \tag{12}$$

Seban[8] has shown that this expression may be expressed as a linear function of the form parameter $\bar{\beta}\,\bar{Z}_i^2$. Thus,

$$\frac{U_1}{2}\frac{d(\theta^2/\nu)}{dS} + \frac{U_1}{r_0}\frac{dr_0}{dS}(\theta^2/\nu) = \frac{1}{2}\frac{U_1}{\nu}\frac{d\bar{\theta}^2}{d\bar{S}} = -A\bar{\beta}\bar{Z}_i^2 + B \tag{13}$$

where A and B are constants. It can be shown also that the form parameter is invariant in the transformation, so that

$$\beta\,Z_i^2 = \bar{\beta}\,\bar{Z}_i^2 \tag{14}$$

Thus the constants determined for the two-dimensional case are applicable hereto.† Then one can write, from Eq. (13),

$$\frac{d\left(\frac{\theta^2}{\nu}\right)}{dS} + \frac{dr_0}{r_0\,dS}\left(\frac{\theta^2}{\nu}\right) = \frac{-A\frac{\theta^2}{\nu}\frac{dU_1}{dS} + B}{U_1} \tag{15}$$

which when rearranged to be in dimensionless form is

$$\frac{d\left(\frac{\theta}{D}\sqrt{\frac{_\infty D}{\nu}}\right)^2}{d(S/D)} + \left\{\frac{2}{r_0/D}\frac{d\left(\frac{r_0}{D}\right)}{d\,(S/D)} + A\frac{U_\infty}{U_1}\frac{d\left(\frac{U_1}{U_\infty}\right)}{d(S/D)}\right\}\left(\frac{\theta}{D}\sqrt{\frac{U_\infty D}{\nu}}\right)^2 = B\left(\frac{U_\infty}{U_1}\right) \tag{16}$$

The solution of Eq. (16) yields the expression

$$\left(\frac{\theta}{D}\sqrt{\frac{U_\infty D}{\nu}}\right)^2 = B\left(\frac{r_0}{D}\right)^{-2}\left(\frac{U_1}{U_\infty}\right)^{-A}\int_0^{S/D}\left(\frac{r_0}{D}\right)^2\times\left(\frac{U_1}{U_\infty}\right)^{A-1}d\left(\frac{S}{D}\right) \tag{17}$$

† The value of the constant A was changed slightly from the value given in reference 8. Change in final results was negligible.

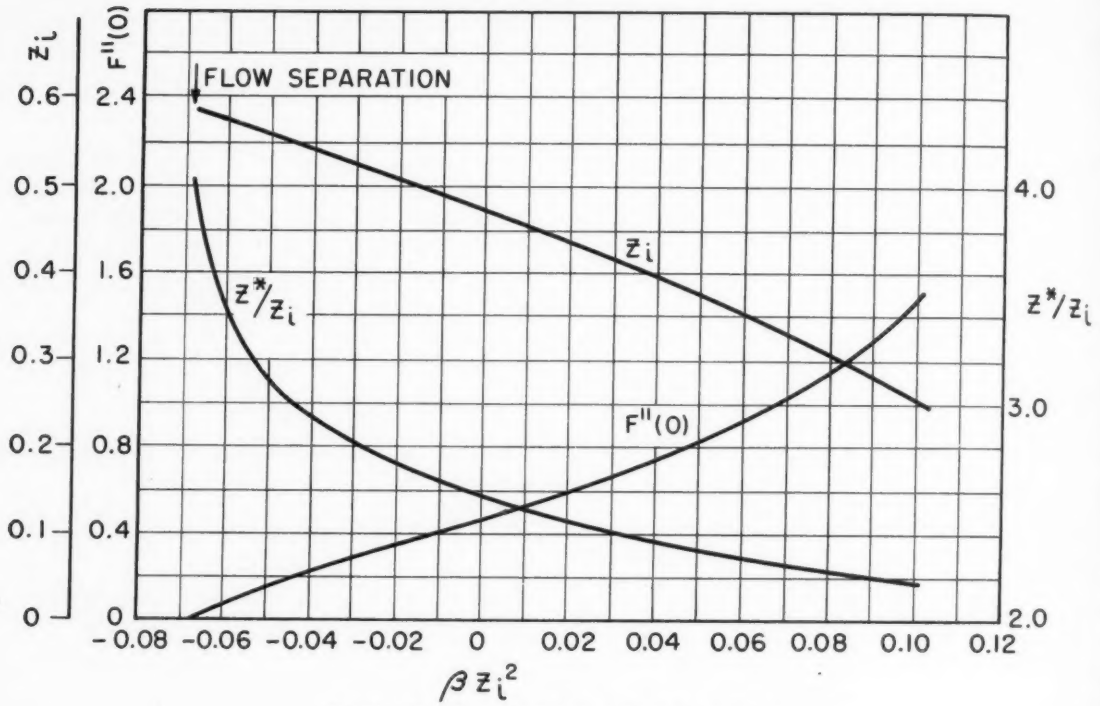

FIG. 2. Functions relating to solutions of Eq. (5).[8]

which gives the momentum thickness as a function of the body shape and the free-stream Reynolds Number for regions away from the stagnation point. At the stagnation point $S/D \to 0$; $U_1/U_\infty \to 0$; $r_0/D \to 0$; thus,

$$\left(\frac{\theta}{D}\sqrt{\frac{U_\infty D}{\nu}}\right)^2 = \lim_{S/D\to 0} \frac{B\int_0^{\frac{S}{D}} \left(\frac{r_0}{D}\right)^2 \left(\frac{U_1}{U_\infty}\right)^{A-1} d\left(\frac{S}{D}\right)}{\left(\frac{r_0}{D}\right)^2 \left(\frac{U_1}{U_\infty}\right)^A} \qquad (18)$$

The limiting solution of Eq. (18) is

$$\frac{\theta}{D}\sqrt{\frac{U_\infty D}{\nu}} = \frac{\sqrt{B/(2+A)}}{\sqrt{\left[d(U_1/U_\infty)/d\ (S/D)\right]_0}} \qquad (19)$$

The values taken for the constants are

$$\begin{aligned} 0 \quad &< \beta Z_i^2 < 0.09, \quad A = 5.23, \quad B = 0.44 \\ -0.068 \ &< \beta Z_i^2 < \quad 0, \quad A = 5.32, \quad B = 0.44 \end{aligned}$$

Applying these constants to Eqs. (17) and (19), the final expressions are obtained for the boundary-layer momentum thickness.

At stagnation point,

$$\frac{\theta}{D}\sqrt{\frac{U_\infty D}{\nu}} = 0.247 \Big/ \sqrt{\left[\frac{d(U_1/U_\infty)}{d(S/D)}\right]_0} \qquad (20)$$

for $0 < \beta Z_i^2 < 0.09$

$$\left(\frac{\theta}{D}\sqrt{\frac{U_\infty D}{\nu}}\right)^2 = 0.44\left(\frac{r_0}{D}\right)^{-2}\left(\frac{U_1}{U_\infty}\right)^{-5.23} \times \int_0^{\frac{S}{D}} \left(\frac{r_0}{D}\right)^2 \left(\frac{U_1}{U_\infty}\right)^{4.23} d\left(\frac{S}{D}\right) \qquad (21)$$

and for $-0.068 < \beta Z_i^2 < 0$

$$\left(\frac{\theta}{D}\right)\sqrt{\frac{U_\infty D}{\nu}}^2 = 0.44\left(\frac{r_0}{D}\right)^{-2}\left(\frac{U_1}{U_\infty}\right)^{-5.32} \int_0^{S/D} \times \left(\frac{r_0}{D}\right)^2 \left(\frac{U_1}{U_\infty}\right)^{4.32} d\left(\frac{S}{D}\right) \qquad (22)$$

Eqs. (20), (21), and (22), together with the knowledge of the free-stream velocity distribution and the body shape, yield a specification of the boundary-layer momentum thickness as a function of the distance S along the body. The displacement thickness δ^* may be obtained by means of the relationship

$$\delta^*/\theta = Z^*/Z_i = \bar{Z}^*/\bar{Z}_i$$

where Z^* is the dimensionless displacement thickness

$$Z^*/Z_i = \bar{Z}^*/\bar{Z}_i$$

is shown as a function of the form parameter on Fig. 2. From this relationship and a knowledge of θ the values for δ^* may be computed. The form parameter is best calculated from the relationship

$$\beta Z_i^2 = \left\{\frac{\theta}{D}\sqrt{\frac{U_\infty D}{\nu}}\right\}^2 \frac{d(U_1/U_\infty)}{d(S/D)}$$

The values of the form parameter are necessary also for the selection of the values of the constants in the above equations.

Skin-Friction Coefficient. The values of the skin-friction coefficients may be determined from the available results. Thus,

$$C_f = \frac{\tau_0}{\rho(U_\infty{}^2/2)} = \frac{\mu(\partial u/\partial n)_0}{\rho(U_\infty{}^2/2)} = \frac{2\nu}{U_\infty{}^2}\left(\frac{Cr_0}{L}\right)\left(\frac{\partial u}{\partial \bar{n}}\right)_0$$

Since,

$$U_1 = C_3 S^m = C_2 \bar{S}^m$$
$$u/U_1 = F'(\bar{Z})$$
$$\frac{\partial u}{\partial \bar{n}} = U_1 F''(\bar{Z})\frac{d\bar{Z}}{d\bar{n}} = \frac{U_1 F''(\bar{Z})}{\sqrt{2-\bar{\beta}}}\sqrt{\frac{U_1}{\nu \bar{S}}} = U_1 F''(\bar{Z})\frac{\bar{Z}_t}{\bar{\theta}}$$

Thus,

$$C_f = \frac{2\nu U_1}{U_\infty} F''(0)\left(\frac{Cr_0}{L}\right)\frac{\bar{Z}_t}{\bar{\theta}};$$
$$\bar{\theta} = (Cr_0/L)\theta$$

Therefore,

$$\frac{C_f}{2}\sqrt{\frac{U_\infty D}{\nu}} = \left(\frac{U_1}{U_\infty}\right)\frac{F''(0)\,\bar{Z}_t}{\left[(\theta/D)\sqrt{U_\infty D/\nu}\right]} \qquad (23)$$

The functions $F''(0)$ and $\bar{Z}_t$ have been calculated and tabulated as functions of $\bar{\beta}$, Fig. 2.[6, 10] The value of θ is determined from Eqs. (20), (21), and (22).

Comparison with Homann Exact Solution for Stagnation Flows.—The results of the above analysis may be compared with the exact solution given by Homann[11] for the skin-friction coefficient at a three-dimensional stagnation point. In this instance the free-stream velocity is a linear function of the distance S; thus $m = 1$ in the expression $U_1 = C_3 S^m$.

By Eqs. (6) and (7), therefore, $\bar{m} = 1/3$ and $\bar{\beta} = 1/2$. For a value of $\bar{\beta} = 1/2$ the values of $F''(0) = 0.9276$ and $\bar{Z}_t = 0.3502$. The value of the momentum thickness at the stagnation point is given by Eq. (20),

$$\frac{\theta}{D}\sqrt{\frac{U_\infty D}{\nu}} = \frac{0.247}{\sqrt{\left[\frac{d(U_1/U_\infty)}{d(S/D)}\right]_0}} = \frac{0.247}{\sqrt{\left(\frac{U_1/U_\infty}{S/D}\right)_0}}$$

Introducing these values into Eq. (23) gives

$$\frac{C_f}{2}\sqrt{\frac{U_\infty D}{\nu}} = \frac{F''(0)\bar{Z}_t}{0.247}\left(\frac{U_1}{U_\infty}\right)\sqrt{\left(\frac{U_1/U_\infty}{S/D}\right)_0} = 1.311\left(\frac{U_1}{U_\infty}\right)\beta_1{}^{1/2} \qquad (24)$$

wherein β_1 is the velocity gradient at the stagnation point defined by

$$U_1/U_\infty = \beta_1(S/D)$$

The exact result given by Homann for symmetrical three-dimensional stagnation flow is

$$(C_f/2)\sqrt{U_\infty D/\nu} = 1.3172\,(U_1/U_\infty)\beta_1{}^{1/2} \qquad (25)$$

Comparison of Eqs. (24) and (25) shows excellent agreement.

Energy Equation

It will be assumed here that superposition of the solutions of the energy equations to account for the effects of mechanical energy dissipation holds on a local basis as has been outlined in reference 8. The following development will consider first the case wherein dissipation is negligible. The necessary changes to account for dissipation will be indicated.

Exact Solutions.—The energy equation, Eq. (2), neglecting the dissipation term may be transformed by the Mangler transformation in the manner of the momentum equation to yield in the two-dimensional variables, $\bar{\psi}$, $\bar{m}$, and $\bar{s}$,

$$\frac{\partial \bar{\psi}}{\partial \bar{n}}\frac{\partial T}{\partial \bar{s}} - \frac{\partial \bar{\psi}}{\partial \bar{s}}\frac{\partial T}{\partial \bar{n}} = a\frac{\partial^2 T}{\partial \bar{n}^2} \qquad (26)$$

To account for surface temperature variation, the temperature T is considered as a product, one part a function of $\bar{S}$ and the other a function of $\bar{Z}$; there follows:

$$T = T_0(\bar{S})\cdot g(\bar{Z}); \quad \begin{matrix} g(0) = 1 \\ g(\infty) = 0 \end{matrix}$$

Transforming now to the Hartree variables as before, one obtains

$$F'(\bar{Z})g(\bar{Z})\,(2-\bar{\beta})\left(\frac{\bar{S}}{T_0}\frac{dT_0}{d\bar{S}}\right) - F(\bar{Z})g'(\bar{Z}) = \frac{1}{\sigma}\,g''(\bar{Z}) \qquad (27)$$

If $T_0 = A_2\bar{S}^{\bar{\gamma}} = A_3 S^{\bar{\gamma}}$, Eq. (27) reduces to the following form:

$$g''(\bar{Z}) + \sigma F(\bar{Z})g'(\bar{Z}) - \sigma\bar{\gamma}(2-\bar{\beta})F'(\bar{Z})g(\bar{Z}) = 0 \qquad (28)$$

Eq. (28) has been solved for several values of the exponent $\bar{\gamma}$ and for several values of the Prandtl Number, σ, by Levy[7] and for the special case of $\bar{\gamma} = 0$ (i.e., constant wall temperature) by Eckert.[10]

Approximate Solution.—The energy equation may be integrated across the boundary layer to yield, for the rotationally symmetrical case,

$$\frac{1}{r_0}\frac{dr_0}{ds}\int_0^\delta uT\,dn + \frac{d}{ds}\int_0^\delta uT\,dn = -a\left(\frac{\partial T}{\partial n}\right)_0 \qquad (29)$$

or when rearranged to be dimensionless in the integrands,

$$U_1 T_0\frac{1}{r_0}\frac{dr_0}{ds}\int_0^\delta\left(\frac{u}{U_1}\frac{T}{T_0}\right)dn + \frac{d}{ds}\,U_1 T_0\int_0^\delta \times \left(\frac{u}{U_1}\frac{T}{T_0}\right)dn = -a\left(\frac{\partial T}{\partial n}\right)_0 \qquad (30)$$

If

$$\theta_t = \int_0^\delta \frac{u}{U_1}\frac{T}{T_0}\,dn$$

Eq. (30) becomes

$$U_1T_0\theta_t\frac{1}{r_0}\frac{dr_0}{dS} + \frac{d}{dS}(U_1T_0\theta_t) = -a\left(\frac{\partial T}{\partial n}\right)_0 \quad (31)$$

Application of the Mangler transformation yields, for Eq. (31), the equivalent two-dimensional statement,

$$\frac{d}{dS}(U_1T_0\bar{\theta}_t) = -a\left(\frac{\partial T}{\partial \bar{n}}\right)_0 \quad (32)$$

Eq. (32) is satisfied on a local basis by the solutions of Eq. (28) within the range of the possible discrepancies previously noted regarding the variability of $\bar{\beta}$ as a parameter.[8] It should be noted here, however, that the range of $\bar{\beta}$ needed for the three-dimensional calculation is $0.5 < \bar{\beta} < -0.20$, whereas for the two-dimensional calculation the range of $\bar{\beta}$ needed is $1.0 < \beta < -0.20$; therefore, whatever the error involved by neglecting $d\bar{\beta}/d\bar{S}$ will be diminished in the three-dimensional case.

Heat Transfer to the Boundary Layer.—The heat rate is given as follows:†

$$q_0 = -k\left(\frac{\partial T}{\partial n}\right)_0 = -kA_2\bar{S}^\gamma g'(0)\frac{d\bar{Z}}{d\bar{n}}\left(\frac{Cr_0}{L}\right)$$

$$q_0 = -kA_2\bar{S}^\gamma g'(0)\frac{\bar{Z}_t}{\theta} = -kA_3S^\gamma g'(0)\frac{\bar{Z}_t}{\theta} \quad (33)$$

The momentum thickness is determined from Eqs. (20), (21), (22), while $g'(0)$ and $\bar{Z}_t$ are the two-dimensional functions corresponding to the applicable form parameter as determined from θ. $g'(0)$ as is shown in Eq. (7) is relatively insensitive to $\bar{\beta}$ but depends most critically upon the value of $\bar{\gamma}$.

The heat rate determined from Eq. (33) may be expressed in terms of the usual dimensionless parameters as follows:

$$\frac{(hD/k)}{\sqrt{U_\infty D/\nu}} = \frac{-g'(0)\bar{Z}_t}{(\theta/D)\sqrt{U_\infty D/\nu}} \quad (34)$$

It should be noted here that solutions for a power function variation in the wall heat rate may be computed on a similar basis to the method outlined above for the variation in the wall temperature. Briefly the method is as follows: From Eq. (33),

$$q_0 = -kA_3S^\gamma g'(0)\frac{\bar{\theta}}{\theta}\frac{\sqrt{U_1/\nu\bar{S}}}{\sqrt{2-\bar{\beta}}} \quad (35)$$

wherein, by means of the transformation, it can be shown that

$$\bar{\theta}/\theta = Cr_0/L = \sqrt{3}\sqrt{\bar{S}/S} \quad (36)$$

Inserting Eq. (36) into Eq. (35), one obtains,‡

$$q_0 = -kA_3S^\gamma g'(0)\sqrt{3}\sqrt{\frac{\bar{S}}{S}}\frac{\sqrt{U_1/\nu\bar{S}}}{\sqrt{2-\bar{\beta}}} \quad (37)$$

From Eq. (37),

$$q_0 = KS^{\gamma+[(m-1)/2]} = KS^{\gamma-[(1-\beta)/(2-\beta)]} = KS^p$$

wherein $p = \gamma - [(1-\beta)/(2-\beta)]$, the exponent for a power-function heat-rate distribution. Thus it can be seen that the problem may be presented on the basis of either heat-rate distribution or surface-temperature distribution. Knowledge of one allows a determination of the other. For instance, if the heat-rate distribution is given, the temperature distribution is defined by the exponents γ, β, or the corresponding two-dimensional values $\bar{\gamma}$, $\bar{\beta}$,

$$\gamma = p + [(1-\beta)/(2-\beta)]$$

As an example, if a constant heat rate is specified, $p = 0$ and the temperature distribution exponent becomes

$$\gamma = (1-\beta)/(2-\beta)$$

whereas if the temperature distribution is constant (isothermal wall), the heat rate must conform to values of p given by

$$p = (\beta-1)/(2-\beta)$$

Other examples involving arbitrary distributions of the heat rate or surface temperature may be easily considered.

Effect of Frictional Heating.—The assumption of superposition of solutions to account for the frictional heating effect on arbitrarily shaped bodies has been noted in reference 8 and to a great degree confirmed experimentally in reference 12. The method briefly is as follows:

For wall-temperature variation $T_0 = T_0(S)$: The heat rate is computed from solutions of Eqs. (28) and (33) (which neglect dissipation), with an effective temperature difference of

† The heat rate as calculated here does not satisfy the integral energy equation, Eq. (29), for the approximate case. It could be made to do so at the expense of not satisfying the momentum equation; however, the results of this approximation when applied to experimental data, Eq. (12), is satisfactory, which fact when considered in conjunction with the rapidity of calculation makes the approximation acceptable.

‡ Eq. (37) states the analogy between flat plates and supersonic cones (U_1 = constant along surface) as originally stated by Handzsche and Wendt[14]—i.e., that the local heat transfer on the surface of a supersonic cone was related to the local heat transfer on the surface of flat plate by the factor $\sqrt{3}$ when the distance from stagnation point to the point under consideration was the same for each. Eq. (37) gives, for the condition $S = \bar{S}$ and $\bar{\beta} = 0$, $q_{0\ \text{cone}} = \sqrt{3}\ q_{0\ \text{flat plate}}$.

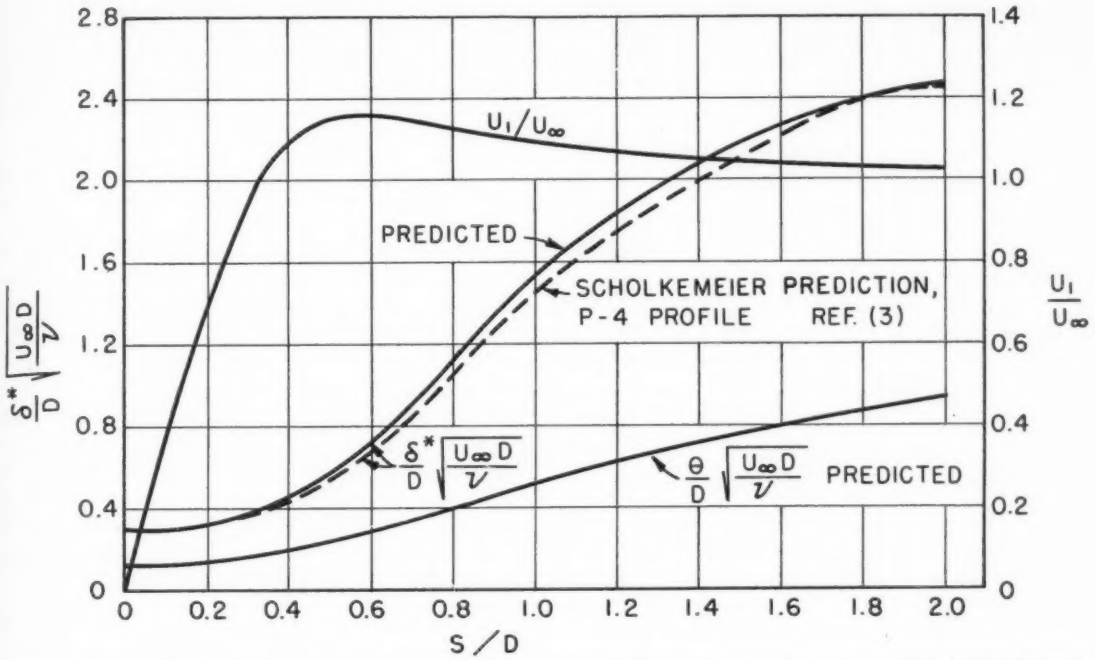

FIG. 3. Free-stream velocity distribution, momentum thickness, and displacement thickness for three-dimensional half-body.

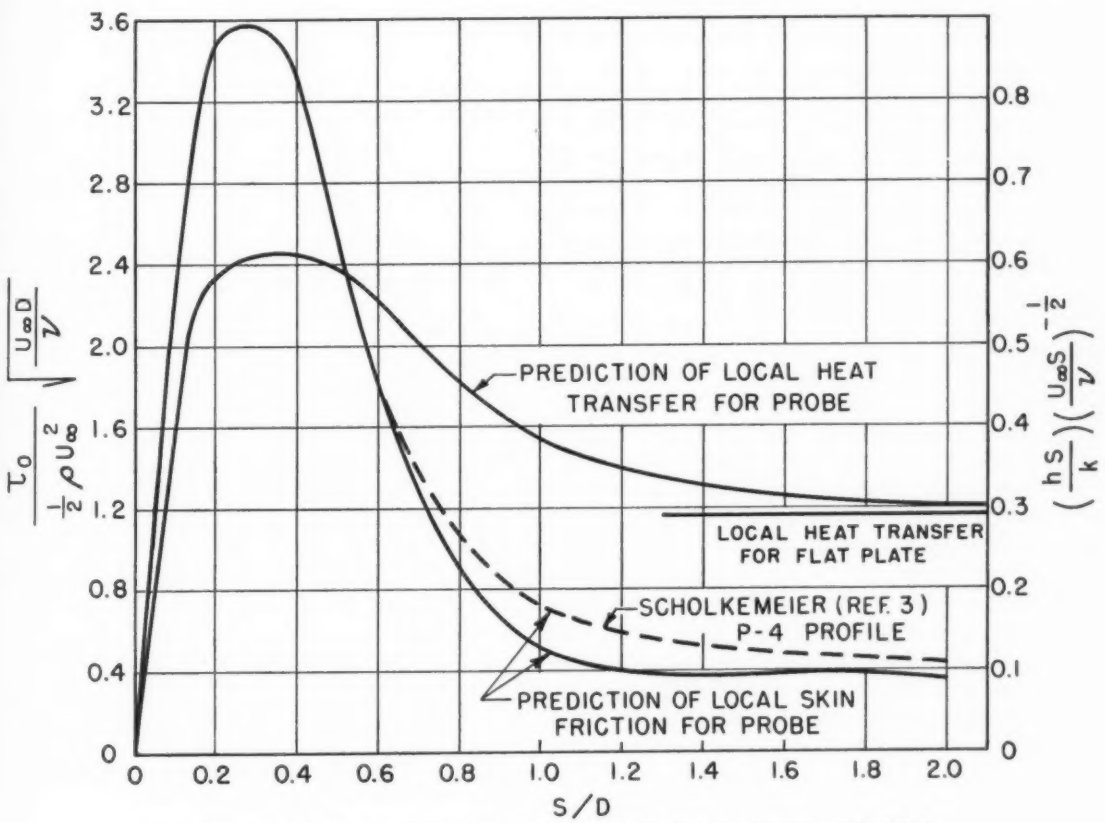
PREDICTION OF LOCAL HEAT TRANSFER FOR PROBE
LOCAL HEAT TRANSFER FOR FLAT PLATE
SCHOLKEMEIER (REF. 3) P-4 PROFILE
PREDICTION OF LOCAL SKIN FRICTION FOR PROBE
$\frac{\tau_0}{\frac{1}{2}\rho U_\infty^2}\sqrt{\frac{U_\infty D}{\nu}}$
$\left(\frac{hS}{k}\right)\left(\frac{U_\infty S}{\nu}\right)^{-\frac{1}{2}}$
S/D

FIG. 4. Predicted skin-friction and heat-transfer coefficient for three-dimensional half-body

$$T_0 - T_{aw} = T_0 - T_1 - r\frac{U_1^2}{2gJc_p} = T_0 - T_{s_1} + (1 - r)\frac{U_1^2}{2gJc_p} \quad (38)$$

wherein T_{s_1} is the free-stream stagnation temperature and r is the thermal recovery factor.[13] The thermal recovery factor may be taken as the $\sqrt{\sigma}$ for the region $(1/2) < \bar{\beta} < 0$ as a satisfactory approximation for the laminar boundary layer.

For a wall heat rate given as $q_0 = q_0(S)$: The wall-temperature distribution is calculated by the method neglecting dissipation as $T_0 = T_0(S)$, and the actual wall-temperature distribution is

$$T_{ACT} = T_0(S) + T_1 + r\frac{U_1^2}{2gJc_p} = T_0(S) + T_{s_1} - (1 - r)\frac{U_1^2}{2gJc_p} \quad (39)$$

Example

Example results of this calculation method are shown for a three-dimensional source shape or half-body. The free-stream velocity distribution for this half-body is depicted on Fig. 3 with the predicted boundary-layer momentum and displacement thicknesses. The predicted skin-friction and heat-transfer coefficients are shown on Fig. 4 in the form of the usual dimensionless parameters.

As a matter of interest, the results obtained here are compared with similar results presented by Scholkemeier[3] for the same half-body. The comparison is made on the basis of the displacement thickness and the skin-friction coefficient. It can be observed that the two results are in good accord near the stagnation point and immediately downstream therefrom; however, at a greater distance from the stagnation point, the results diverge somewhat. This divergence is the result of the selected velocity profiles in the boundary layer, Scholkemeier making use of the Pohlhausen P-4 profiles, while the present method considers the Hartree "wedge flow" profiles. Although insufficient experimental data exist to enable a selection of one velocity profile over the other, the use of the Hartree profiles is preferred by reason of the increased versatility in the solutions of the energy equation to account for a variety of surface temperature and surface heat-rate variations. Enough experimental evidence exists[12] to substantiate the results of such calculations.

A prediction of the heat-transfer coefficient for the half-body with a constant surface temperature is shown on Fig. 4 in comparison with similar results for a flat plate. It can be observed that the local values of the heat-transfer coefficients on the half-body approach the value for the flat plate in the limit wherein the velocity along the half-body becomes constant.

Summary

A calculation method has been presented which will enable a rapid prediction of the distribution of the local skin-friction and heat-transfer coefficients to be made for rotationally symmetrical bodies having arbitrarily specified free-stream velocities and surface-temperature variations for constant-property, incompressible, laminar boundary-layer flows.†

Example results utilizing the proposed method have been presented in the form of the boundary-layer momentum and displacement thicknesses, the skin-friction coefficients, and the heat-transfer coefficients for a three-dimensional half-body with constant surface temperature. These results utilizing the Hartree velocity profiles have been compared with similar results obtained by Scholkemeier utilizing the Pohlhausen P-4 velocity profiles.

References

[1] Millikan, C. B., *The Boundary Layer and Skin Friction for a Figure of Revolution*, Trans. A.S.M.E., Vol. 54, 1932.

[2] Frössling, Nils, *Verdunstung, Wärmeübergang und Geschwindigkeitsverteilung bei zweidimensionaler und rotationssymmetrischen laminarer Grenzschichtströmung*, Lunds, Univ. Arsskr., Vol. 35, 1940.

[3] Scholkemeier, F. W., *Die laminare Reibungsschicht an rotionssymmetrischen Körpern*, Dissertation; Techn. Hochschule Carola-Wilhemina, Braunsweig, 1943.

[4] Tomotika, S., *Laminar Boundary Layer on the Surface of a Sphere in a Uniform Stream*, A.R.C. R. & M. 1678, 1935.

[5] Whitehead, L. G., and Canetti, G. S., *The Laminar Boundary Layer on Solids of Revolution*, Philosophical Magazine, Vol. 41, October, 1950.

[6] Hartree, D. R., *On an Equation Occurring in Falkner and Skan's Approximate Treatment of the Equation of the Boundary Layer*, Proc. Camb. Phil. Soc., Vol. 33, pp. 223–239, 1937.

[7] Levy, S., *Heat Transfer to Constant-Property Laminar Boundary-Layer Flows with Power-Function Free-Stream Velocity and Wall-Temperature Variation*, Journal of the Aeronautical Sciences, Vol. 19, No. 5, p. 341, May, 1952.

[8] Seban, R. A., *Calculation Method for Two Dimensional Laminar Boundary Layers with Arbitrary Free Stream Velocity Variation and Arbitrary Wall Temperature Variation*, University of California, Institute of Engineering Research Report 2–12, May, 1950.

[9] Mangler, W., *Zustammenhang zwischen ebenen und rotationssymmetrischen Grenzschichten in kompressiblen Flüssigkeiten*, ZAMM, Vol. 28, 1948.

[10] Eckert, E., *Die Berechnung des Wärmeübergangs in der laminaren Grenzchicht umströmter Körper*, VDI-Forschungsheft 416 September/October, 1942. (Translation, R. Kay, University of California, Berkeley.)

[11] Homann, F., *Der Einfluss grosser Zähigkeit bei der Strömung um den Zylinder und um die Kugel*, ZAMM, Vol. 16, No. 3, 1936,

† The calculation method for the axisymmetrical, three-dimensional, laminar boundary layer given here may be reduced to the form applicable to the two-dimensional case if r_0 is considered to be no function of S and if the free-stream velocity U_1 is considered in terms of the distance $\bar{S}$. If these changes are made, the resulting formulations for the boundary-layer characteristic dimensions, the skin friction, and the heat transfer are shown to be identical with the results presented by Seban.[8]

(*Concluded on page 330*)

Statistical Aspects of Dynamic Loads

Y. C. FUNG†

California Institute of Technology

ABSTRACT

In many dynamic stress problems, the knowledge of the physical phenomena is not precise enough to justify exact predictions with respect to the results of each individual observation. On the one hand, the loading is never exactly known, and on the other, the physical system may be so complicated that detailed calculations for the prediction of dynamic responses are difficult and the numerical results are often uncertain. In such cases the physical data can be regarded as a set of statistical data of random processes. Logical statements of the forcing functions are therefore statistical. The chief object of an analysis is then to draw valid inferences about the statistical statements of the responses.

In this paper the statistical theory is illustrated by the gust- and landing-load problems. A method of determining the mean intensity of the dynamic response is presented. Through a study of the distribution of the extreme values, an "envelope" representing the most probable largest stress (or other response quantities of interest) at any point in the structure can be found. Such an envelope, if used as a basis for specifying the design stresses, can be regarded as one that yields, in the long run, a uniform factor of safety over the entire structure with respect to a random forcing function. The probability of exceeding a given maximum stress being known, the life expectancy of an aircraft can be determined as a function of the specified load intensity and vice versa.

SYMBOLS

b = semichord of airfoil
c = wing chord
U = flight speed of airplane
ω = circular frequency, rad. per sec.
w = gust speed, component of turbulent velocity normal to the flight path
z = vertical translation of airplane
S = wing area (sq.ft.)
L = scale of turbulence
$k = \omega b/U$ = reduced frequency based on wing semichord
$\xi = \omega L/U$ = reduced frequency based on scale of turbulence
$s = b/L$, ratio of wing semichord to the scale of turbulence
l = wing span

(I) INTRODUCTION

ALTHOUGH AIRCRAFT DESIGN is an art well established, it is still useful to re-examine periodically the basic point of view from which the design criteria are formulated. This paper is concerned with one phase of aircraft design—the dynamic loads as they arise from flying through gusty air, landing impacts, take-off over rough surfaces, buffeting, etc. In particular, the statistical aspects of these dynamic loading problems are considered. It will be shown that, in certain occasions, it is logical to recognize the statistical nature of these problems and is perhaps wise to deviate somewhat from the current design philosophy.

Statistical methods have been used extensively in theoretical physics, electrical engineering, and the theory of turbulence.‡ Recently, their application to buffeting has been pointed out by Liepmann.[1] The present paper extends Liepmann's ideas to some other problems.

(II) RANDOM ELEMENTS IN DYNAMIC STRESS PROBLEMS

In a classic approach to the dynamic stress problem, the response to a specific forcing function is sought. Whenever it is permissible to linearize the governing equations, the mathematical principles for treating such problems are well known, although in aeroelasticity it usually leads to a set of complicated equations.

For example, in the gust-load problem, a sharp-edged gust is often considered. Under a number of simplifying assumptions, it is possible to derive a "sharp-edged gust formula" giving the normal acceleration experienced by an airplane in encountering such a gust. The simplifying assumptions are rarely fulfilled. Yet the formula is useful, for, as Rhode pointed out,[6] if the gust speed is based upon an "*effective*" value obtained by acceleration measurements made on airplanes over a long period of time and if the data are reduced according to the sharp-edged gust formula, the result will correctly represent the actual load factor. The effective gust speed will be different, however, for each particular type of airplane, because the effects of the simplifying assumptions are different for different airplane size, flexibility, flight speed, and type of construction. This approach has been found satisfactory until recently, when new models with high structural flexibility appear so frequently that the measurements of the effective gust speeds cannot keep pace with the designs.

A theoretically more satisfactory procedure is to measure directly the atmospheric disturbances (gusts) and then design the structures accordingly. It is generally thought that a few typical types of gust profile can be defined which will produce the critical dynamic stresses in the structures. The intensity of these typical gusts can then be determined statistically by flight measurements. Thus the gust-loading problem is reduced to a well-defined problem of finding the

Presented at the Structures Session, Annual Summer Meeting, I.A.S., Los Angeles, July 16–18, 1952.

† Assistant Professor of Aeronautics.

‡ See reference 1 for a brief historical review and references to fundamental works. See also references 2–5.

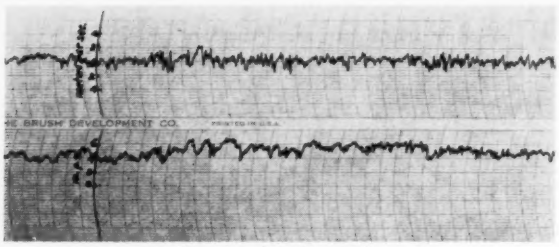

FIG. 1. A gust record.

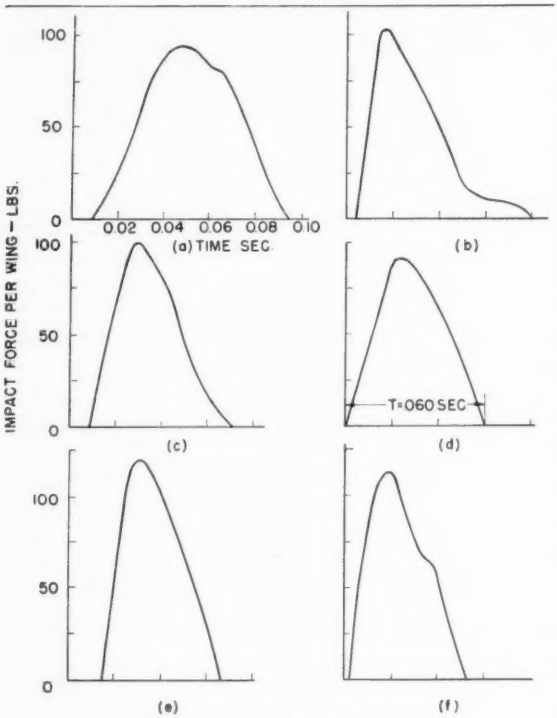

FIG. 2. Landing impact curves.

response of an elastic airplane to some specified gust profiles.[7]

In applying such an analysis to the practical design of an aircraft, one must know how to specify the gust profile. A deeper consideration will lead to the question whether such a formulation is sensible in physical reality—that is, whether such a profile can ever be determined by experimental measurements.

Fig. 1 shows a record of gusts measured by an anemometer 146 m. above the ground (suspended in space by a balloon that is tied to the ground by three wires).† It is similar in nature to the anemometer records of wind-tunnel turbulences. From such a figure it is indeed impossible to say what kind of an isolated gust profile can characterize the real picture. Although there is a certain regularity in each record, it is impossible to predict the exact shape, height, and duration of each peak.

A similar question arises in other dynamic stress problems. In practice, most dynamic stress problems are characterized by the unpredictable nature of the forcing functions. The exact form of the forcing function is always uncertain to some extent because of the large number of variables entering the problem. Thus, when a few important ones are considered in a theory, other variables appear as external disturbing influences. The random nature of the atmospheric turbulence as shown in the records of Fig. 1 is due to the influences of the viscosity, pressure, density, temperature, humidity, and velocity distributions, varying in such a complicated manner that mechanistic predictions based on the hydrodynamic equations are practically impossible.

Consider the landing impact as another example. In addition to the landing speed, drop height, and the airplane attitude as ordinarily considered in the landing analysis, there are a number of factors beyond the control of an airplane designer, such as the softness of the ground, the tire pressure, the change of temperature and its effect on the viscosity of the fluid in the oleo strut and the air cushion, the surface friction, the bumpiness of the ground, the pilot technique, etc. The list of possible factors is almost unlimited, and it is of little interest to compile such a list because it would not be useful. In the landing analysis, the assumption usually made is that it is possible to introduce *average* values of these factors and that the practical variations of these factors from their average values introduce only small errors. When the secondary stresses due to the variations of the neglected variables are not negligible, we are left with two ways to account for them: (1) by introducing a sufficiently large factor of safety (or a higher load factor), or (2) by studying the variations and introducing some allowances based on statistical inferences. The second alternative is, of course, more attractive if it can be accomplished without causing too much difficulty in the analysis.

In Fig. 2 are shown the experimental results of Ramberg and McPherson of the National Bureau of Standards on the landing impact force.[9] In their tests a model single-spar wing having only flexural degrees of freedom was fitted with an oleo strut. The model was dropped from a carefully controlled height. The landing conditions were varied by changing the softness of the rubber on which the model was dropped, the initial spring loading, and the opening of pressure relief ports in the damper. The transient bending stresses were measured both at the wing root and at an outboard station. The test results are summarized in Table 1 and Fig. 2. It is seen that considerable variations exist in the maximum impact force, bending moment, acceleration at the fuselage, and the shape of the impact force curves. These variations will cause variations

† This figure is obtained by MacCready.[8] The upper curve is the vertical component of the gusts; the lower curve is the horizontal component.

TABLE 1

Maximum Values of the Applied Impact Force (Sum of Spring and Damper Forces), Bending Moments at 1.5- and 14.5-In. Stations, and Accelerations at Root (from Reference 9)

Record	Maximum Impact Force per Half-Wing (Lbs.)	Bending Moment $M_{b,1.5}$ (Lbs.-In.)	Bending Moment $M_{b,14.5}$ (Lbs.-In.)	Maximum Acceleration at Root (In./Sec.²)	Maximum Acceleration at Root g	Impact Duration (Sec.)
a	95	750	370	1,580	4.1	0.086
b	105	1,130	650	1,930	5.0	0.076
c	100	1,060	550	1,580	4.1	0.062
d	92	970	540	1,510	3.9	0.060
e	120	1,370	820	2,220	5.8	0.052
f	113	1,170	600	1,620	4.2	0.050

in the dynamic stresses in the airplane, especially if the airplane structure is flexible. Hence, if a typical impact force-time curve is chosen among all the curves of Fig. 2, it is necessary to increase the amplitude of this curve by a factor (of safety) of considerable magnitude in order to overshadow the maximum stresses that may be induced by other impact force-time curves. Under such circumstances it seems desirable to make a more rational approach so that a more realistic design specification may be obtained. It is from considerations of this nature that a statistical theory is originated.

Let the curve shown on the left-hand side of Fig. 3 be taken as a typical average curve.† The individual impact curves of Fig. 2 can be represented by superpositions as shown in Fig. 3. An essential feature of the curves on the right-hand side of this figure is their irregularity. Remembering that such irregularities are caused by a large number of factors, it is not surprising that no definite rule can be stated which will predict their possible form.

If the uncertainty of predicting the forcing function is recognized, the problem becomes statistical. One then tries to state the main features of the response, as well as those of the forcing function, in terms of statistical averages and probability distributions.

(III) The Probability Distribution

It was stated in the last section that in some dynamic stress problems our knowledge of the physical phenomena is not precise enough to justify exact predications with respect to the results of each individual observation. On the one hand, the loading is never exactly known, and on the other, the physical system is so complicated that detail calculations for the prediction of dynamic responses are difficult and the numerical results are often uncertain. In such cases, we shall regard the physical data as a set of *statistical data* of *random variables*. The chief object of an analysis is then to draw valid inferences from the data.

† This curve is the mean of all the curves of Fig. 2—i.e., the mean value of the impact force at each instant of time following the contact of the landing gear with the ground.

The statistical nature of a random variable is characterized by its *distribution function*. For a random variable y, the distribution function $F(x)$ is the probability of the event $y \leq x$:

$$F(x) = P(y \leq x) \tag{1}$$

Obviously, $F(x)$ is a nondecreasing function, and

$$F(-\infty) = 0, \quad F(+\infty) = 1 \tag{2}$$

If the derivative $F'(x) = f(x)$ exists, as will be assumed hereafter, $f(x)$ is called the *probability density* or the *frequency function* of the random variable. A probability density is nonnegative and has the integral 1 over $(-\infty, \infty)$, since, by definition,

$$P(a < y \leq b) = F(b) - F(a) \tag{3}$$

In the limit it is seen that the probability that the

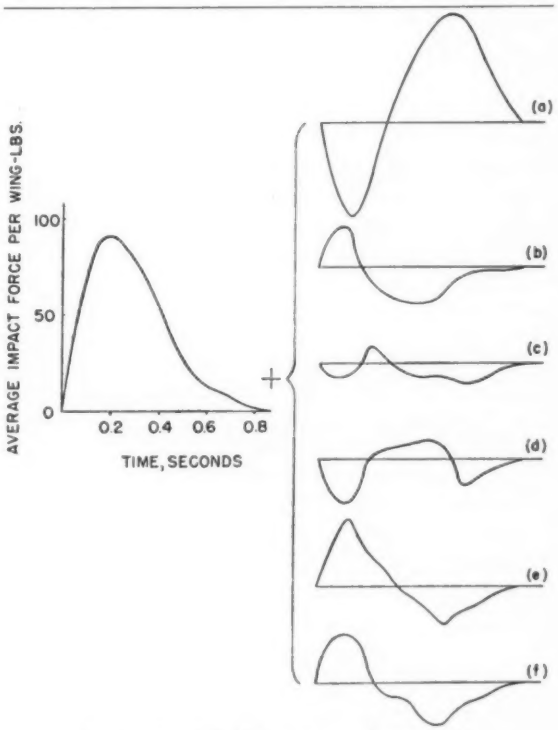

FIG. 3. Landing impact curves, decomposed.

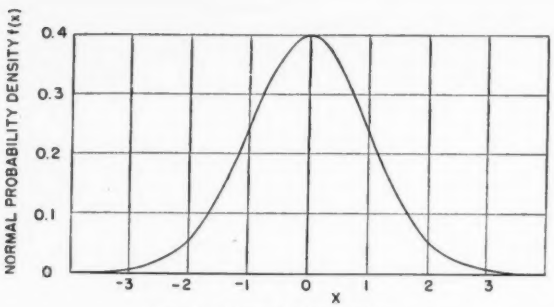

FIG. 4. Normal distribution.

variable y takes a value belonging to the interval

$$x < y < x + \Delta x$$

is for small Δx asymptotically equal to $f(x)\Delta x$, which is written in the usual differential notation

$$P(x < y < x + dx) = f(x)\,dx \tag{4}$$

Moments

The integrals

$$\alpha_\nu = \int_{-\infty}^{\infty} x^\nu f(x)\,dx, \quad (\nu = 1, 2, 3, \ldots) \tag{5}$$

if absolutely convergent, are called the first, second, third, . . . , moment of the distribution function. The first moment, called the *mean*, is often denoted by the letter m:

$$m = \int_{-\infty}^{\infty} xf(x)\,dx \tag{6}$$

The integrals

$$\mu_\nu = \int_{-\infty}^{\infty} (x - m)^\nu f(x)\,dx \tag{7}$$

are called the *central moments*.

The *mean* m is a kind of measure of the *location* of the variable y. It gives a *typical value* of the variable, which may be conceived as a *central point* of the distribution.

The second central moment μ_2 gives an idea of how widely the values of the variable are spread on either side of the mean. This is called the *variance* of the variable. We have, of course, always $\mu_2 \geq 0$; $\mu_2 = 0$ if, and only if, the variable assumes only one value. Generally, the smaller the variance, the greater the concentration, and conversely.

In order to obtain a quantity of the first dimension in units of the variable, it is often preferable to use the nonnegative square root of μ_2, which is called the *standard deviation* of the variable and is denoted by σ,

$$\sigma^2 = \mu_2 = \alpha_2 - m^2 \tag{8}$$

Example: The Normal Distribution

The *normal distribution function* is defined by the relation

$$F(x) = \frac{1}{\sqrt{2\pi}} \int_{-\infty}^{x} e^{-t^2/2}\,dt \tag{9}$$

The corresponding *normal probability density* is

$$f(x) = (1/\sqrt{2\pi})\, e^{-x^2/2} \tag{10}$$

Diagrams of the function $f(x)$ is given in Fig. 4. The mean value of the distribution is 0, and the standard deviation is 1.

A random variable ξ is said to be *normally distributed with the parameters m and σ*—or in brief, *normal* (m, σ)—if the distribution function of ξ is $F[(x - m)/\sigma]$, where F is given by Eq. (11) and $\sigma > 0$ and m are the standard deviation and the mean, respectively. The probability density is then

$$f(x) = (1/\sigma\sqrt{2\pi})\, e^{-(x-m)^2/2\sigma^2} \tag{11}$$

(IV) Statistical Averages†

The concept of *time averages* is well known. Thus, the mean and the mean square of a function of time $u(t)$ over a time interval $2T$ are

$$\bar{u} = \frac{1}{2T} \int_{t_0 - T}^{t_0 + T} u(t)\,dt \tag{12}$$

$$\overline{(u - \bar{u})^2} = \frac{1}{2T} \int_{t_0 - T}^{t_0 + T} u^2(t)\,dt - \bar{u}^2 \tag{13}$$

If $\bar{u}$ and $\overline{(u - \bar{u})^2}$ are dependent neither on t_0 nor on T, provided that T is sufficiently large, then $u(t)$ is called a *stationary random process*.

The concept of *ensemble average* is important. A set of observations forms an *ensemble* of events. In the example of landing impact measurements such as those represented in Fig. 2, each impact force-time curve is a member in an ensemble of such curves.

Imagine that a large number of experiments be made simultaneously on identical models under similar conditions. Let the records be numbered and denoted by $u_1(t), u_2(t), \ldots, u_N(t)$. If the total number of records is N, the following averages may be formed:

$$\bar{u} = (u_1 + u_2 + \ldots + u_N)/N \tag{14}$$

$$\overline{(u - \bar{u})^2} = \sum_{i=1}^{N} (u_i - \bar{u})^2/N \tag{15}$$

Assume that $\bar{u}$ and $\overline{(u - \bar{u})^2}$ tend to definite limits m and σ^2, respectively, as $N \to \infty$. Then $\bar{u}$, $\overline{(u - m)^2}$, or m, σ^2 are ensemble averages of the random process $u(t)$.

If the ensemble averages of $u(t)$ are independent of time, then $u(t)$ is said to be *stationary*. For a stationary random process, the ensemble averages are identical with the time averages.

There are many flows of interest that are approximately homogeneous and stationary when the time

† See references 1–5 for greater detail and more precise discussions.

and distance scales are properly chosen. Such is the case of atmospheric turbulence within a suitable expanse of time and space.

It is natural to expect that the behavior of a dynamic system depends on the manner in which the excitation changes in successive instants of time. Simply knowing the mean and intensity of the excitation is not sufficient to establish the corresponding mean and intensity of the response. Additional information expressing the sequential time characteristics of the excitation is necessary. One of the measures describing the sequential behavior has its origin in the harmonic analysis and is called the *power spectrum*. Alternatively, a more easily defined quantity called the *correlation function* may be used.

The Power Spectrum

Let us consider a stationary random process $u(t)$ with mean $m = 0$ and define the mean square of $f(t)$ over an interval $2T$ as in Eq. (13).

Let $u(t)$ be truncated so that it becomes zero outside the interval $(-T, T)$. Let the truncated function be written as $u_T(t)$. The Fourier integral of $u_T(t)$ exists, and we may write

$$u_T(t) = \frac{1}{\sqrt{2\pi}} \int_{-\infty}^{\infty} \mathfrak{F}(\omega) e^{i\omega t}\, d\omega \tag{16}$$

$$\mathfrak{F}(\omega) = \frac{1}{\sqrt{2\pi}} \int_{-T}^{T} u_T(t)\, e^{-i\omega t}\, dt \tag{17}$$

It is well known (Parseval theorem) that

$$\int_{-\infty}^{\infty} u_T^2(t)\, dt = \int_{-T}^{T} u_T^2(t)\, dt = \int_{-\infty}^{\infty} |\mathfrak{F}(\omega)|^2\, d\omega \tag{18}$$

Hence,

$$\overline{u^2(t)} = \frac{1}{2T} \int_{-\infty}^{\infty} |\mathfrak{F}(\omega)|^2\, d\omega = \int_0^{\infty} \frac{|\mathfrak{F}(\omega)|^2}{T}\, d\omega \tag{19}$$

For a stationary random process $\overline{u^2(t)}$ tends to a constant, so $|\mathfrak{F}(\omega)|^2/T$ tends to a definite limit. Let

$$p(\omega) = \lim_{T \to \infty} \frac{|\mathfrak{F}(\omega)|^2}{T} \tag{20}$$

then

$$\overline{u^2(t)} = \int_0^{\infty} p(\omega)\, d\omega \tag{21}$$

Following Taylor, $p(\omega)$ is called the *power spectrum* of $u(t)$. The element $p(\omega)d\omega$ gives the contribution to $\overline{u^2(t)}$ from simple harmonic elements with frequencies ranging from ω to $\omega + d\omega$. The integral

$$\int_0^{\omega} p(\omega)\, d\omega$$

represents the contribution to $u^2(t)$ from frequencies less than ω.

Correlation Functions

Consider again a stationary random process $u(t)$. The average value

$$\psi(\tau) = \overline{u(t)u(t+\tau)} = \frac{1}{2T} \int_{-T}^{T} u(t)\, u(t+\tau)\, dt \tag{22}$$

is well defined, provided that T is sufficiently large. $\psi(\tau)$ is a function of τ and is called a *correlation function*.

The following properties of the correlation function can be easily seen:

$$\psi(0) = \overline{u^2(t)} \tag{23}$$

$$\lim_{\tau \to \infty} \psi(\tau) = 0 \quad (\text{if } \bar{u} = 0) \tag{24}$$

$$\psi(\tau) = \psi(-\tau) \tag{25}$$

Moreover, the reciprocal relations between the power spectrum and the correlation function can be established[1]

$$\psi(\tau) = \int_0^{\infty} p(\omega) \cos \omega\tau\, d\omega \tag{26}$$

$$p(\omega) = \frac{2}{\pi} \int_0^{\infty} \psi(\tau) \cos \omega\tau\, d\omega \tag{27}$$

(V) The Power Spectra of the Excitation and the Response

Suppose that the response y and the excitation f are connected by the differential equation

$$\frac{d^2y}{dt^2} + \beta \frac{dy}{dt} + \omega_0^2 y = f(t) \tag{28}$$

If $f(t)$ is a harmonic function

$$f(t) = Ae^{i\omega t} \tag{29}$$

where A is real, the solution $y(t)$ which represents a steady motion is

$$y(t) = Ae^{i\omega t}/Z(i\omega) \tag{30}$$

where

$$Z(i\omega) = \omega_0^2 - \omega^2 + i\beta\omega \tag{31}$$

is called the *impedance* of the system represented by Eq. (28). Generalizing this result to an arbitrary forcing function $f(t)$ represented by a Fourier integral

$$f(t) = \frac{1}{\sqrt{2\pi}} \int_{-\infty}^{\infty} A(\omega)\, e^{i\omega t}\, d\omega \tag{32}$$

we have the response

$$y(t) = \frac{1}{\sqrt{2\pi}} \int_{-\infty}^{\infty} \frac{A(\omega)}{Z(i\omega)}\, e^{i\omega t}\, d\omega \tag{33}$$

which is valid if the integral converges.

If $f(t)$ is a stationary random function, it does not tend to zero as $t \to \infty$ and its Fourier Transform does not exist. But a truncated function can be defined so

that Eqs. (32) and (33) hold within a large time interval $(-T, T)$. The following relation can be proved:

$$\overline{y^2(t)} = \int_0^\infty \frac{p(\omega)}{|Z(i\omega)|^2}\, d\omega \tag{34}$$

where $p(\omega)$ is the power spectrum of $f(t)$. The phase relationship between the excitation and the response, represented by the argument of the complex number $Z(i\omega)$, is completely obliterated in the power spectra relations.

The preceding conclusion holds for a much wider class of dynamic systems than that represented by Eq. (28). It holds for higher order linear differential equations, linear integral equations, or linear integral-differential equations under mild restrictions.

(VI) The Response of a Rigid Airplane to Atmospheric Turbulences

As an illustration of the statistical approach, let us consider the motion of an airplane in response to atmospheric turbulences. For simplicity, let us introduce the assumptions that the airplane can be regarded as rigid, having uniform forward speed U and responding only to gusts normal to the flight path, and that only the vertical translation degree of freedom is permitted.

The atmospheric turbulence (gusts) may depend on the condition of flow and the thermal stability of the air. Therefore the statement of the characteristics of turbulences must be based on measurements relevant to specific meteorological conditions.† However, Clementson[13] has shown that the correlation functions (and the power specra) of atmospheric turbulence in different conditions (unstable air mass, water-land discontinuities, thunderstorms, and mountainous terrain) have remarkable similarity to each other.

The following analysis will not refer to any particular weather condition but to the isotropic turbulence as measured in wind tunnels. Obviously, however, the analysis can be extended to other turbulence fields.

It is assumed, therefore, that the gust field has a power spectrum given by[1]

$$p(\omega) = \overline{w^2}\,\frac{L}{\pi U}\,\frac{1 + 3\xi^2}{(1 + \xi^2)^2}, \quad \xi = \frac{\omega L}{U} \tag{35}$$

where $\overline{w^2}$ is the mean square (intensity squared) of the gust, L is the scale of turbulence, and U is the speed of the general flow.

The scale of turbulence is defined by the area under the correlation curve,

$$L = \int_0^\infty R(r)\, dr \tag{36}$$

† At the present time no general conclusion has been reached in relating the distribution function of the gust velocity components, the power spectra, and the correlation functions to the velocity gradient, lapse rate, and other meteorological factors. For available information, see, for example, references 10–12.

where

$$R(r) = \frac{\overline{w(x, t)\, w(x + r, t)}}{\overline{w^2}} \tag{37}$$

Let us consider a strip of unit length of an airfoil of infinite span in a two-dimensional flow. The mean-flow velocity is U parallel to the mean position of the airfoil chord. The thickness and the amplitude of the displacement of the airfoil are assumed small in comparison with the chord. To the mean velocity of flow U is superposed a small turbulent motion that has only one component of velocity w in a direction normal to the chord. The turbulent motion in the fluid is transported with the mean flow, so that w is given by a function

$$w = w[t - (x/U)]$$

The lift of the airfoil is partly induced by the disturbance w and partly by the motion of the airfoil itself. Within the framework of the linearized theory, the lift induced by these two parts are superposable. The equation of motion of the airfoil (having the translational degree of freedom only) can be written as

$$m\ddot{z} + L(z) = -L(w) \tag{38}$$

where $L(w)$ indicates the lift corresponding to $w(t)$ and $L(z)$ that for the motion of the airfoil. It is clear that the problem of the response of an airfoil to a turbulent flow can be separated into two problems: (1) the determination of the lift produced by the turbulent flow on an airfoil which is stationary relative to the mean-flow velocity, and (2) the determination of the disturbed motion of the airfoil to an exciting force, with the flow regarded as uniform and without turbulence.

Let $p_g(\omega)$ and $p_l(\omega)$ denote the power spectra of the turbulent flow and the lift, and let $\chi_a(\omega)$, $\chi_z(\omega)$ denote the square of the absolute values of the frequency response (admittance) of the lift and the airplane acceleration, respectively; then

$$p_l(\omega) = \chi_a(\omega)\, p_g(\omega) \tag{39}$$

$$p_{\ddot{z}}(\omega) = \chi_z(\omega)\chi_a(\omega)\, p_g(\omega) \tag{40}$$

Hence the problem is really the determination of the quantities $\chi_a(\omega)$ and $\chi_z(\omega)$.

Let the vertical gust velocity be

$$w(x, t) = w_0\, e^{i\omega[t - (x/U)]} \tag{41}$$

The expression of lift is given by Sears[14]

$$L = 2\pi\rho b U\, w_0\, e^{i\omega t}\, \varphi(k) \tag{42}$$

where k is the reduced frequency

$$k = \omega b/U \tag{43}$$

and $\varphi(k)$ is a complex function

$$\varphi(k) = [J_0(k) - iJ_1(k)]\, C(k) + i\, J_1(k) \tag{44}$$

J_0, J_1 are the Bessel functions of the first kind and

$C(k)$ is the Theodorsen function. The resultant lift acts through the one-quarter-chord point from the leading edge. The factor $2\pi\rho bU\ \varphi(k)$ represents the frequency response (admittance) of the lift.

Liepmann has shown[1] that a simple approximation of $|\varphi(k)|^2$ is

$$|\varphi(k)|^2 = 1/(1 + 2\pi k) \tag{45}$$

Admittance of the Airplane

The equation of motion of a two-dimensional airfoil subject to a sinusoidal force can be reduced into the following form:

$$\left\{-m\frac{\bar{U}^2}{b^2}k^2 + \frac{\pi\rho U^2}{2}\frac{S}{b}[2C(k)\ ik - k^2]\right\} z_0 = P_0 \tag{46}$$

where $P = P_0 e^{i\omega t}$ is the exciting force and $z = z_0 e^{i\omega t}$ is the wing displacement. The quantity in the braces $\{\ \}$ is the complex impedance from $F(t)$ to $z(t)$. Its inverse multiplied by $-\omega^2 = -(Uk/b)^2$ gives the admittance of the acceleration $\ddot{z}$. Let

$$\kappa = 2m/\pi\rho Sb \tag{47}$$

be the *density ratio* of the airplane; then the admittance can be written as

$$\frac{\ddot{z}}{P} = \frac{2}{\pi\rho Sb}\frac{k}{(1+\kappa)k + 2G - 2iF} \tag{48}$$

The Gust Response

The intensity of the acceleration $\sqrt{\overline{\ddot{z}^2}}$ can now be computed. Assume the power spectrum of the gust to be given by Eq. (35). Neglecting the lift on the tail surfaces, and using strip theory, the lift on the wing due to a gust can be obtained by multiplying Eq. (42) by the wing span. Then in the notation of Eq. (40), we have

$$\chi_a = (\pi\rho SU)^2|\varphi(k)|^2 \tag{49}$$

$$\chi_s = \left|\frac{\ddot{z}}{P}\right|^2 = \left(\frac{2}{\pi\rho Sb}\right)^2 \times \frac{k^2}{4(F^2+G^2) + 4Gk(1+\kappa) + k^2(1+\kappa)^2} \tag{50}$$

The mean square of the acceleration is, therefore,

$$\overline{\ddot{z}^2} = \int_0^\infty \chi_a(k)\chi_s(k)p_g(\omega)d\omega, \qquad \left(k = \frac{\omega b}{U}\right) \tag{51}$$

The exact integration of the above expression is difficult because of the complicated manner in which the Bessel functions are involved. To obtain an approximate solution, the approximation for $|\varphi(k)|^2$ given by Eq. (45) may be used. As to χ_s, we note that, in the full range $(0, \infty)$, G^2 is much less than F^2. Hence we may neglect terms involving G^2 in Eq. (16). Moreover, since

$$|F| \leq 1, \qquad |G| < 0.2$$

while in practice, κ varies from a number of order 40 for trainers and transports to 150 for high-speed fighters, a fair approximation of Eq. (16) is simply

$$\chi_s = \left(\frac{2}{\pi\rho Sb}\right)^2 \frac{k^2}{4 + k^2(1+\kappa)^2} \tag{52}$$

Using the approximations, Eqs. (45) and (52) and introducing the notations

$$s = b/L \tag{53}$$

$$a = 2/s(1+\kappa) \tag{54}$$

where s is the ratio of the wing semichord to the turbulence scale, we obtain

$$\overline{\ddot{z}^2} = \overline{w^2}\frac{4U^2}{\pi b^2(1+\kappa)^2}\int_0^\infty \frac{\xi^2}{a^2+\xi^2}\frac{1}{1+2\pi s\xi}\frac{1+3\xi^2}{(1+\xi^2)^2}\,d\xi \tag{55}$$

By partial fractions,

$$\frac{\xi^2}{a^2+\xi^2}\frac{1+3\xi^2}{(1+\xi^2)^2} = \frac{A}{a^2+\xi^2} + \frac{B}{1+\xi^2} + \frac{C}{(1+\xi^2)^2}$$

where

$$A = \frac{a^2(3a^2-1)}{(a^2-1)^2}, \qquad B = -\frac{5a^2-3}{(a^2-1)^2}, \qquad C = \frac{2}{a^2-1} \tag{56}$$

Furthermore,

$$I_1(a, s) = \int_0^\infty \frac{d\xi}{(1+2\pi s\xi)(a^2+\xi^2)} = \frac{2\pi s}{1+4\pi^2 s^2 a^2}\left(\log 2\pi s + \log a + \frac{1}{4as}\right) \tag{57}$$

Differentiating both sides with respect to a and then dividing through by $(-2a)$, we obtain

$$I_2(a, s) = \int_0^\infty \frac{d\xi}{(1 + 2\pi s\xi)(a^2 + \xi^2)^2} = \frac{8\pi^3 s^3}{(1 + 4\pi^2 s^2 a^2)^2}\left(\log 2\pi s + \log a + \frac{1}{4as}\right) + \frac{\pi s}{(1 + 4\pi^2 s^2 a^2)a^2}\left(\frac{1}{4sa} - 1\right) \quad (58)$$

Hence, from Eq. (55),

$$\overline{\ddot{z}^2} = \overline{w^2}\,[4U^2/\pi b^2(1 + \kappa)^2]\, I\,(a, s) \quad (59)$$

where $I(a, s) = AI_1(a, s) + BI_1(1, s) + CI_2(1, s)$ (60)

$I_1(1, s), I_2(1, s)$ are given, respectively, by Eqs. (57) and (58), with the parameter a replaced by 1; and A, B, and C are given by Eq. (56). The variation of $I(a, s)$ is shown in Fig. 5. Note that $\overline{\ddot{z}^2} \to 0$ both when $s \to 0$ and when $s \to \infty$. Hence, as the scale of turbulence becomes either negligibly small or infinitely large in comparison with the wing chord, the intensity of the acceleration experienced by the airplane will tend to zero. This can be expected, because when the wing chord is extremely large in comparison with the turbulence scale, the "gusts" are smoothed out by canceling each other over the wing. On the other hand, when the chord length is extremely small in comparison with the scale of turbulence, the airfoil behaves quasi-stationary. Since a rigid airplane having only the translation degree of freedom will experience no acceleration in a stationary flow, the limiting case $\overline{\ddot{z}^2} \to 0$ as $s \to 0$ is to be expected.

The factor $I(a, s)$ shows clearly the effect of the size of the airplane relative to the scale of turbulence. The effect of finite span is neglected. Liepmann[1] has shown that essentially the finite span effect is to multiply the right-hand side of Eq. (59) by a factor

$$(L/l)\,[1 - e^{-l/L}] \quad (61)$$

where l is the length of the wing span.

(VII) Housner's "Stress Envelope"

In structural designs, it is often required to find the maximum stresses expected at any point in a structure. In this connection it is interesting to notice an approach used by Housner[15] in the study of strong-motion earthquakes, which is a nonstationary random process.

Consider the following specific problem: A beam is clamped at one end and free at the other. The clamping wall is subjected to a variable acceleration that is a random function of time. Find the response of the beam.

If the variable acceleration of the wall is $a(t)$ and if $a(t) = 0$ for $t \leq 0$, it is not difficult to derive the beam displacement $u(x, t)$,

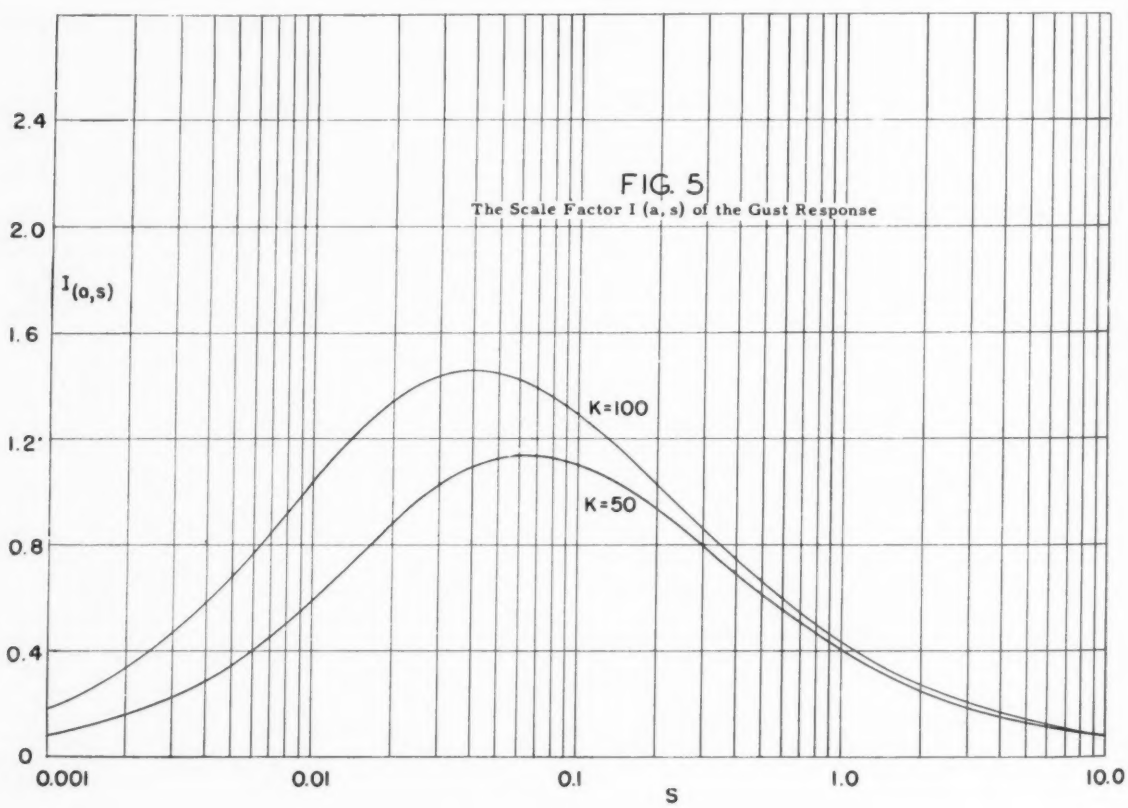

FIG. 5
The Scale Factor I (a, s) of the Gust Response

$$u(x, t) = \sum_i \frac{K_i}{\omega_i} f_i(x) \int_0^t a(\tau) \sin \omega_i(t - \tau)\, d\tau \tag{62}$$

where

$f_i(x)$ = the ith normal mode of the beam
ω_i = the circular frequency of vibration of the ith mode
K_i = $\int f_i\, d\rho / \int f_i^2\, d\rho$, $d\rho$ being a mass element of the beam, and the integrals are taken over the entire mass

This can be written as

$$\left.\begin{aligned} u &= \sum_i \frac{K_i}{\omega_i} f_i(x) \left[\sin \omega_i t \int_0^t a(\tau) \cos \omega_i \tau\, d\tau - \cos \omega_i t \int_0^t a(\tau) \sin \omega_i \tau\, d\tau\right] \\ &= \sum_i \frac{K_i}{\omega_i} f_i(x) \left\{\left[\int_0^t a(\tau) \cos \omega_i \tau\, d\tau\right]^2 + \left[\int_0^t a(\tau) \sin \omega_i \tau\, d\tau\right]^2\right\}^{1/2} \sin \omega_i (t - \alpha_i) \end{aligned}\right\} \tag{63}$$

where α_i is a phase factor that depends on the values of the integrals. Introducing the notation

$$R_i = \left[\left(\int_0^t a(\tau) \cos \omega_i \tau\, d\tau\right)^2 + \left(\int_0^t a(\tau) \sin \omega_i \tau\, d\tau\right)^2\right]^{1/2} \tag{64}$$

Eq. (63) becomes

$$u = \sum_i \frac{K_i}{\omega_i} f_i(x)\, R_i \sin \omega_i(t - \alpha_i) \tag{65}$$

The quantity R_i is a function of t, $a(t)$, and ω_i. It characterizes the acceleration $a(t)$.

Housner[16, 17] has shown that, if $a(t)$ represents the ground acceleration encountered in strong-motion earthquakes, the maximum values of R_i (reached at certain time t) vary erratically with the frequency ω_i. For two frequencies close to each other, R_i may have markedly different values. On the basis of analyses of many past earthquake records, it cannot be concluded that the maximum R_i will necessarily be larger at one frequency of vibration than at another. In fact, on averaging a number of such R_i vs. ω_i curves, it is found that the maximum R_i is essentially independent of ω_i, except for very high frequencies ($R_i \to 0$ as $\omega_i \to \infty$). Housner shows[16] that this should really be expected if the earthquake waves consist of a series of impulses arriving at random intervals.

If R_i is a constant independent of ω_i, we may write R_i as R, which is a measure of the intensity of the earthquake. In this case Eq. (65) may be rewritten in terms of R,

$$u = R \sum_i \frac{K_i}{\omega_i} f_i(x) \sin \omega_i(t - \alpha_i) \tag{66}$$

Examining the trigonometric term, it is seen that, because of the variable phase factor α_i, the effect of the modes may be additive or they may tend to cancel each other. Either of these possibilities may occur, and whether or not they do depends upon the earthquake. The worst case is when the maximum contributions of each mode are additive—that is, when $\sin \omega_i(t - \alpha_i) = 1$ and $f_i(x)$ has its absolute value $|f_i(x)|$. The maximum displacement at any point is then

$$u = R \sum_i \frac{K_i}{\omega_i} |f_i(x)| \tag{67}$$

It should be noted that Eq. (67) does not represent the actual displacement at any time, but at any t it represents the maximum that would occur if all modes were additive. In this sense, Eq. (67) may be said to represent the envelope of maximum displacements.

The argument that a certain envelope can be constructed which represents the worst possible combination of all the modes can be applied to the more general case in which R_i does depend on the frequency ω_i. Then the envelope of displacement at any point is

$$u = \sum_i \frac{K_i}{\omega_i} |R_i(\omega_i)|\, |f_i(x)| \tag{68}$$

Example: A Uniform Cantilever Beam

Consider a uniform cantilever beam that has a uniform distribution of mass and rigidity and which deflects with bending deformation only. Let the mass per unit length be m and the flexural rigidity be EI. The free vibration modes $f_i(x)$ and the frequencies ω_i are well known and will not be quoted here.

The envelope of maximum displacements for a cantilever beam is given by Eq. (67) if we assume random impulses so that R is a constant. The envelope of maximum bending moments is given by

$$M = EI \frac{d^2u}{dx^2} = REI \sum_i \frac{K_i}{\omega_i} \left|\frac{d^2 f_i}{dx^2}\right| = Rl \sqrt{mEI}\, X_m \tag{69}$$

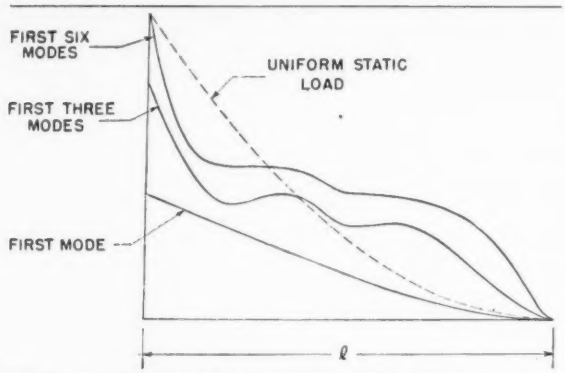

FIG. 6. The envelope of bending moment in a uniform cantilever beam.

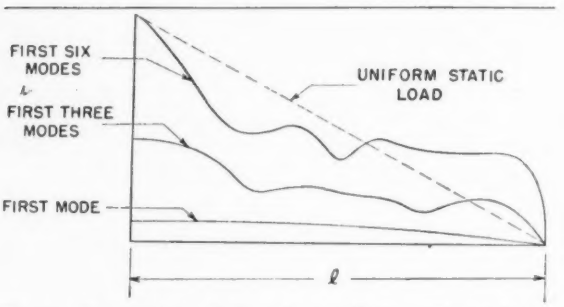

FIG. 7. The envelope of shear in a uniform cantilever beam.

where

$$X_m = \sum_i \frac{K_i}{p_i^2} \left| \frac{d^2 f_i}{dx^2} \right| \tag{70}$$

and p_i is the ith root of the equation

$$\cos p \cdot \cosh p + 1 = 0 \tag{71}$$

The shape of the envelope of maximum bending moments is given by X_m. The absolute magnitude depends upon the intensity of disturbance R and upon the mass per unit length and stiffness, $\sqrt{mEI}$. The shape X_m is shown in Fig. 6 for the first mode, the sum of the first three modes, and the sum of the first six modes.

On the same figure, for comparison, the shape of a bending moment curve corresponding to a uniformly distributed load is shown by the dotted line.

Similarly, the envelope of maximum shearing force can be obtained from the equation

$$S = EI \frac{d^3 u}{dx^3} = R\, EI \sum_i \frac{K_i}{\omega_i} \left| \frac{d^3 f_i}{dx^3} \right| \tag{72}$$

The shape of the maximum shear envelope is given in Fig. 7. The shear that would have developed if a uniformly distributed load is applied statically is shown by the dotted line in the same figure.

(VIII) Extreme Values†

In a sample of n values of any random variable, there are always two finite and uniquely determined *extreme values*. Let us consider the case when the population has a distribution of the continuous type, with a distribution function $F(x)$ and a probability density $f(x) = F'(x)$. Let x denote the *largest value* in a sample of n from this population. The probability element $g(x)dx$ in the sampling distribution of x is identical with the probability that, among the n sample values, $n - 1$ are $< x$ and 1 falls between x and $x + dx$. Hence, by the rules of multiplication of independent combined events and the definition of the distribution function, we have

$$g(x)\, dx = n\, [F(x)]^{n-1} f(x)\, dx \tag{73}$$

Let us introduce a new variable ξ by the substitution

$$\xi = n\, [1 - F(z)] \tag{74}$$

Since $F(x)$ varies between 0 and 1, we have

$$0 \leq \xi \leq n \tag{75}$$

By differentiation, $d\xi = -n\, f(x)\, dx$. The expression (73) is therefore transformed into

$$g(x)\, dx = -[1 - (\xi/n)]^{n-1}\, d\xi \tag{76}$$

The probability density of the new variable ξ is, therefore,

$$h(\xi) = [1 - (\xi/n)]^{n-1} \tag{77}$$

for $0 \leq \xi \leq n$ and $h(\xi) = 0$ outside $(0, n)$. As $n \to \infty$, $h(\xi)$ converges for any $\xi \leq 0$ to the limit

$$\lim_{n \to \infty} h(\xi) = e^{-\xi} \tag{78}$$

When the initial distribution function F is given, it is sometimes possible to solve Eq. (74) explicitly for x. The extreme value x is then obtained in terms of an auxiliary variable ξ whose probability density is known. Generally, however, such explicit solution cannot be given, but the limiting form of the distribution of the largest value when n is extremely large can often be found.

For example, if the population distribution is *normal* (m, σ) and if x is the largest value in a sample of n values from this distribution, Eq. (74) gives

$$\xi = \frac{n}{\sigma\sqrt{2\pi}} \int_x^\infty e^{-(t-m)^2/2\sigma^2}\, dt \tag{79}$$

The asymptotic solution of this equation, for large values of n, is

† The method that follows here is given by Cramer, reference 18, pp. 370–378, where further references to papers by Fisher, Tippet, Irwin, Pearson, Davies, and Hartley are given. Further references to a series of papers by Gumbel, Kimball, and Kendall can be found in references 19 and 20.

$$x = m + \sigma\sqrt{2\log n} - \sigma\frac{\log\log n + \log 4\pi}{2\sqrt{2\log n}} + \frac{\sigma}{\sqrt{2\log n}}v \quad (80)$$

where

$$v = -\log \xi \quad (81)$$

The variable v, by virtue of Eqs. (81) and (78), has the probability density $j(v)$:

$$j(v) = e^{-v-e^{-v}} \quad (82)$$

which is shown in Fig. 8. The distribution function is

$$J(v) = e^{-e^{-v}} \quad (83)$$

The complement $J^*(v)$, which gives the probability that v be larger than a specified value,

$$J^*(v) = 1 - e^{-e^{-v}} \quad (84)$$

is tabulated by Press in Table 1 of reference 19.

As another example, consider the *Laplace distribution* defined by the probability density

$$f(x) = (1/2\lambda)e^{-|x-\mu|/\lambda} \quad (85)$$

for which the mean is μ, the first moment about the mean is zero, and the second moment about the mean is $2\lambda^2$. The distribution function $F(x)$ is obtained by an integration. Eq. (74) gives, when $x > \mu$,

$$\xi = n\,[1 - F(x)] = (n/2)e^{-|x-\mu|/\lambda} \quad (86)$$

Hence,

$$x = \mu + \lambda\log(n/2) + \lambda v \quad (87)$$

where $v = -\log \xi$ has exactly the same distribution function as given by Eq. (83).

Application to Gust-Load Problem

It was shown by Press[19] that the "effective" gust velocity and the peaks of the increment of normal acceleration experienced by an airplane in flight have a probability distribution that is approximately Laplacian. Therefore, if the parameters μ and λ were determined from flight-test records, it would be possible to calculate the probability of encountering a gust of specified intensity.

Following Gumbel and Press, the transformation (87) will be written as

$$v = \alpha(x - u) \quad (88)$$

Identifying with Eq. (87), it is seen that

$$\alpha = 1/\lambda \quad (89)$$

$$u = \mu + \lambda\log(n/2) \quad (90)$$

As shown in Fig. 8, the frequency function $j(v)$ has one, and only one, maximum, reached when $v = 0$. Hence,

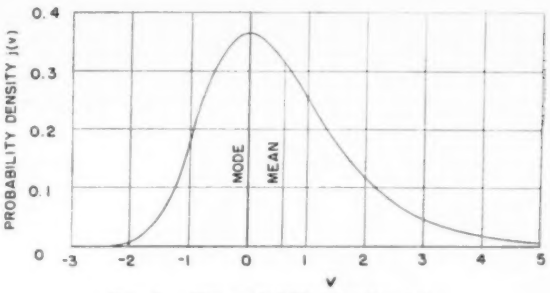

FIG. 8. The probability density $j(v)$.

$v = 0$ is the so-called *mode* of the distribution $j(v)$ and is in a sense a measure of the most probable value of v. From Eq. (88) it is seen that $v = 0$ implies $x = u$, and, hence, u represents a most probable value of the extreme value x in a sample of size n.

In practical applications to the gust problem, samples of the extreme values are readily obtainable from the N.A.C.A. V-G Recorders. From a V-G record it is impossible to tell the time history of the gusts, but the extreme values of the acceleration are obtained. If a number of such records are available, each representing approximately the same number of hours of flight, the statistical distribution of the extreme values can be estimated. The probability of experiencing an acceleration exceeding a specific value can then be calculated. From the acceleration data the so-called "effective" gust velocity can be calculated on the basis of the sharp-edged gust formula.

In order to utilize the type of data named above, it is necessary to estimate the parameters α and u directly from the samples of extreme values. The parameters α and u can be determined from the mean $\tilde{m}$ and the standard deviation $\tilde{\sigma}$ of the distribution of the largest value from the following equations, which are given by Gumbel:[20]

$$u = \tilde{m} - (\gamma/\alpha) \quad (91)$$

$$1/\alpha = (\sqrt{6}/\pi)\,\tilde{\sigma} \quad (92)$$

where γ is Euler's constant and is approximately equal to 0.5772. If Eqs. (91) and (92) are assumed to be true when the parameter values $\tilde{m}$ and $\tilde{\sigma}$ are replaced by their respective sample estimates $\bar{x}$ and s,

$$s = \sqrt{\Sigma(x - \bar{x})^2/(N - 1)} \quad (93)$$

where N is the total number of observations and Σ sums over the N observed values of x, then,

$$u = \bar{x} - (\gamma/\alpha) \quad (94)$$

$$1/\alpha = (\sqrt{6}/\pi)s \quad (95)$$

For samples of data, estimates of the values of u and α may be determined from Eqs. (94) and (95). By means of the transformation law, Eq. (88), the equivalent values between x and v are found. Since the distribution function of v is known, the probabilities that

a value of v and the associated value of x will be exceeded may then be obtained simply from the tables of $J^*(v)$.

In an example given by Press,[19] gust velocity measurements from 485 traverses of thunderstorms from the 1946 operations of the U.S. Weather Bureau Thunderstorm Project are analyzed. The parameters u and α are calculated according to Eqs. (94) and (95). The transformation (88) now appears as

$$v = 0.2072\ (w_e - 12.837) \tag{96}$$

where w_e is the "effective" gust velocity. For a given value of w_e, the equivalent value v can be computed from Eq. (96), and then the associated probability of exceeding w_e in each traverse can be found.

From the known probability of exceeding a specified gust velocity, the average miles of flight required to exceed that gust velocity can be determined by the equation

$$\text{mileage} = (U/P)\tau \tag{97}$$

where U is the average flight speed, P is the probability that a given value of w_e will be exceeded on each record, and τ is the average flight-hours per record.

(IX) Dynamic Stresses in an Elastic Structure-Stationary Random Process

For a stationary random process the time average is the same as the ensemble average. This remark, together with a result on the distribution of extreme values, gives a new significance to the root mean square of the random process. Eventually, it will make possible the determination of not only the most probable value of the largest stress at any point in a structure but also the life expectancy of a given structure with respect to the random process considered.

Let us consider the gust problem. The atmospheric turbulence will be regarded as a stationary random process with a mean zero. The root mean square (averaged over time) of the turbulent velocity component w, normal to the flight path of an aircraft, is also the standard deviation at any time of a large number of records of velocity measurements performed simultaneously under similar conditions. Similar interpretation applies to the mean and standard deviation of the airplane response (the elastic displacement, the acceleration at c.g., or the dynamic stresses, etc.).

However, the probabilistic structure of the gust response is not entirely given by the mean and standard deviation. Additional information is required to characterize the gust response as a random process.

It is generally assumed that the velocity component in a turbulent flow is normally distributed. If the aeroelastic system is assumed linear, the response will also be normally distributed.

Let us assume, then, that the probability distribution of the gust response is normal. The mean and standard deviation being known, the probabilistic structure is completely defined. In particular, the distribution of the extreme values is defined.

Let the displacement $\boldsymbol{u}$ of the elastic body be described by the generalized coordinates $f_n(\boldsymbol{x})$ and generalized displacements $q_n(t)$,

$$\boldsymbol{u}\ (\boldsymbol{x}, t) = \sum_n q_n(t)\, f_n(\boldsymbol{x}) \tag{98}$$

The stress at any point in the elastic body is a linear function of the derivatives of $\boldsymbol{u}$ with respect to the position vector $\boldsymbol{x}$. Hence, we may write

$$\tau\ (\boldsymbol{x}, t) = \sum_n q_n(t)\ g_n(\boldsymbol{x}) \tag{99}$$

where τ denotes a component of stress at $\boldsymbol{x}$ at time t and $g_n(\boldsymbol{x})$ being functions of $\boldsymbol{x}$ derived from $f_n(\boldsymbol{x})$. Accordingly,

$$|\tau(\boldsymbol{x}, t)|^2 = \sum_m \sum_n q_m(t) q_n^*\ (t)\ g_m(\boldsymbol{x})\ g_n(\boldsymbol{x}) \tag{100}$$

where $q_n^*(t)$ is the complex conjugate of $q_n(t)$. Taking averages over a sufficiently long period of time, we obtain

$$\overline{|\tau(\boldsymbol{x}, t)|^2} = \sum_m \sum_n \overline{q_m(t)\ q_n^*(t)}\ g_m(\boldsymbol{x})\ g_n(\boldsymbol{x}) \tag{101}$$

The left-hand side is a function of $\boldsymbol{x}$. The right-hand side is real, for Eq. (101) may be written as

$$\overline{|\tau(\boldsymbol{x}, t)|^2} = \sum_m \overline{|q_m(t)|^2}\ g_m^2(\boldsymbol{x}) + \sum_{m \neq n} \overline{[q_m(t) q_n^*(t) + q_m^*(t) q_n(t)]}\ g_m(\boldsymbol{x})\ g_n(\boldsymbol{x}) \tag{102}$$

the second summation being taken *once* over all pairs of (m, n) under the stipulation $m \neq n$.

The variance of the stress component at $\boldsymbol{x}$ is $\overline{\tau^2}$. Assuming normal distribution, the probability density of the stress τ at $\boldsymbol{x}$ is

$$f(\tau) = (1/\sigma\sqrt{2\pi}) e^{-\tau^2/2\sigma^2} \tag{103}$$

where

$$\sigma^2 = \overline{\tau(\boldsymbol{x}, t)^2} \tag{104}$$

The maximum stress expected at any point in a structure can be found by the method described in Section (VIII). It is shown there that, if the distribution of a random variable x is normal with mean $m = 0$ and standard deviation σ, the maximum value of x in n sample values has the following probability density as $n \to \infty$:

$$j(v) = e^{-v - e^{-v}} \tag{105}$$

where

$$v = \alpha (x - u) \tag{106}$$

$$u = \sigma \left(\sqrt{2 \log n} - \frac{\log \log n + \log 4\pi}{2\sqrt{2 \log n}} \right) \tag{107}$$

$$1/\alpha = \sigma / \sqrt{2 \log n} \tag{108}$$

The point $v = 0$ is the *mode* of the frequency function $j(v)$. Hence, the "most probable" value of the largest value of x in n samples ($n \to \infty$) is, from Eq. (106),

$$x = u \tag{109}$$

Let the random variable x stand for the stress τ. It is seen that for a fixed large value of n the most probable value of the largest stress is

$$\tau_{max.}(\boldsymbol{x}) = \text{const.} \sqrt{\overline{\tau(\boldsymbol{x}, t)^2}} \tag{110}$$

Therefore the most probable largest stress is proportional to the root mean square of $\tau(\boldsymbol{x}, t)$ and is a function of the space coordinates $\boldsymbol{x}$.

A surface representing the most probable largest stress as a function of $\boldsymbol{x}$ can serve as a rational basis for structural design. It is, in a sense, an envelope of expected most severe stress in the elastic body. It must be remarked that such a stress distribution does not occur in any particular one loading but is only the most probable value for a large number of loadings.

From Eq. (108) it is seen that the standard deviation of the largest value of stress is also proportional to $\sqrt{\overline{\tau^2}}$ [cf. Eq. (92)]. Hence, following the example in Section (VIII), the life expectancy is inversely proportional to $\sqrt{\overline{\tau^2}}$.

(X) Concluding Remarks

The preceding analyses are based on simplified models and are not immediately applicable to practical problems encountered in aircraft designs. The lines of thinking, however, are demonstrated, and it is not difficult to imagine various avenues of applications. For example, gust responses and landing and take-off loads during taxiing over rough grounds or water surfaces may be regarded as stationary random processes, while the disturbances to the landing impact—deviations from a mean curve, such as those represented by the curves on the right-hand side of Fig. 3—may be regarded as a nonstationary random process.†

It is obvious that the calculation of the mean square response can be extended to systems having many degrees of freedom. Such calculations will show, in particular, the *scale effect*—i.e., the effect of size of the aircraft on the dynamic responses (gusts, tail buffeting in fully developed wing wake, etc.). Housner's "envelope" treats a process that can hardly be regarded as stationary. It is directly applicable only to the particular type of excitation discussed. Nevertheless, it is indicative of the general form of the result to be expected with regard to the spatial distribution of stresses. It shows in particular, that the equivalent static inertia loading, commonly used in current aircraft design, can be misleading and unconservative.

The application of the theory of extreme values to the ensemble averages leads to an envelope of the most probable largest stress in a structure. Such an envelope can be used as follows: When the distribution of the largest stress over space is known, it is necessary only to measure experimentally the intensity of the largest stress at a few points on the structure. Such measurements, taken over a long period of time, will determine the time interval in which a specified maximum intensity of stress will occur *once*, in association with a given probability. Thus the life expectancy of the aircraft can be determined for a given specification of the largest stress. Conversely, with the service life of the aircraft specified, the specification of the design load can be made. The reasoning is analogous to the determination of the maximum load factor by the V-G diagram.

It is important to realize that the stress envelope relates to a large number of experiments and not to any specific forcing function. If the design stress is based on such an envelope, it will ensure, *in the long run*, a uniform factor of safety over the entire structure.

As was shown above, the solution of the structural admittance requires the solution of aeroelastic equations similar to those governing flutter, dynamic stability, etc. Hence, it is clear that the proximity of the flight speed to any of the critical speeds of aeroelastic instabilities will induce excessive dynamic stresses.

Some additional results relating to less restrictive models are available. However, too brief a presentation of quantitative results might prevent an intelligent interpretation. Hence, these results will be reserved for future publications.

† The response to the mean curve can be treated as an "exact" problem. The present approach is entirely different from an earlier proposal made by Biot and Bisplinghoff.[21] See reference 9.

References

[1] Liepmann, H. W., *On the Application of Statistical Concepts to the Buffeting Problem*, Journal of the Aeronautical Sciences, Vol. 19, No. 12, p. 793, December, 1952. Also, *An Approach to the Buffeting Problem from Turbulence Considerations*, Rept. No. SM-13940, Douglas Aircraft Company, Inc., 1951.

[2] Wang, M. C., and Uhlenbeck, G. E., *On the Theory of the Brownian Motion II*, Reviews of Modern Physics, Vol. 17, 1945.

[3] Chandrasekhar, S., *Stochastic Process in Physics and Astrophysics*. Reviews of Modern Physics, Vol. 15, 1943.

[4] James, H. M., Nichols, N. B., and Phillips, R. S., *Theory of Servomechanisms;* McGraw-Hill Book Company, Inc., 1947.

[5] Lawson, J. L., and Uhlenbeck, G. E., *Threshold Signals;* McGraw-Hill Book Company, Inc., 1950.

[6] Rhode, R. V., and Lundquist, E. E., *Preliminary Study of Applied Load Factors in Bumpy Air*, N.A.C.A. T.N. No. 374, 1931.

(*Concluded on next page*)

[7] Donely, Philip, *Summary of Information Relating to Gust Loads in Airplanes*, N.A.C.A. T.R. No. 997, 1950. Formerly, N.A.C.A. T.N. No. 1976.

[8] MacCready, P., *Atmospheric Turbulence*, Ph.D. Thesis, California Institute of Technology, 1952.

[9] Ramberg, W., and McPherson, A. R., *Experimental Verification of Theory of Landing Impact*, Bureau of Standards Report, presented before the Sixth International Congress for Applied Mechanics, Paris, September, 1946.

[10] Mook, C. P., *A Meteorological Analysis of Reports of Turbulence Encountered by Aircraft in Clear Air*, Aeronautical Engineering Review, Vol. 11, No. 9, p. 22, September, 1952.

[11] Tolefson, H. B., *An Analysis of the Variation with Altitude of Effective Gust Velocity in Convective Type Clouds*, N.A.C.A. T.N. No. 1628, 1948.

[12] Press, H., and Thompson, J. K., *An Analysis of the Relation Between Horizontal Temperature Variations and Maximum Effective Gust Velocities in Thunderstorms*, N.A.C.A. T.N. No. 1917, 1949.

[13] Clementson, G. C., *An Investigation of the Power Spectral Density of Atmospheric Turbulence*, Thesis, M.I.T., 1950.

[14] Sears, W. R., *Some Aspects of Non-Stationary Airfoil Theory and its Practical Application*, Journal of the Aeronautical Sciences, Vol. 8, pp. 104–108, 1941.

[15] Housner, G. W., *Calculating the Response of an Oscillator to Arbitrary Ground Motion*, Bull. Seism. Soc. Amer., Vol. 31, pp. 143–149, 1941.

[16] Housner, G. W., *Characteristics of Strong Motion Earthquakes*, Bull. Seism. Soc. Amer., Vol. 37, pp. 19–31, 1947.

[17] Alford, J. L., Housner, G. W., and Martel, R. R., *Spectrum Analysis of Strong-Motion Earthquakes*, California Institute of Technology Report to ONR, Contract N6 onr-244, August, 1951.

[18] Cramer, H., *Mathematical Methods of Statistics*, Princeton University Press, 1946.

[19] Press, Harry, *The Application of the Statistical Theory of Extreme Values to Gust-Load Problems*, N.A.C.A. T.R. No. 991, 1950. Formerly, N.A.C.A. T.N. No. 1926, 1949.

[20] Gumbel, E. J., *Les Valeurs Extremes des Distributions Statistiques*, Ann. de L'Institute Henri Poincare, Vol. 5, No. 2, pp. 115–158, 1935.

[21] Biot, M. A., and Bisplinghoff, R. L., *Dynamic Loads on Airplane Structures During Landing*, N.A.C.A. Wartime Report W-92, ARR 4 H10, October, 1944.

Calculation Method for Three-Dimensional Rotationally Symmetrical Laminar Boundary Layers with Arbitrary Free-Stream Velocity and Arbitrary Wall-Temperature Variation

(*Concluded from page 316*)

p. 153. (Translation by D. C. Ipsen, University of California, Institute of Engineering Research Report 19–6, July, 1951.)

[12] Drake, R. M., Seban, R. A., Doughty, D. L., and Levy, S., *Local Heat Transfer Coefficients on the Surface of an Elliptical Cylinder, Axis Ration 1:3, in a High Speed Air Stream*, University of California, Institute of Engineering Research Report 41–7, April, 1952.

[13] Eckert, E., and Drewitz, O., *Die Berechnung des Temperaturefeldes in der laminaren Grenzschicht schnell angeströmter unbeheizter Körper*, Luftfahrtforschung, Vol. 19, 1942.

[14] Handzsche, W., and Wendt, H., *Die laminare Grenzschicht an einem mit Überschallgeswindigkeit angeströmeten nicht angestellten Kegel*, Jahrbuch der deutsche Luftfahrtforschung, I, Vol. 76, 1941.

An Experimental Study of Natural Vibrations of Cantilevered Triangular Plates*

P. N. GUSTAFSON,† W. F. STOKEY,‡ AND C. F. ZOROWSKI‡

Carnegie Institute of Technology

ABSTRACT

Experimental results are obtained for the lowest six natural frequencies and the associated nodal lines of triangular plates of uniform thickness clamped on one edge. Two series of plates are examined. In one series, a delta-wing plan form of fixed span is maintained, and five plates are examined having aspect ratios ranging from 2 to 20. In the other series, a fixed span and a fixed root chord are maintained, and five plates are examined having mean chord-line sweepback angles ranging from 0 to 45°. Test results are presented by graphs and photographs. These results show that in the delta-wing plan form of fixed span, the frequency of each of the six modes *increases* as the aspect ratio *increases*—that is, as the root chord is made smaller. No such general property is exhibited by the plates in the sweepback series, except for the "bending" modes, where the frequencies decrease with increasing angle of sweepback. A simple method is described for finding the natural frequencies of a plate of any size, thickness, and material as long as its plan form is similar to one of the plates used in the experiments, or any other plate whose frequencies are known.

INTRODUCTION

THE UNIFORM FLAT TRIANGULAR PLATE serves as an approximation to rudimentary wing and tail surfaces on rockets, bombs, and some aircraft. There is also some evidence that flat-plate vibrations may be correlated with actual delta wings of hollow tapered construction.

The determination of the natural modes and frequencies of any thin flat plate may be reduced to the following boundary-value problem:[1]

$$\Delta\Delta w = (\sigma/D)\,\lambda w \tag{1}$$

with the boundary conditions

$$w = \frac{\partial w}{\partial n} = 0 \tag{2}$$

along a clamped edge, and

$$\left.\begin{aligned} &(\partial^3 w/\partial n^3) + (2-\mu)\partial^3 w/\partial n \partial s^2 = 0 \\ &\frac{\partial^2 w}{\partial n^2} + \frac{\mu\,\partial^2 w}{\partial s^2} = 0 \end{aligned}\right\} \tag{3}$$

along a free edge, where

$$\left.\begin{aligned} w &= \text{transverse displacement} \\ \sigma &= \text{mass per unit area} \\ D &= \text{flexural rigidity} = Eh^3/12(1-\mu^2) \\ \lambda &= \text{square of angular frequency} \\ n &= \text{normal coordinate at any edge} \\ s &= \text{tangential coordinate at any edge} \\ E &= \text{modulus of elasticity} \\ \mu &= \text{Poisson's Ratio} \\ h &= \text{plate thickness} \end{aligned}\right\} \tag{4}$$

There is no exact analytical solution available for this problem at the present time. Some success has been achieved with Rayleigh and Rayleigh-Ritz methods, but thus far only a few modes and a few plate shapes have been examined. There appears to be a great need for experimental solutions of this problem, not only to supply immediate answers but also to serve as a check for approximate analytical solutions as they are developed.

It was decided to explore the effects that plate shape might have on modes and frequencies by studying the separate effects of the two parameters necessary and sufficient to describe the plan form of any triangular plate—namely, aspect ratio and sweepback angle. The usual definitions are assumed but will be repeated for clarity, as shown in Fig. 1. The plate configurations adopted for the experiment and their designations are given in Figs. 2 and 3.

Note that plates A2 and S3 are identical so that only nine different plates are represented in the two groups. All of the plates in the "S" series have a fixed span and a fixed aspect ratio of 4.0. The sweepback angles vary from 0 (isosceles triangle) to 45°. However, the plates in the "A" series do not have a fixed sweepback angle. Rather, they are all of the delta-wing shape—that is, the trailing edge is a straight line from wing tip to wing tip. This represents a concession to the widespread interest in such configurations.

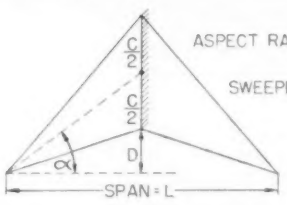

$$\text{ASPECT RATIO} = \frac{(\text{SPAN})^2}{\text{AREA}} = \frac{L^2}{CL/2} = \frac{2L}{C} \tag{5}$$

$$\text{SWEEPBACK ANGLE} = \tan^{-1}\frac{D + C/2}{L/2} \tag{6}$$

FIG. 1. Eqs. (5) and (6).

Received November 5, 1952.

* This report is based on research conducted in part under a contract between the Flight Research Laboratory of the U.S. Air Force and Carnegie Institute of Technology.

† Department of Mathematics.

‡ Department of Mechanical Engineering.

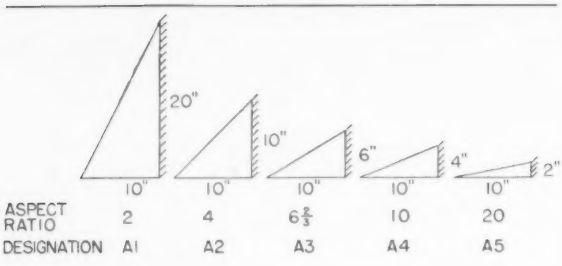

FIG. 2. Delta-wing configurations

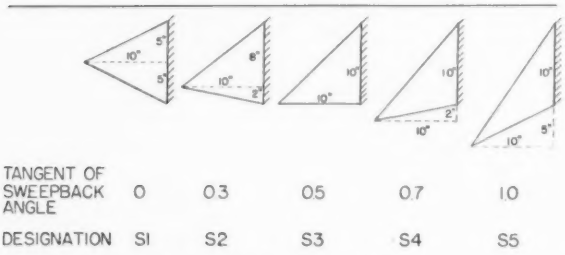

FIG. 3. Sweptback-wing configurations.

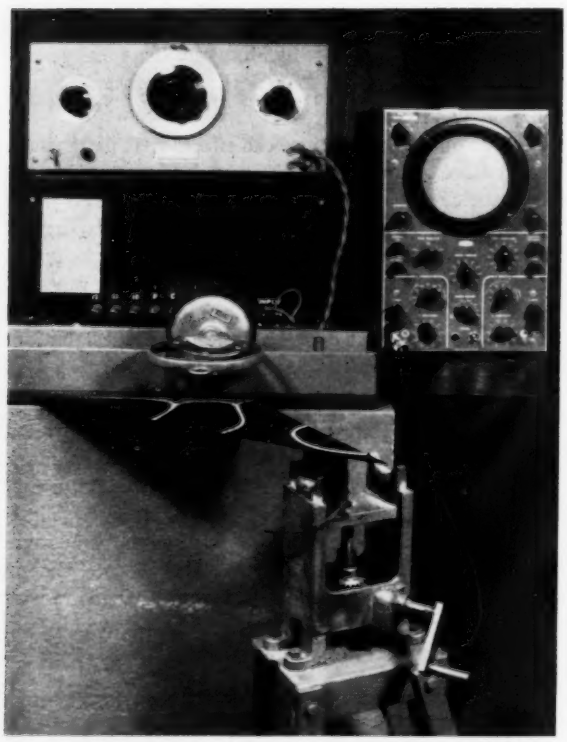

FIG. 4. Equipment for measuring frequencies and indicating nodal lines.

DESCRIPTION OF TESTS

Equipment.—Fig. 4 is a photograph showing one of the plates being tested. The plates were cut from sheet steel averaging 0.061 in. in thickness. Each plate had at its base a 6-in. projection for mounting. The support consisted of a $^1/_4$-in. steel plate to which the plate projection was clamped by another piece of $^1/_4$-in. steel plate and a length of 6-in. steel channel. The entire assembly was held together and clamped firmly to a heavy concrete base by means of two $^1/_2$-in. studs embedded in the concrete and three $^1/_2$-in. bolts anchored in expansion nuts in the concrete.

The method of exciting the natural vibrations is essentially that described in reference 2. The plates were vibrated by a U-shaped electromagnet to which power was supplied by a 25-watt amplifier. The amplifier was drived by a Hewlett-Packard Model 200a audio oscillator. The magnet was mounted on a pedestal that could be moved about, since the best place at which to drive the plate depended on the shape of the plate and the mode of vibration. In particular, it was impossible to excite a mode with the magnet directly beneath a node line for that mode. The magnet mount was equipped with a screw mechanism for vertical adjustments.

A microphone was placed above the plate and its output fed to the Y-input of a cathode-ray oscilloscope. This microphone picked up the sound emitted by the vibrating plate, and, since the intensity of the sound depended on the amplitude of vibration, the oscilloscope served as an indicator of changes in amplitude. Since the magnet pulled twice on the plate for each cycle of the oscillator, the plate usually vibrated at twice the oscillator frequency. However, in certain cases it was found that the plate could be driven at some natural frequency by setting the oscillator at a value other than one-half the plate frequency. For instance, the fundamental frequencies were excited in most cases by setting the oscillator at the natural frequency. This made it necessary to have some means of determining the ratio of plate frequency to oscillator frequency. This was done by feeding the oscillator output to the X-axis of the oscilloscope to which the microphone was connected and observing the Lissajous patterns. A further check was made where possible by measuring the plate frequency directly with a strobotac. Power-line frequency was used as a standard in all tests, the oscillator being calibrated against this over the range of frequencies used.

Procedure.—The plate to be tested was clamped firmly in the support, and the magnet was placed beneath it. The oscillator frequency was increased until the plate vibrated at its fundamental frequency, which was indicated by a large amplitude. The oscillator frequency was next increased gradually until resonance occurred at the second mode. This again was indicated by a marked increase in amplitude and also by an increase in the intensity of the sound emitted, which could be heard and was also observed on the oscilloscope. This same procedure was followed for each higher mode in turn up to six modes.

The closest possible estimate of the natural frequency was determined in each case by reducing the power input to the magnet to the lowest value at which vibration could be observed, at the same time carefully adjusting the oscillator frequency to give maximum vibration as observed by the microphone output on the oscilloscope. This technique narrowed the range of frequencies at which resonance could be detected. Some of the plates had fundamental frequencies lower than the lowest oscillator frequency. For such cases the fundamental frequency was determined by plucking the plate and measuring the frequency with a strobotac.

The nodal lines were determined by the well-known method of sprinkling the plate with a light granular material. Ordinary table salt proved satisfactory and afforded sharp contrast with the plates, which were painted with a thin coat of black lacquer. When the salt was sprinkled over the plate, the crystals either went off the edge or settled along a nodal line. These lines were photographed after the power input was reduced and the vibrations had damped out. The frequency values presented in this report were determined before the plates were painted. It was observed that the paint altered the natural frequencies slightly but had no noticeable effect on the nodal lines.

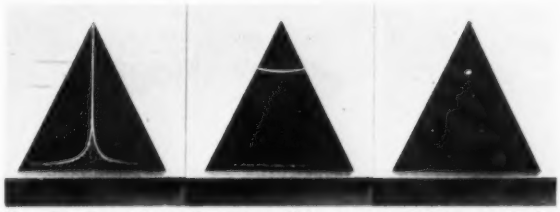

FIG. 5. Second, third, and combined modes of 10- by 10-in. isosceles plate.

An interesting phenomenon occurs when two successive natural frequencies of a plate are close together or when a natural frequency is nearly an integral multiple of another. In either event the plate may vibrate in a superposition of the two individual modes,[3] and the only point (or points) permanently at rest are therefore at the intersection of the nodal lines associated with the individual modes. In fact, it is sometimes difficult to make the plate vibrate in the individual modes concerned without artificially restraining it at several points along a nodal line. This behavior is shown in Fig. 5, which gives the second mode (166 cycles per sec.), third mode (169 cycles per sec.) and combination of the second and third modes for the 10- by 10-in. isosceles plate.

In attempting to find the sixth mode of plate A5, a series of four node *points* was observed, indicating a

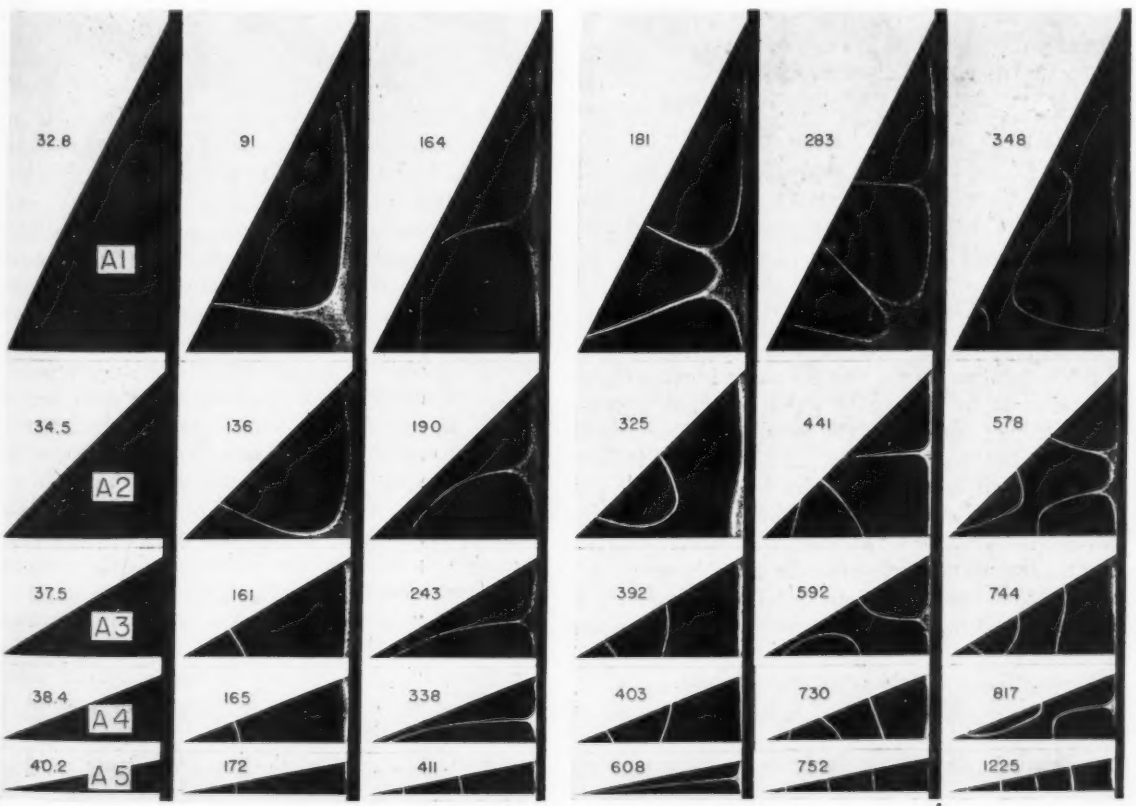

FIG. 6. Nodal lines and frequencies for delta-wing series.

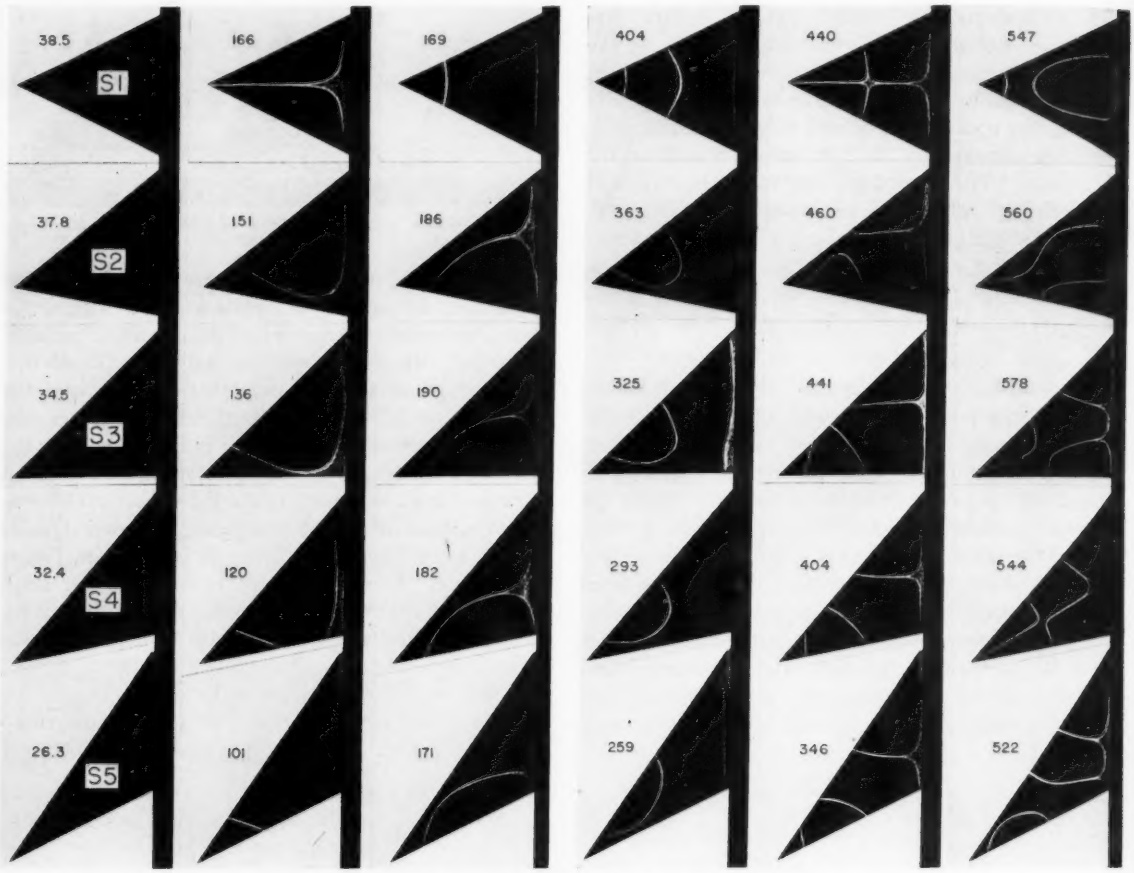

FIG. 7. Nodal lines and frequencies for sweptback-wing series.

superposition of the fourth mode (608 cycles per sec.) and the sixth mode (1,225 cycles per sec.). In this instance, the sixth-mode frequency was nearly double the fourth-mode frequency.

DISCUSSION OF RESULTS

Delta-Wing Series.—Fig. 6 shows the photographs of the nodal lines for the first six natural modes of the five plates in the delta-wing series, arranged in order of increasing frequency. The frequency of each mode accompanies the photograph. Definite trends in both frequency and mode shape may be observed if one selects a given mode of the widest plate and traces through its behavior to the narrowest plate. In each case the frequency *increases* as the chord becomes narrower. The fundamental mode of all five plates is primarily a "bending" mode, resembling the behavior of a simple cantilever beam. However, some chordwise variation in displacement is present. For the wide plate, A1, the fundamental is the only mode of the six examined which can be given any such simple classification. But as the plates become narrower they approach more nearly the behavior of a beam, until in the plate designated A5 all of the modes are roughly speaking "bending" modes except the fourth, which is a "torsional" mode.

A better picture of the variation of frequency with aspect ratio is afforded by the graphs of Fig. 8, where frequency is plotted against aspect ratio for each of the six modes. If we are to expect a smooth behavior from the curves, it is essential to fix our attention on those vibration modes belonging to the same "shape family," as determined from an inspection of the nodal lines of Fig. 6. Family "A" on Fig. 8 consists of the fundamental modes of all five plates. Family "B" consists of all the second modes. Family "C" consists of the third modes of plates A1, A2, A3, and A4, and the fourth mode of plate A5. That is, the mode shape that starts out as the third mode of the lower aspect ratios becomes the fourth mode of the high aspect ratio plates, and vice versa, at an aspect ratio of approximately 12.5, as seen on Fig. 8. Families "E" and "F" consist of the fifth and sixth modes, respectively, for all plates, so that in this series there is only one instance of an interchange of frequency.

Sweptback Wing Series.—Photographs of the nodal lines for the first six modes of each plate in the sweptback series are shown in Fig. 7, with the modes arranged

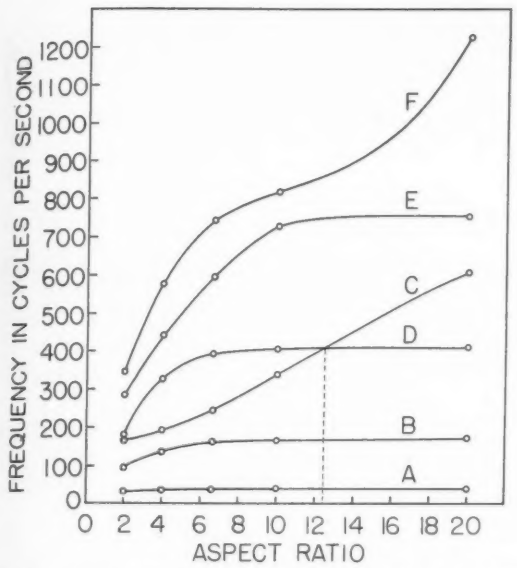

FIG. 8. Frequency vs. aspect ratio for plates of delta-wing shape.

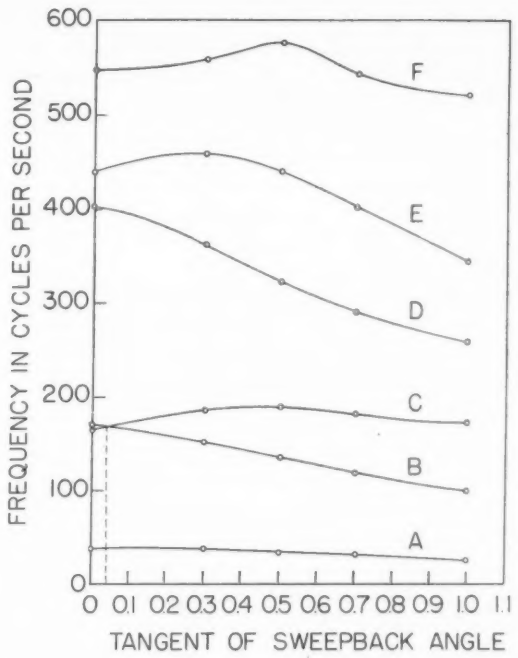

FIG. 9. Frequency vs. sweepback angle for a fixed span of aspect ratio 4.

in order of increasing frequency. The graphs of Fig. 9, where frequency is plotted against tangent of the sweepback angle, show clearly how the frequency changes as the plates are swept back through increasing angles. As in the case of the preceding series, one must be careful in plotting these curves to consider only mode shapes belonging to the same family. With one exception, all modes of a given order also belong to the same "shape family." That exception is in the isosceles plate, S1, where the third mode is essentially a "bending" mode and belongs in family "B," while the second mode is essentially a torsional mode and belongs in family "C." These are the two modes previously discussed in connection with Fig. 5. The point of interchange of the frequencies occurs at a sweepback angle of approximately $\tan^{-1} 0.035$. Several general observations may be made from inspection of Fig. 7 and Fig. 9. First, it is again noted that the fundamental mode of each plate is primarily a "bending" mode. Family "B" may also be roughly classified as a "bending" mode. The frequencies in families "A," "B," and "D" drop off as the sweepback angle is increased. For "bending" modes, this may be explained by the fact that, for a fixed span, an increase in the sweepback angle also increases the effective length of each wing half, with a consequent drop in frequency. For the other mode families "C," "E," and "F," the frequency is observed to increase up to sweepback angles of from $\tan^{-1} 0.3$ to $\tan^{-1} 0.5$ before dropping off.

Contrast Between Plates and Beams.—The results of this experiment serve to emphasize several important differences between beam and plate vibrations. In the case of a cantilever beam the natural frequencies of vibration are, on the whole, widely separated. For example, in a uniform cantilever beam, the first five bending frequencies are in the ratios of 1, 6.27, 17.55, 34.4, and 56.8.[4] On the other hand, the natural frequencies of flat plates are much closer together, as for example in the 10- by 10-in. right triangular plate, where the first six frequencies are in the ratios 1, 3.94, 5.50, 9.42, 12.8, and 16.74. It would appear that approximately *twice* as many modes of plate vibrations must be examined to cover the same frequency range as in beam vibrations. Probably the same observation applies in comparing delta wings with conventional wings. This suggests that, if three natural modes are required in the flutter analysis of a conventional wing, then six natural modes would be needed for a comparable flutter analysis of a delta wing.

Another point of difference arises in connection with the number of node points and nodal lines. In a cantilever beam, each higher bending mode is accompanied by the addition of one more node point. However, in the case of flat plates there is no corresponding relationship involving the nodal lines. In fact, many cases exist where a higher mode actually possesses *fewer* nodal lines than a lower mode, as evidenced by the fifth and sixth modes of plate A1 or the third and fourth modes of plate A5.

THE FREQUENCIES OF PLATES OF SIMILAR PLAN FORM

In order to make use of the experimental data, it is necessary to convert from the frequency of any given plate to the frequency of a plate of an exactly similar plan form but having different size, thickness, and material properties. Suppose the frequency of plate (A)

in Fig. 10 is known, and it is desired to find the frequency of plate (B) in which all dimensions except thickness are some scale factor α times the corresponding dimension of plate (A).

In the following development, primed quantities will refer to plate (B) and unprimed quantities to plate (A). Now suppose the exact displacement, $w(x,y)$ is known for a vibration mode of plate (A). This function will satisfy the differential Eq. (1) and also the boundary conditions (2) and (3).

Next one might predict that, in the corresponding natural mode of plate (B), the displacement would be exactly similar to plate (A), and since the magnitude of displacement has no effect on frequency (as long as all displacements are small), one might guess

$$w'(x',y') = w(x,y) \tag{7}$$

provided that

$$\left.\begin{aligned} x' &= \alpha x \\ y' &= \alpha y \end{aligned}\right\} \tag{8}$$

We then inquire under what conditions the function w' will satisfy the differential equation

$$\Delta'\Delta'(w') = (\sigma'/D')\lambda' w' \tag{9}$$

with the boundary conditions

$$w' = \partial w'/\partial n' = 0 \tag{10}$$

along a clamped edge and

$$\left.\begin{aligned} (\partial^3 w'/\partial n'^3) + (2-\mu')(\partial^3 w'/\partial n \partial s'^2) &= 0 \\ (\partial^2 w'/\partial n'^2) + \mu'(\partial^2 w'/\partial s'^2) &= 0 \end{aligned}\right\} \tag{11}$$

along a free edge. Now

$$\frac{\partial w'}{\partial x'} = \frac{\partial w'}{\partial x}\frac{dx}{dx'} = \frac{1}{\alpha}\frac{\partial w}{\partial x} \tag{12a}$$

$$\frac{\partial^2 w'}{\partial x'^2} = \frac{\partial}{\partial x}\left(\frac{\partial w'}{\partial x'}\right)\frac{dx}{dx'} = \frac{1}{\alpha^2}\frac{\partial^2 w}{\partial x^2} \tag{12b}$$

Similarly,

$$\left.\begin{aligned} \frac{\partial^2 w'}{\partial y'^2} &= \frac{1}{\alpha^2}\frac{\partial^2 w}{\partial y^2} & \frac{\partial^3 w'}{\partial n'^3} &= \frac{1}{\alpha^3}\frac{\partial^3 w}{\partial n^3} \\ \frac{\partial w'}{\partial n'} &= \frac{1}{\alpha}\frac{\partial w}{\partial n} & \frac{\partial^3 w'}{\partial n' \partial s'^2} &= \frac{1}{\alpha^3}\frac{\partial^3 w}{\partial n \partial s^2} \\ \frac{\partial^2 w'}{\partial n'^2} &= \frac{1}{\alpha^2}\frac{\partial^2 w}{\partial n^2} & \Delta'\Delta'(w') &= \frac{1}{\alpha^4}\Delta\Delta w \\ \frac{\partial^2 w'}{\partial s'^2} &= \frac{1}{\alpha^2}\frac{\partial^2 w}{\partial s^2} \end{aligned}\right\} \tag{13}$$

Substituting Eq. (7) into Eq. (9) and using Eqs. (13), we obtain

$$(1/\alpha^4)\Delta\Delta w = (\sigma'/D')\lambda' w$$

or

$$\Delta\Delta w = \alpha^4(\sigma'/D')\lambda' w \tag{14}$$

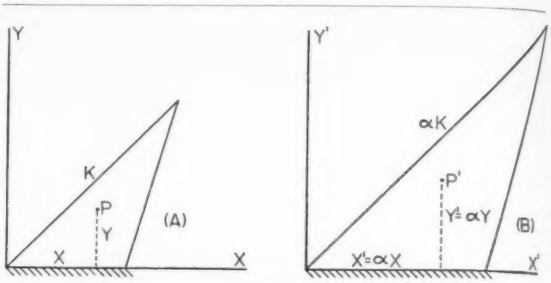

FIG. 10.

By comparison with Eq. (1), this will be satisfied if

$$\alpha^4 \frac{\sigma'}{D'}\lambda' = \frac{\sigma}{D}\lambda$$

or

$$\lambda' = \frac{1}{\alpha^4}\frac{D'}{D}\frac{\sigma}{\sigma'}\lambda \tag{15}$$

The boundary condition (10) is also satisfied upon substitution of Eqs. (7), (2), and (13) into Eq. (10). Turning now to boundary conditions (11) and using the relations (13), we obtain

$$\frac{\partial^3 w'}{\partial n'^3} + (2-\mu')\frac{\partial^3 w'}{\partial n' \partial s'^2} = \frac{1}{\alpha^3}\left[\frac{\partial^3 w}{\partial n^3} + (2-\mu')\frac{\partial^3 w}{\partial n \partial s^2}\right] \tag{16}$$

$$\frac{\partial^2 w'}{\partial n'^2} + \mu'\frac{\partial^2 w'}{\partial s'^2} = \frac{1}{\alpha^2}\left[\frac{\partial^2 w}{\partial n^2} + \mu'\frac{\partial^2 w}{\partial s^2}\right] \tag{17}$$

It is clear from Eq. (3) that the right-hand sides of Eqs. (16) and (17) will vanish only if $\mu' = \mu$. Thus, although a similar displacement will satisfy the biharmonic equation, it will not satisfy the free-edge boundary conditions unless the two plates have equal Poisson ratios. However, most metals do not differ by much in this respect, so that Eq. (11) should be closely approximated by similar displacement functions even for different materials. Then Eq. (15) may be used to compare the two frequencies and may be written as

$$\lambda' = \frac{1}{\alpha^4}\frac{E'h'^3}{Eh^3}\frac{(1-\mu^2)}{(1-\mu'^2)}\frac{\rho h}{\rho' h'}\lambda = \frac{1}{\alpha^4}\frac{E'\rho h'^2(1-\mu^2)}{E\rho' h^2(1-\mu'^2)} \tag{18}$$

where

$$\left.\begin{aligned} h &= \text{plate thickness} \\ \rho &= \text{mass per unit volume} \end{aligned}\right\} \tag{19}$$

Or, since $\lambda = \omega^2 = (2\pi f)^2$,

$$f' = \frac{1}{\alpha^2}\frac{h'}{h}\left[\frac{E'}{E}\frac{\rho}{\rho'}\frac{(1-\mu^2)}{(1-\mu'^2)}\right]^{1/2} \tag{20}$$

To summarize, Eq. (20) may be used to convert frequency from a given plate of one size to any other plate of similar plan form but of different size, thickness, and material. The transformation is exact for plates of the same Poisson ratio and provides a good approximation for plates having Poisson ratios not greatly different.

Conclusion

Several recent papers[5-7] deal with natural vibrations of *rectangular* cantilevered plates, considering the effects of aspect ratio and sweepback. The same two parameters are considered in this report, but in the aspect ratio series a delta-wing plan form is preserved, which results in a variable sweepback as the aspect ratio changes. A more systematic (and more comprehensive) program would consist of the selection of, say, five sweepback angles, as in series "S." For each angle examine five aspect ratios. The delta-wing plan form could be included as a special case for each angle. Then 25 plates would be required in all, as compared with nine covered by this report. There is also the clipped-wing plan form to consider, and possibly a simple correlation may be found which would enable one to predict truncated plate vibrations (trapezoidal plan form) from the vibrations of the complete triangular plate. These progams may be undertaken if a sufficient demand should arise.

The authors hope that this report will prove useful to design engineers and also to those interested in comparing analytical solutions with experimental evidence.

References

[1] Lord Rayleigh, *Theory of Sound*, Vol. I, pp. 357, 358; Dover Publications, New York, 1945.

[2] Campbell, Wilfred, *Protection of Steam Turbine Disc Wheels from Axial Vibration*, Transactions of A.S.M.E., p. 31, 1924.

[3] Lord Rayleigh, *op. cit.*, Vol. I, pp. 377, 383.

[4] Den Hartog, J. P., *Mechanical Vibrations*, 3rd Ed., p. 459; McGraw-Hill Book Company, Inc., New York, 1947.

[5] Martin, H. C., and Gursahaney, H. J., *On the Deflection of Swept Cantilevered Surfaces*, Journal of the Aeronautical Sciences, Vol. 18, No. 12, p. 805, December 1951.

[6] Dalley, J. W., and Ripperger, E. A., *Experimental Values of Natural Frequencies for Skew and Rectangular Cantilever Plates*, Society for Experimental Stress Analysis Proceedings, Vol. 9, No. 2, p. 51, 1952.

[7] Barton, M. V., *Vibration of Rectangular and Skew Cantilever Plates*, J. of Appl. Mech., Vol. 18, No. 2, p. 129, June, 1951.

Library Facilities of the
Institute of the Aeronautical Sciences

To serve Institute members and others in the aeronautical industry, the Institute of the Aeronautical Sciences offers the facilities of:

The W. A. M. Burden Library

2 East 64th Street
New York 21, N.Y.

The facilities of this library are available for reference study at the Institute.

The Paul Kollsman Lending Library

2 East 64th Street
New York 21, N.Y.

This library loans books without charge to members and others in the United States over eighteen years of age. Full information will be sent on request.

The Pacific Aeronautical Library

7660 Beverly Boulevard
Los Angeles 36, Calif.

This is a service and reference library for West Coast members and organizations. Full information as to its facilities will be sent on request.

Some Effects of Surface Curvature on Laminar Boundary-Layer Flow*

JAMES S. MURPHY†
University of Michigan

SUMMARY

The laminar flow of a viscous incompressible fluid over a two-dimensional curved surface is investigated for two cases, one in which the curvature is "large" and the other in which it is "moderate." The boundary-layer equations applicable to these cases are obtained as approximations from the exact equations of motion by an order-of-magnitude analysis. These equations are solved for flow over a particular surface with zero surface pressure gradient. In this analysis, the pressure gradient normal to the surface is included, and the outer boundary conditions are modified in accordance with the requirements of flow over a curved surface.

The results indicate that for equal Reynolds Numbers, the stress on convex surfaces is less than the flat-plate value, while the stress on concave surfaces is greater than for a flat plate. The most important effect of surface curvature, for the cases considered, is the modification of the shape of the velocity profile near the "outer edge" of the boundary layer. The requirement that a smooth transition exist between the viscous flow and the potential flow at the outer edge of the layer causes the profile to have a negative slope near the outer edge for convex surface curvature and a positive slope for concave surface curvature.

Received November 18, 1952.

*This paper is based on part of a Ph.D. Thesis in Aeronautical Engineering in the University of Michigan, June, 1952. The author gratefully acknowledges the guidance of Profs. A. M. Kuethe and R. C. F. Bartells during the course of work.

†Associate Research Engineer, Engineering Research Institute. Now with El Segundo Division, Douglas Aircraft Company, Inc.

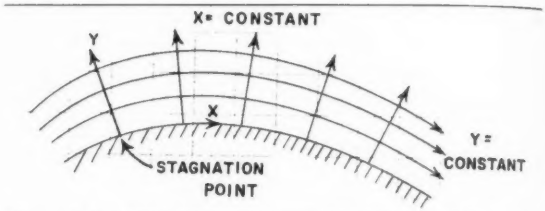

FIG. 1. Coordinate system for two-dimensional motion past an arbitrary cylindrical surface.

EQUATIONS OF MOTION

CONSIDER THE MOTION OF A viscous incompressible fluid along a curved two-dimensional surface. Let x represent distance measured along the surface from the stagnation point and y represent the distance normal to the surface, as shown in Fig. 1. Designate the velocity components in the directions x and y by u and v, respectively. Also denote the curvature of the surface by $K = K(x)$, which is a continuous function of x and is positive for convex and negative for concave curvature. Then for steady motion the Navier-Stokes equations may be written (see reference 1) as

$$\frac{1}{1+Ky}u\frac{\partial u}{\partial x}+v\frac{\partial u}{\partial y}+\frac{Kuv}{1+Ky}=-\frac{1}{\rho(1+Ky)}\frac{\partial p}{\partial x}+\nu\left[\frac{1}{(1+Ky)^2}\frac{\partial^2 u}{\partial x^2}+\frac{\partial^2 u}{\partial y^2}-\frac{y}{(1+Ky)^3}\frac{\partial K}{\partial x}\frac{\partial u}{\partial x}+\frac{K}{1+Ky}\frac{\partial u}{\partial y}-\frac{K^2u}{(1+Ky)^2}+\frac{2K}{(1+Ky)^2}\frac{\partial v}{\partial x}+\frac{v}{(1+Ky)^3}\frac{\partial K}{\partial x}\right] \quad (1a)$$

$$\frac{1}{1+Ky}u\frac{\partial v}{\partial x}+v\frac{\partial v}{\partial y}-\frac{Ku^2}{1+Ky}=-\frac{1}{\rho}\frac{\partial p}{\partial y}+\nu\left[\frac{1}{(1+Ky)^2}\frac{\partial^2 v}{\partial x^2}+\frac{\partial^2 v}{\partial y^2}-\frac{y}{(1+Ky)^3}\frac{\partial K}{\partial x}\frac{\partial v}{\partial x}+\frac{K}{1+Ky}\frac{\partial v}{\partial y}-\frac{K^2v}{(1+Ky)^2}-\frac{u}{(1+Ky)^3}\frac{\partial K}{\partial x}-\frac{2K}{(1+Ky)^2}\frac{\partial u}{\partial x}\right] \quad (1b)$$

The equation of continuity is

$$(\partial u/\partial x)+(\partial/\partial y)[(1+Ky)v]=0 \quad (2)$$

These equations may be made nondimensional by introduction of the quantities

$$\left.\begin{aligned} u' &= u/U_0, & v' &= v/U_0 \\ y' &= y/L, & x' &= x/L \\ K' &= KL, & p' &= p/\rho U_0^2 \end{aligned}\right\} \quad (3)$$

where U_0 and L are characteristic velocity and length in any flow under consideration. In terms of these non-dimensional quantities the equations of motion are

$$\frac{1}{1+K'y'}u'\frac{\partial u'}{\partial x'}+v'\frac{\partial u'}{\partial y'}+\frac{K'u'v'}{1+K'y'}=-\frac{1}{1+K'y'}\frac{\partial p'}{\partial x'}+\frac{1}{R}\left[\frac{1}{(1+K'y')^2}\frac{\partial^2 u'}{\partial x'^2}+\frac{\partial^2 u'}{\partial y'^2}-\frac{y'}{(1+K'y')^3}\frac{\partial K'}{\partial x'}\frac{\partial u'}{\partial x'}+\frac{K'}{(1+K'y')}\frac{\partial u'}{\partial y'}-\frac{K'^2u'}{(1+K'y')^2}+\frac{2K'}{(1+K'y')^2}\frac{\partial v'}{\partial x'}+\frac{v'}{(1+K'y')^3}\frac{\partial K'}{\partial x'}\right] \quad (4a)$$

$$\frac{1}{1+K'y'}u'\frac{\partial v'}{\partial x'}+v'\frac{\partial v'}{\partial y'}-\frac{K'u'^2}{1+K'y'}=-\frac{\partial p'}{\partial y'}+\frac{1}{R}\left[\frac{1}{(1+K'y')^2}\frac{\partial^2 v'}{\partial x'^2}+\frac{\partial^2 v'}{\partial y'^2}-\frac{y'}{(1+K'y')^3}\frac{\partial K'}{\partial x'}\frac{\partial v'}{\partial x'}+\frac{K'}{1+K'y'}\frac{\partial v'}{\partial y'}-\frac{K'^2v'}{(1+K'y')^2}-\frac{u'}{(1+K'y')^3}\frac{\partial K'}{\partial x'}-\frac{2K'}{(1+K'y')^2}\frac{\partial v'}{\partial x'}\right] \quad (4b)$$

where

$$R=\rho U_0 L/\mu = \text{Reynolds Number}$$

and the equation of continuity is

$$(\partial u'/\partial x')+(\partial/\partial y')[(1+K'y')v']=0 \quad (4c)$$

Boundary-Layer Equations of Motion

The above exact equations of motion are extremely difficult to solve. Indeed, only a few such exact solutions have been found. Hamel found one by restricting the stream lines of the viscous flow to coincide with those of a potential flow. The resulting viscous motion has stream lines in the form of logarithmic spirals.[2] Another solution of the complete equations of motion was obtained by von Kármán for the case of steady motion about a rotating disc.[3] However, by means of the order of magnitude analysis[4] we may simplify the equations of motion and continuity and obtain the "boundary-layer equations." The boundary-layer thickness parameter δ' is taken as small, and all terms in the equations are arranged according to the hierarchy of orders of magnitude.

$$\ldots \ll O(\delta'^2) \ll O(\delta') \ll O(1) \ll O\frac{1}{\delta'} \ll O\left(\frac{1}{\delta'^2}\right) \ll \ldots \quad (5)$$

Physical experience also shows that the following assumptions are valid for boundary-layer flow,

$$\left.\begin{aligned} u' &= O(1), \quad \partial u'/\partial x' = O(1) \\ \partial^2 u'/\partial x'^2 &= O(1), \quad \partial p'/\partial x' = O(1) \end{aligned}\right\} \quad (6)$$

where the primed quantities are nondimensional. Then moderately curved surfaces may, in the spirit of the foregoing definition of order of magnitude, be characterized by the condition

$$K' = O(1) \quad (7a)$$

while surfaces with large curvature may be said to be of order

$$K' = O(1/\delta') \quad (7b)$$

The conditions (7a) and (6) when applied to the continuity equation indicate that the orders of magnitude of the velocity component v' and its derivatives are

$$v' = O(\delta'), \qquad \frac{\partial v'}{\partial y'} = O(1),$$

$$\frac{\partial v'}{\partial x'} = O(\delta'), \qquad \frac{\partial^2 v'}{\partial x' \partial y'} = O(1) \quad (8)$$

provided that the derivative of the curvature has an order of magnitude no greater than

$$\partial K'/\partial x' = O(1/\delta') \quad (9)$$

For example, integration of Eq. (4c) yields

$$(1+K'y')v' = -\int_0^{y'} \frac{\partial u'}{\partial x'}\,dy'$$

Hence, if the orders of magnitude (6) hold, we may write for any point in the boundary layer

$$|v'| \leq \frac{O(1)}{|1+K'y'|}\int_0^{y'} dy' = \frac{O(\delta')}{|1+K'y'|}$$

Then for a convex surface satisfying the condition (7a), $(K' > 0)$,

$$\frac{1}{|1+K'y'|} \leq \frac{1}{1+|K'y'|} \leq \frac{1}{1+O(\delta')} = O(1)$$

while for a concave surface, $(K' < 0)$,

$$\frac{1}{|1+K'y'|} \leq \frac{1}{1-|K'y'|} \leq \frac{1}{1-O(\delta')} = O(1)$$

so that

$$v' = O(\delta')$$

In this manner, all terms involving the velocity components and their derivatives which appear in the

equations of motion may be assigned an order of magnitude. Inspection of the orders of magnitude of the terms in the first component of the equation of motion, Eq. (4a), reveals that all terms in the square bracket on the right may be neglected in comparison to $\partial^2 u'/\partial y'^2$, which is $O(1/\delta'^2)$. Also the term $K'u'v'/(1 + K'y')$ on the left side may be neglected in comparison to the others. All remaining terms are $O(1)$ except the term on the right involving the Reynolds Number, which has an unknown order of magnitude. Hence, we conclude that this term can be of order no greater than unity and find that

$$1/R = O(\delta'^2) \tag{10}$$

This result, applied to the second component of the equation of motion, shows that all terms may be neglected in comparison to the term $K'u'^2/(1 + K'y')$ on the left side. Since this term is $O(1)$, we conclude that

$$\partial p'/\partial y' = O(1) \tag{11}$$

Hence, the dimensional form of the equations governing the motion in the boundary layer on a curved two-dimensional surface, which is consistent with the above orders of magnitude, is

$$u\frac{\partial u}{\partial x} + v\frac{\partial u}{\partial y} = -\frac{1}{\rho}\frac{\partial p}{\partial x} + \nu\frac{\partial^2 u}{\partial y^2} \tag{12a}$$

$$Ku^2 = (1/\rho)(\partial p/\partial y) \tag{12b}$$

and continuity is

$$(\partial u/\partial x) + (\partial v/\partial y) = 0 \tag{12c}$$

when the surface curvature satisfies the conditions,

$$K' = O(1), \quad \partial K'/\partial x' = O(1/\delta') \tag{12d}$$

and the Reynolds Number, the condition (10).

In a similar manner, it can be shown that for convex surfaces with large curvature, the boundary-layer equations of motion are

$$\frac{1}{1 + Ky}\,u\frac{\partial u}{\partial x} + v\frac{\partial u}{\partial y} + \frac{Kuv}{1 + Ky} = -\frac{1}{\rho(1 + Ky)}\frac{\partial p}{\partial x} + \nu\left(\frac{\partial^2 u}{\partial y^2} + \frac{K}{1 + Ky}\frac{\partial u}{\partial y} - \frac{K^2 u}{1 + Ky^2}\right) \tag{13a}$$

$$Ku^2/(1 + Ky) = (1/\rho)(\partial p/\partial y) \tag{13b}$$

while the continuity equation is

$$(\partial u/\partial x) + (\partial/\partial y)[(1 + Ky)v] = 0 \tag{13c}$$

when the curvature satisfies the conditions

$$K' = O\left(\frac{1}{\delta'}\right), \qquad \frac{\partial K'}{\partial x'} = O\left(\frac{1}{\delta'}\right), \quad k' > 0 \tag{13d}$$

The restriction to convex curvature is imposed by the singularity in the equations of motion at $Ky = -1$. As would be expected, the equations of motion for large convex curvature are also valid for moderate curvature and should yield, actually, a more accurate solution for moderate curvature than do the Eqs. (12). Therefore, Eq. (13) may be applied to both concave and convex surfaces when the curvature is moderate.

Boundary Conditions

The no-slip condition at the surface requires that the velocity vanish at $y = 0$. This yields the two boundary conditions

$$u = v = 0 \tag{14}$$

at $y = 0$. In addition, a smooth transition is required between the motion of the fluid in the boundary layer, and the motion represented by the potential flow in the region exterior to the layer. Thus, it is necessary that at the "outer edge" of the boundary layer, the solution of the boundary layer tends asymptotically to an expression representing approximately the potential flow in the neighborhood of the surface. This approximate representation characterizing the nature of the potential flow near the surface depends upon the magnitude of the surface curvature and therefore will be different for the two cases considered here. In both cases, however, it is necessary to consider only thin boundary layers.

It is supposed, as in the case of the flow within the boundary layer, that in a neighborhood of the surface the potential flow is such that

$$u' = O(1), \quad \frac{\partial u'}{\partial x'} = O(1), \quad \frac{\partial^2 u'}{\partial x'^2} = O(1) \tag{15}$$

where the nondimensional quantities are introduced as before. Then it follows from the equation of continuity that, in the neighborhood of a surface having moderate or large curvature, in which $y' = O(\delta')$, the potential flow satisfies the further order relations,

$$v' = O(\delta'), \quad \frac{\partial v'}{\partial x'} = O(\delta'), \quad \frac{\partial v'}{\partial y'} = O(1) \tag{16}$$

We therefore seek an approximate representation of the potential flow consistent with these order relationships. Since the potential flow is irrotational, the components of velocity satisfy a condition that, in terms of the curvilinear coordinate system, can be written in the nondimensional form

$$\frac{1}{1 + K'y'}\frac{\partial v'}{\partial x'} - \frac{\partial u'}{\partial y'} - \frac{K'u'}{1 + K'y'} = 0 \tag{17}$$

If the boundary layer is extremely thin, Eq. (17) is valid at $y' = \delta'$. For the case of moderate curvature, if terms of $O(\delta')$ are neglected in Eq. (17), the condition of irrotationality may be expressed in dimensional form as

$$(1/u)(\partial u/\partial y) = -K \tag{18}$$

This differential equation requires that

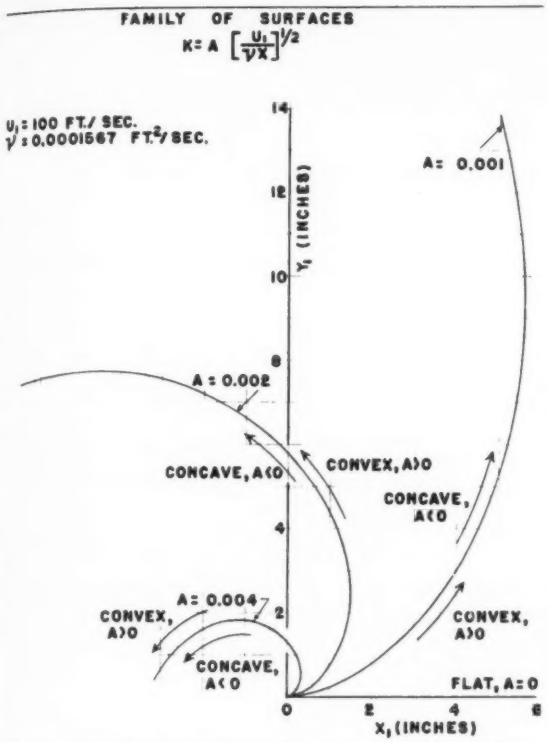

FIG. 2. Family of surfaces considered in particular solution.

$$u = C(x)e^{-Ky} \tag{19}$$

where the arbitrary function $C(x)$ is determined by the value of u prescribed by the potential flow at the surface. If, on the surface, $u = u_0(x)$ then an approximate representation of the potential flow in the neighborhood of a surface with moderate curvature is given by

$$u = u_0(x)e^{-Ky} \tag{20}$$

Thus for convex curvature ($K > 0$),

$$\partial u/\partial y]_{y=\delta} < 0$$

while for concave curvature ($K < 0$),

$$\partial u/\partial y]_{y=\delta} > 0$$

In the case of large convex curvature, the approximate condition of irrotationality expressed in dimensional form is

$$\frac{1}{u}\frac{\partial u}{\partial y} = -\frac{K}{1 + Ky} \tag{21}$$

This equation requires that

$$u = D(x)/(1 + Ky)$$

where the arbitrary function $D(x)$ is determined by the value of u prescribed by the potential flow at the surface. If, as before, $u = u_0(x)$ on the surface, then an approximate representation of the potential flow near the surface is

$$u = u_0(x)/(1 + Ky) \tag{22}$$

Hence, for the case of moderate surface curvature, the outer boundary condition for the solution of the boundary-layer equations is taken as

$$u \to u_0(x)e^{-Ky}, \quad y > 0 \tag{23}$$

For the case of large convex surface curvature, the outer boundary condition is

$$u \to \frac{u_0(x)}{1 + Ky}, \quad y > 0 \tag{24}$$

Perhaps it should be noted here that these outer boundary conditions can also be developed by a combination of the second component of the equation of motion and the Bernoulli equation.

Flow Along a Particular Surface

In order to determine the influence of normal pressure gradient and the outer boundary condition, developed above, on wall stress for laminar flow, we shall consider flow along a particular surface. The effects of surface pressure gradient will be eliminated by considering an idealized flow past the surface, such that the potential flow velocity at the surface is a constant, chosen to be U_1.

This flow would be difficult to obtain experimentally, but a theoretical solution shows the effects of surface curvature and allows a comparison to be made with the Blasius solution[5] for flow along a flat surface.

The family of surfaces we shall consider has a curvature distribution given by

$$K = A(U_1/\nu)^{1/2}x^{-1/2} \tag{25}$$

where A is a constant of proportionality, U_1 is the constant potential flow velocity at the surface, and ν is the coefficient of kinematic viscosity. We shall seek a solution for those surfaces for which

$$-0.05 < A < +0.05 \tag{26}$$

Several surfaces of the family for $U_1 = 100$ ft. per sec. and $\nu = 0.0001567$ are shown on Fig. 2.

Consider Eqs. (13), which are valid for large curvature, with the boundary conditions (14) and (24). Eq. (13c) may be satisfied by introduction of a stream function ψ, such that

$$u = \frac{\partial \psi}{\partial y}, \quad v = -\frac{1}{1 + Ky}\frac{\partial \psi}{\partial x} \tag{27}$$

Now make the following transformation of independent variables:

$$\eta = \frac{y}{2}\left(\frac{u_1}{\nu x}\right)^{1/2}, \quad \xi = x \tag{28}$$

We shall seek a solution for which ψ has the form,

$$\psi = (U_1\nu\xi)^{1/2}f(\eta) \tag{29}$$

where $f(\eta)$ is a function of η alone. Then

$$\left.\begin{aligned} u &= \frac{1}{2}U_1 f', \quad \frac{\partial u}{\partial x} = -\frac{1}{4}\frac{U_1}{\xi}\eta f'' \\ \frac{\partial u}{\partial y} &= \frac{U_1}{4}\left(\frac{U_1}{\nu\xi}\right)^{1/2} f'' \\ \frac{\partial^2 u}{\partial y^2} &= \frac{U_1}{8}\left(\frac{U_1}{\nu\xi}\right) f''' \\ v &= \frac{1}{2(1+2A\eta)}\left(\frac{U_1\nu}{\xi}\right)^{1/2}(f'\eta - f) \\ Ky &= 2A\eta \end{aligned}\right\} \quad (30)$$

Substitution of these values into Eq. (12b) yields

$$\frac{\partial p}{\partial \eta} = \frac{\rho A U_1^2 f'^2}{2(1+2A\eta)} \quad (31)$$

and using this result in Eq. (12a), along with Eq. (30), gives the single equation of motion,

$$f''' + ff'' + 2Aff' + 2A\eta ff'' + 4A\eta f'' + 4A^2\eta^2 f''' + 2Af'' + 4A^2\eta f'' - 4A^2 f' = 0 \quad (32)$$

for the condition

$$\partial p/\partial \xi = 0 \quad (33)$$

which is required for a constant potential flow velocity along the surface.

The boundary conditions (11) become

$$f = f' = 0, \qquad \eta = 0 \quad (34a)$$

and the condition (24) at the outer edge of the boundary layer is

$$f' \to \frac{2}{1+2A\eta}, \qquad \eta > 0 \quad (34b)$$

Assume a solution of (32) of the form

$$f = \sum_{i=0}^{\infty} \frac{C_i \eta^i}{i!} \quad (35)$$

where the C_i are constants. In view of the conditions (34a), the first two coefficients are zero. Then substituting Eq. (35) in Eq. (32) and expanding and equating coefficients of powers of η to zero gives

$$\left.\begin{aligned} C_2 &\\ C_5 &= -(C_2^2 + 96A^3C_2) \\ C_8 &= 11C_2^2 + 1832A^3C_2^2 + 161{,}280A^6C_2 \\ C_{11} &= -375C_2^4 - 203{,}784A^3C_2^3 - 10{,}623{,}744A^6C_2^2 - 928{,}972{,}800A^9C_2 \end{aligned}\right.$$
$$\left.\begin{aligned} C_3 &= -2AC_2 \\ C_6 &= 10AC_2^2 \\ C_9 &= -324AC_2^3 - 29{,}520A^4C_2 - 2{,}580{,}480A^7C_2 \end{aligned}\right.$$
$$\left.\begin{aligned} C_4 &= 12A^2C_2 \\ C_7 &= -128A^2C_2^2 - 11{,}520A^5C_2 \\ C_{10} &= 8{,}184A^2C_2^3 + 531{,}936A^5 \times C_2^2 + 46{,}448{,}640A^8C_2 \end{aligned}\right\} \quad (36)$$

Hence, the function f has the form

$$f = C_2^{1/3}F_0(C_2^{1/3}\eta) - AG_1(C_2^{1/3}\eta) + \frac{A^2}{C_2^{1/3}}G_2(C_2^{1/3}\eta) - \ldots + \frac{(-1)^n A^n}{C_2^{(n-1)/3}}G_n(C_2^{1/3}\eta) + \ldots \quad (37)$$

where

$$\left.\begin{aligned} F_0(C_2^{1/3}\eta) &= \frac{(C_2^{1/3}\eta)^2}{2!} - \frac{(C_2^{1/3}\eta)^5}{5!} + \frac{11(C_2^{1/3}\eta)^8}{8!} - \frac{375(C_2^{1/3}\eta)^{11}}{11!} + \frac{27{,}897(C_2^{1/3}\eta)^{14}}{14!} - \frac{3{,}817{,}742(C_2^{1/3}\eta)^{17}}{17!} + \ldots \\ G_1(C_2^{1/3}\eta) &= \frac{2(C_2^{1/3}\eta)^3}{3!} - \frac{10(C_2^{1/3}\eta)^6}{6!} + \frac{324(C_2^{1/3}\eta)^9}{9!} - \frac{22{,}896(C_2^{1/3}\eta)^{12}}{12!} + \frac{2{,}854{,}146(C_2^{1/3}\eta)^{15}}{15!} - \frac{595{,}343{,}808(C_2^{1/3}\eta)^{18}}{18!} + \ldots \\ G_2(C_2^{1/3}\eta) &= \frac{12(C_2^{1/3}\eta)^4}{4!} - \frac{128(C_2^{1/3}\eta)^7}{7!} + \frac{8{,}184(C_2^{1/3}\eta)^{10}}{10!} - \ldots \\ G_3(C_2^{1/3}\eta) &= \frac{96(C_3^{1/3}\eta)^5}{5!} - \frac{1{,}832(C_2^{1/3}\eta)^8}{8!} + \frac{203{,}784(C_2^{1/3}\eta)^{11}}{11!} - \ldots \end{aligned}\right\} \quad (38)$$

etc.

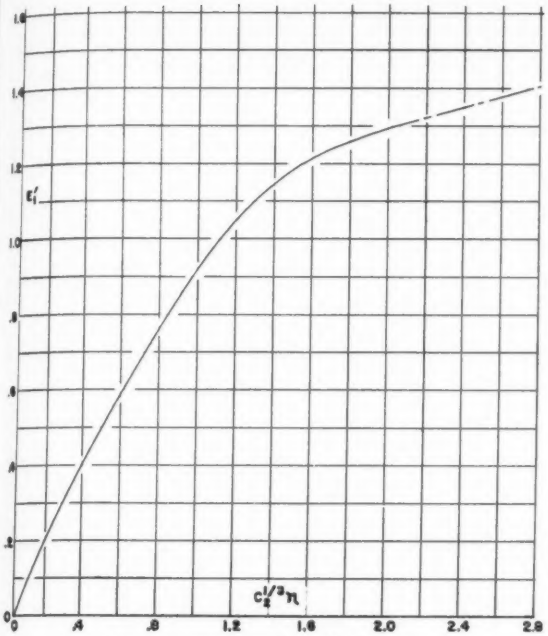

FIG. 3. The function $E_1'(C_2^{1/3}\eta)$.

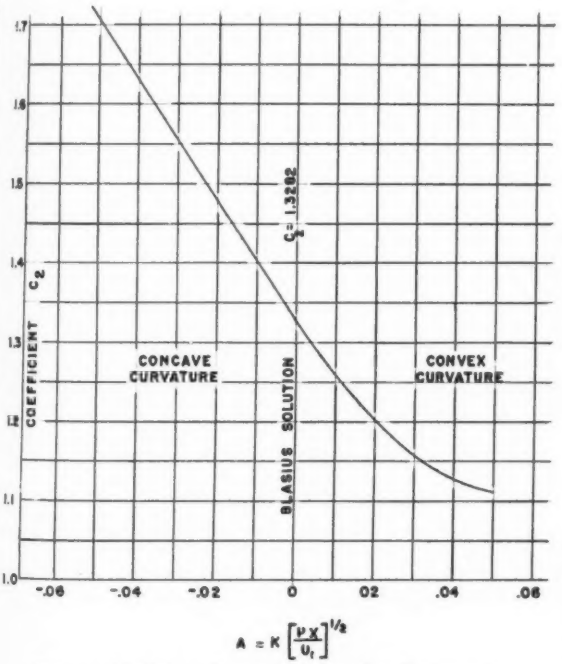

FIG. 4. Coefficient C_2 as a function of wall curvature.

The series F_0 is that obtained by Blasius for flow over a flat surface—i.e., a surface for which $K = A = 0$. Therefore the above solution is a double power series in η and the curvature that passes over into the Blasius solution as $K \to 0$. For small values of curvature such that $|A| \ll 1$, it may be expected that the higher powers of A will be small and may be neglected. Thus for $-0.005 < A < +0.05$, we may approximate solution (37) by

$$f = C_2^{1/3}F_0(C_2^{1/3}\eta) - AG_1(C_2^{1/3}\eta) \tag{39}$$

The outer boundary condition specifies the dependence of the unknown coefficient C_2 on the curvature. In general, this condition requires that

$$C_2^{2/3}F_0' - AC_2^{1/3}G_1' + A^2G_2' - \ldots + \frac{(-1)^nA^nG_n'}{C_2^{(n-2)/3}} + \ldots \to \frac{2}{1 + 2A\eta}, \quad \eta > 0 \tag{40}$$

which can be written in the form

$$C_2^{2/3}[F_0' - A\eta E_1' + A^2\eta^2E_2' - \ldots (-1)^nA^n\eta^nE_n' + \ldots] \to \frac{2}{1 + 2A\eta}, \quad \eta > 0 \tag{41a}$$

where

$$E_n' = G_n'/(C_2^{1/3}\eta)^n \tag{41b}$$

For small values of A, this condition can be approximated by

$$C_2^{2/3}[F_0'(C_2^{1/3}\eta) - A\eta E_1'(C_2^{1/3}\eta)] \to \frac{2}{1 + 2A\eta}, \quad \eta > 0 \tag{42}$$

It has been shown[1] that the value of F_0' for large $(C_2^{1/3}\eta)$ is

$$F_0'(C_2^{1/3}\eta) = 1.65562, \quad C_2^{1/3}\eta > 3.3 \tag{43}$$

The approximate value of $E_1'(C_2^{1/3}\eta)$ can be determined by summation of the series expansion of this function. The value of E_1' computed in this manner is shown on Fig. 3, where, for values of $(C_2^{1/3}\eta) > 2$, the function has been approximated by the tangent at $(C_2^{1/3}\eta) = 2$ in order to avoid lengthy computation of further terms in the series. The equation of the tangent is

$$E_1'(C_2^{1/3}\eta) \approx 0.144C_2^{1/3}\eta + 1.002, \quad (C_2^{1/3}\eta) > 2 \tag{44}$$

Use of Eqs. (44) and (43) in Eq. (42) yields

$$C_2^{2/3}[1.65562 - 0.144AC_2^{1/3}\eta^2 - 1.002A\eta] \to \frac{2}{1 + 2A\eta}, \quad \eta > 3 \tag{45}$$

Evaluation of C_2 as a function of A has been accomplished numerically for $-0.05 < A < +0.05$ and large η. The results are shown on Fig. 4. Velocity profiles for $A = -0.05$, -0.02, and $+0.05$ are shown on Fig. 5, along with the Blasius profile for $A = 0$.

Discussion of Results

Study of the velocity profiles on Fig. 5 shows that the most important effect of surface curvature is the modification of the profile shape for large η. This modification is imposed by the outer boundary condition. The profile for convex curvature would appear to be more sensitive to an adverse pressure gradient $(\partial p/\partial x > 0)$

than the profiles for concave surfaces. In addition, at points in the layer on a convex surface where $\partial u/\partial y < 0$, the flow will be considerably less stable to two-dimensional disturbances than points closer to the surface.[6]

The laminar shearing stress at the wall is given by

$$\tau_0 = \mu(\partial\mu/\partial y)_{y=0} \tag{46a}$$

which for the particular flow considered here is

$$\tau_0 = \mu \frac{U_1}{4}\left(\frac{U_1}{\nu x}\right)^{1/2} C_2 \tag{46b}$$

The variation of C_2 with curvature shown on Fig. 4 indicates that wall stress for convex curvature is less than the flat-plate value, while that for concave curvature is greater than the flat-plate value.

An estimate of the errors involved in Eqs. (13) is possible by consideration of the equations of motion made nondimensional by introduction of the following quantities:

$$x_1 = \frac{x}{L}, \quad y_1 = R^{1/2}\frac{y}{L}, \quad u_1 = \frac{u}{U_0}$$

$$v_1 = R^{1/2}\frac{v}{U_0}, \quad p_1 = \frac{p}{\rho U_0^2}, \quad K_1 = KL \tag{47}$$

where U_0 and L are characteristic velocity and length and R = Reynolds Number.

It can be shown by means of this transformation that the errors in Eqs. (13a) and (13b) are of order R^{-1} and $(\partial K_1/\partial x)R^{-3/2}$, while the equation of continuity is exact. Previous solutions in which all terms involving the surface curvature were neglected contained, in addition to the above errors, errors of order $K_1R^{-1/2}$ (see reference 1, page 121). Perhaps the greatest improvement introduced here, however, is associated with the new outer boundary condition that is valid to order K_1, whereas previous solutions contained an error in this condition of order K_1.

A solution for flow along the surface considered above, using the more approximate equations of motion, Eq. (12), and the corresponding outer boundary condition, Eq. (23), has also been obtained. The equation of motion is simpler, in this case, being

$$f''' + ff'' + 2A\eta f'^2 = 0 \tag{48}$$

with the boundary conditions

$$\left.\begin{aligned} f = f' = 0, \quad \eta = 0 \\ f' \to 2 - 4A\eta, \quad \eta > 0 \end{aligned}\right\} \tag{49}$$

The solution of Eq. (48) agrees closely with the above solution, Eq. (37), for convex curvature, but the results for concave curvature indicate a smaller value of wall stress than Eq. (37). The difference between the two solutions may be attributed, essentially, to the differences between the outer boundary conditions (23) and (24).

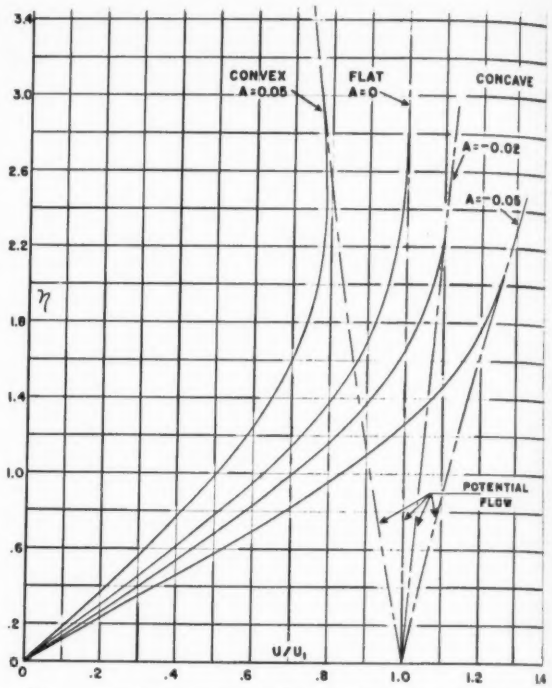

FIG. 5. Typical velocity profiles for flow along convex, flat, and concave surfaces of the family considered in particular solution.

It should also be noted that the numerical values obtained in the solution presented here could be improved upon by the numerical integration of Eq. (32) with the boundary conditions (34).

REFERENCES

[1] Goldstein, S., *Modern Developments in Fluids Dynamics*, 1st Ed., Vol. 1, pp. 90–120; Oxford University Press, 1938.

[2] Hamel, George, *Spiralförmige Bewegungen Zäher Flüssigkeiten*, Jahresbericht der Deutschen Mathematiker—Vereinigung, Band 25, pp. 34–60, 1917.

[3] von Kármán, Th., *Über laminare und turbulente Reibung*, Zeitschr. für Angewandte Math. und Mech., Band 1, pp. 244–247, 1921.

[4] Prandtl, L., *Über Flüssigkeitbewegung bei sehr kleiner Reibung*, Verhandlungen des Dritten Internationalen Mathematiker—Kongress, Heidelberg, pp. 484–491, 1904.

[5] Blasius, H., *Grenzschichten in Flüssigkeiten mit kleiner Reibung*, Zeitschr. für Mathematik und Physik, Band 16, p. 1, 1908.

[6] Kuethe, A. M., and Schetzer, J. D., *Foundations of Aerodynamics*, 1st Ed., p. 285; John Wiley & Sons, Inc., New York, 1950.

Shock-Wave Effects on the Laminar Skin Friction of an Insulated Flat Plate at Hypersonic Speeds*

TING-YI LI† AND H. T. NAGAMATSU‡
California Institute of Technology

ABSTRACT

An approximate theory on the phenomena of interaction between the shock wave and the laminar boundary layer on an insulated flat plate at hypersonic speeds has been formulated. Results on the rate of growth of the boundary-layer thickness and the rate of decay of the shock-wave strength have been found that hold for $M_1^{2(2+\omega)} R_1^{-1} = 0(1)$. A new set of formulas for the average skin-friction coefficient, C_F, over an insulated flat plate at hypersonic speeds has been obtained. Calculations on the basis of the new C_F formulas yield the data shown in Figs. 5 and 6. Contrary to the conventional theory that predicts a steady decrease in C_F as M_1 increases, the present results indicate that C_F may increase with M_1 at hypersonic Mach Numbers.

NOMENCLATURE

L = chord of the flat plate
x_0 = interaction distance
C_F = average skin friction coefficient
M_1 = free-stream Mach Number
x, y = Cartesian coordinates (Fig. 1)
u, v = velocity components in x, y directions, respectively
p = pressure
ρ = density
T = absolute temperature
μ = coefficient of viscosity
k = coefficient of conductivity
R = gas constant
C_p = specific heat at constant pressure
ω = constant index of the power law of viscosity
$R_{1x} = \rho_1 u_1 x/\mu_1$ = free-stream Reynolds Number based on the distance x from the leading edge
$R_1 = \rho_1 u_1 L/\mu_1$ = free-stream Reynolds Number based on the chord of the flat plate
δ = boundary-layer thickness
$Pr = \mu C_p/k$ = Prandtl Number
$\tau_w = \mu_w(\partial u/\partial y)_w$ = laminar skin friction of the flat plate

Subscripts 1 and 2 refer to the conditions pertaining to the free stream and the outer boundary of the viscous layer, respectively. Subscript w refers to the conditions on the flat-plate surface.

Received September 23, 1952. Revised and received January 26, 1953.

* This report is the condensed version of a GALCIT report of the same title.[1] The work was sponsored by the Army Ordnance and the Air Force.

† Senior Research Engineer, Guggenheim Aeronautical Laboratory.

‡ Senior Research Fellow, Guggenheim Aeronautical Laboratory.

(I) INTRODUCTION

IN RECENT YEARS, a considerable amount of information concerning the skin friction of a two-dimensional thin flat plate moving edgewise through the air at high speeds has been obtained through the study of compressible boundary-layer equations.[2] The usual basic assumption is that viscous effects are confined to a narrow region close to the plate surface. The flow field outside this narrow region is regarded as nonviscous and not effected by the presence of the boundary layer. However, when the plate is moving at supersonic speeds, disturbances due to the viscous effects in the boundary layer can drastically influence the outside flow field.[3] Thus, the retarded flow in the boundary layer causes the stream lines to turn slightly away from the plate surface, and this results in a shock wave extending from the plate into the free stream. This shock wave, moreover, decays in its strength as it intersects successive expansion waves originating from the boundary layer. There is, therefore, a close relationship between the rate of growth of the boundary-layer thickness in the viscous flow region and the rate of decay of the shock-wave strength in the outside flow field. In the lower supersonic speed range, the boundary layer and the shock wave are so far apart that their interaction effects can probably be neglected as in the existing theories.[2] The situation is quite different when the hypersonic speed range is approached. One may define the hypersonic flow régime such that $M_1(v_2/u_2) = 0(1)$ (reference 4). By the familiar argument, the boundary-layer thickness must be such that

$$\delta/x = 0(v_2/u_2) = 0(1/M_1)$$

Therefore, in the hypersonic speed range, the shock wave, which has a wave angle of the order of the quantity $1/M_1$, is so close to the plate surface that the entire region between the shock wave and the plate surface should be considered as a viscous flow layer.** Consequently, for the determination of the shock-wave characteristics, viscous effects must be considered,[5] and for the estimation of the plate skin friction, due care must be exercised to account for the shock-wave effects. In

** Lees[15] postulates the region between shock wave and the plate surface as consisting of hot and cold layers; thus, his formulation is somewhat different from ours.

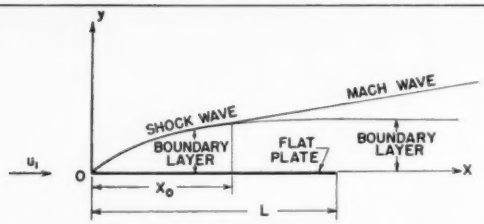

FIG. 1 — THE COORDINATE SYSTEM AND THE FLAT PLATE

the present paper, an approximate theory of the shock-wave effects on the hypersonic laminar friction on an insulated flat plate will be presented.

(II) Basic Equations and Assumptions

The thickness of the shock wave[6, 7] is assumed infinitesimally thin.† The flow variables in the region bounded by the shock wave and the plate surface satisfy the compressible boundary-layer equations,

$$\rho u \frac{\partial u}{\partial x} + \rho v \frac{\partial u}{\partial y} = -\frac{dp_2}{dx} + \frac{\partial}{\partial y}\left(\mu \frac{\partial u}{\partial y}\right) \tag{1}$$

$$\frac{\partial}{\partial x}\rho u + \frac{\partial}{\partial y}\rho v = 0 \tag{2}$$

$$\rho u \frac{\partial}{\partial x}(C_p T) + \rho v \frac{\partial}{\partial y}(C_p T) = u \frac{dp_2}{dx} + \frac{\partial}{\partial y}\left(k \frac{\partial T}{\partial y}\right) + \mu \left(\frac{\partial u}{\partial y}\right)^2 \tag{3}$$

The order of magnitude arguments responsible for the derivation of the above equations can be carried through in hypersonic flow problems (cf. Appendix of reference 1; also reference 8). However, these arguments can fail near the base of the shock wave.[9] In the present analysis, the shock wave is assumed to start from the plate leading edge (Fig. 1). Therefore, the above equations do not hold in the vicinity of the origin, $0 \leq x < \epsilon$. The flat plate possesses, in a certain sense, a fictitious curvature because of the presence of the viscous layer. It is because of the fictitious curvature effects that the terms containing dp_2/dx are retained in Eqs. (1) and (3).

The problem is then to seek the solution of the boundary-layer equations, Eqs.(1)–(3), with the appropriate boundary conditions. The conditions of no slip and heat insulation are assumed valid at the surface of the flat plate. At the outer boundary of the viscous layer, besides the usual conditions, the pressure jump condition across an oblique shock wave must be satisfied. Thus, one has the following conditions:

At $y = 0$, $u = v = 0$,

$$(\partial T/\partial y)_w = 0 \tag{4}$$

At $y = \delta$, $u = u_2$,

$$\left.\begin{aligned} (\partial u/\partial y)_\delta &= (\partial^2 u/\partial y^2)_\delta = 0 \\ \frac{p_2}{p_1} &= \frac{2\gamma}{\gamma+1}\left(M_1 \frac{d\delta}{dx}\right)^2 - \frac{\gamma-1}{\gamma+1} \end{aligned}\right\} \tag{5}$$

It may happen that the rate of decay of the shock-wave strength is such that at $x = x_0$ the shock wave already degenerates into a Mach wave. When this happens, a new phase in the interaction between the outside flow and the boundary layer begins so that the entire problem must be formulated differently.† The present problem is therefore to find the solution satisfying Eqs. (1)–(5) in the domain $0 \leq y \leq \delta$, $\epsilon < x \leq x_0$.

In the present analysis, the following simplifying assumptions are made: (1) The perfect gas law $p = R\rho T$ is assumed valid; (2) the air viscosity coefficient is a function of temperature only, and the simple law $\mu \alpha T^\omega$ is assumed; (3) the specific heat at constant pressure is assumed constant, and the Prandtl Number is assumed unity. Then, the particular energy integral

$$C_p T + (1/2)u^2 = \text{constant} \tag{6}$$

which satisfies the conditions in Eq. (4), reduces Eq. (3) identically to Eq. (1). Integrating Eqs. (1) and (2) across the boundary layer and combining the results yield the familiar momentum integral relation, which can be written as

$$\frac{\tau_w}{\rho_1 u_1^2} = \frac{d}{dx}\frac{\rho_2 u_2^2}{\rho_1 u_1^2}\int_0^\delta \frac{\rho u}{\rho_2 u_2}\left(1 - \frac{u}{u_2}\right)dy + \frac{p_1}{\rho_1 u_1^2}\frac{d}{dx}\left(\frac{p_2}{p_1}\right)\int_0^\delta \left(\frac{\rho u}{\rho_2 u_2} - 1\right)dy \tag{7}$$

By Eq. (6), one can show that

$$\frac{T}{T_2} = 1 + \frac{\gamma-1}{2} M_1^2 \frac{T_1}{T_2}\left(\frac{u_2}{u_1}\right)^2\left(1 - \frac{u^2}{u_2^2}\right)$$

which for $M_1 >> 1$ can be approximated in the layer

$$0 \leq y < \delta[1 - (\Delta_1/\delta)]$$

as

$$\frac{T}{T_2} \simeq \frac{\gamma-1}{2} M_1^2 \frac{T_1}{T_2}\left(\frac{u_2}{u_1}\right)^2\left(1 - \frac{u^2}{u_2^2}\right) \tag{8}$$

Therefore, Eq. (7) can be rewritten as

† The ratio of the shock-wave thickness X and the boundary-layer thickness δ can be expressed as[6]

$$\frac{X}{\delta} = \frac{8\gamma}{\gamma+1}\frac{\mu^*}{\rho^* u_n^* \delta}\frac{(M_{1n}^* + 1)}{(M_{1n}^* - 1)}$$

where the superscript * denotes the quantities at conditions pertaining to the critical speed of sound and the subscript n denotes the normal component to the shock-wave front. For the present problem, calculations show that, except in the region of the leading edge of the plate, $X/\delta \ll 1$ if

$$M_{1n}^* - 1 \gg M_1^{2\gamma/(1-\gamma)}$$

† One may assume that for $x > x_0$ the boundary-layer growth is so slow that the nonlinear interactions between the shock and the boundary layer appear only as higher order effects and are negligible. x_0 can therefore be designated as the "interaction distance." For $x > x_0$, the ordinary boundary-layer theory is assumed valid.

$$\frac{\tau_w}{\rho_1 u_1^2} = \frac{2}{(\gamma-1)M_1^2}\frac{d}{dx}\left[\frac{p_2}{p_1}\int_0^{\delta[1-(\Delta_1/\delta)]}\frac{\frac{u}{u_2}}{1+\frac{u}{u_2}}\,dy\right] + \frac{p_1}{\rho_1 u_1^2}\frac{d}{dx}\left(\frac{p_2}{p_1}\right)\times$$
$$\int_0^{\delta[1-(\Delta_1/\delta)]}\left[\frac{2}{(\gamma-1)M_1^2}\frac{T_2}{T_1}\left(\frac{u_1}{u_2}\right)^2\frac{\frac{u}{u_2}}{1-\left(\frac{u}{u_2}\right)^2}-1\right]dy + \frac{d}{dx}\times$$
$$\left[\frac{\rho_2 u_2^2}{\rho_1 u_1^2}\int_{\delta[1-(\Delta_1/\delta)]}^{\delta}\frac{\frac{u}{u_2}\left(1-\frac{u}{u_2}\right)}{1+\frac{\gamma-1}{2}M_1^2\frac{T_1}{T_2}\left(\frac{u_2}{u_1}\right)^2\left(1-\frac{u^2}{u_2^2}\right)}\,dy\right] + \frac{p_1}{\rho_1 u_1^2}\frac{d}{dx}\left(\frac{p_2}{p_1}\right)\times$$
$$\left[\int_{\delta[1-(\Delta_1/\delta)]}^{\delta}\frac{\frac{u}{u_2}\,dy}{1+\frac{\gamma-1}{2}M_1^2\frac{T_1}{T_2}\left(\frac{u_2}{u_1}\right)^2\left(1-\frac{u^2}{u_2^2}\right)}-\Delta_1\right] \quad (7a)$$

For $M_1 >> 1$, $\Delta_1/\delta << 1$, Eq. (7a) can finally be approximated as follows:

$$\frac{\tau_w}{\rho_1 u_1^2} = \frac{2}{(\gamma-1)M_1^2}\frac{d}{dx}\left[\frac{p_2}{p_1}\int_0^{\delta}\frac{(u/u_2)}{1+(u/u_2)}\,dy\right] - \frac{\delta}{\gamma M_1^2}\frac{d}{dx}\left(\frac{p_2}{p_1}\right) \quad (9)$$

Eq. (9) was first used by Shen[5] in his research on the viscous effects on the shock-wave shape over an insulated wedge at hypersonic speeds.

(III) Nonlinear Interactions Between the Shock Wave and the Boundary Layer

The momentum integral equation, Eq. (9), can be treated by the approximation method of Pohlhausen.[10, 11] We shall assume a velocity distribution function as follows:

$$f(y^*) = 2y^* - 2y^{*3} + y^{*4} + \frac{\Lambda(x)}{6}\,y^*(1-y^*)^3 \quad (10)$$

where $f = u/u_2$ and $y^* = y/\delta$. Except for the pressure jump condition in Eq. (5), f satisfies the following given boundary conditions:

$$f(1) = 1, \quad f'(1) = f''(1) = 0, \quad f(0) = 0$$
$$f''(0) = -\Lambda = (\delta^2/\mu_w u_1)\,(dp_2/dx)\dagger \quad (11)$$

In reference 5, Shen used a velocity profile linear in y^*, thus satisfying only two of the conditions in Eq. (11)—viz., $f(1) = 1, f(0) = 0$. Eqs. (9), (10), and (11) can be combined to yield

$$\frac{d}{dx}\left(\frac{p_2}{p_1}\delta^2\right) - \frac{2F'(\Lambda)}{1-F(\Lambda)}\frac{d\Lambda}{dx}\left(\frac{p_2}{p_1}\delta^2\right) = M_1^2\,\frac{\mu_w}{\rho_1 u_1}\left[\frac{\gamma-1}{1-F(\Lambda)}\left(2-\frac{5\Lambda}{6}\right)+\gamma\Lambda\right] \quad (12)$$

where

$$F(\Lambda) = \int_0^1 dy^*/(1+f) \quad (13)$$

and $F'(\Lambda) = dF/d\Lambda$. Integration of Eq. (12) yields

$$\frac{p_2}{p_1}\delta^2 = \frac{M_1^2\frac{\mu_w}{\rho_1 u_1}}{[1-F(\Lambda)]^2}\int_0^x [1-F(\Lambda)]^2\times\left[\frac{(\gamma-1)\left(2-\frac{5\Lambda}{6}\right)}{1-F(\Lambda)}+\gamma\Lambda\right]dx \quad (14)$$

The quantity p_2/p_1 must, moreover, satisfy the pressure jump condition mentioned in Eq. (5). Therefore, we have the following equation:

$$\frac{\gamma}{2(\gamma+1)}\left(\frac{d\eta}{dx}\right)^2 - \frac{\gamma-1}{\gamma+1}\frac{\eta}{M_1^2} = \frac{\mu_w/\rho_1 u_1}{[1-F(\Lambda)]^2}\int_0^x [1-F(\Lambda)]^2\times\left\{\frac{(\gamma-1)\,[2-(5\Lambda/6)]}{1-F(\Lambda)}+\gamma\Lambda\right\}dx \quad (15)$$

where

$$\eta = \delta^2 \quad (16)$$

† u_1 and u_2 are related across the shock wave by the relation

$$\frac{u_2}{u_1} = \left(1+\frac{v_2}{u_2}\frac{d\delta}{dx}\right)^{-1}$$

For hypersonic flow, one can take

$$u_2/u_1 = 1 - 0\,(1/M_1^2) \simeq 1$$

On the other hand, the pressure jump condition may be substituted in the last condition in Eq. (11) to yield another equation

$$\Lambda = -\frac{\gamma}{\gamma+1}\frac{M_1^2 p_1}{\mu_w u_1}\frac{d\eta}{dx}\left[\frac{d^2\eta}{dx^2} - \frac{1}{2\eta}\left(\frac{d\eta}{dx}\right)^2\right] \quad (17)$$

The problem is to find Λ and η satisfying Eqs. (15) and (17) simultaneously. η is the boundary-layer thickness function, while Λ is essentially the shock-wave pressure function. Eqs. (15) and (17) show the interdependence of the growth of the boundary layer and the decay of the shock wave. The nonlinear interaction characteristics are clearly exhibited.

(IV) Approximate Solutions of the Basic Equations

To deal with the dual relations in Eqs. (15) and (17) exactly as they stand, one may eliminate Λ between them to obtain one equation defining η. The resulting equation is, however, nonlinear, a rigorous treatment of which would be extremely tedious and difficult.

For hypersonic flow, $M_1 \gg 1$, we shall consider the following approximate equations instead:

$$\frac{\gamma}{2(\gamma+1)}\left(\frac{d\eta}{dx}\right)^2 = \frac{\mu_w/\rho_1 u_1}{[1-F(\Lambda)]^2} \times \int_0^x [1-F(\Lambda)]^2 \left\{\frac{(\gamma-1)\,[2-(5\Lambda/6)]}{1-F(\Lambda)} + \gamma\Lambda\right\} dx \quad (15a)$$

$$\Lambda = -\frac{\gamma}{\gamma+1}\frac{M_1^2 p_1}{\mu_w u_1}\frac{d\eta}{dx}\left[\frac{d^2\eta}{dx^2} - \frac{1}{2\eta}\left(\frac{d\eta}{dx}\right)^2\right] \quad (17)$$

The omission of the term $-[(\gamma-1)/(\gamma+1)]\,(\eta/M_1^2)$ can be justified *a posteriori* in a certain limited range of x's [cf. Section (V)]. Notice that some of the nonlinearity properties of Eqs. (15) and (17) have been preserved; the treatment of the approximate system should provide an initial step toward the understanding of the exact system. From Eq. (15a), η is easily obtained as follows:

$$\eta = \left[\frac{2(\gamma+1)}{\gamma}\frac{\mu_w}{\rho_1 u_1}\right]^{1/2} \int_0^x [1-F(\Lambda)]^{-1}\left(\int_0^{x_1}[1-F(\Lambda)]^2\left\{\frac{(\gamma-1)\,[2-(5\Lambda/6)]}{1-F(\Lambda)} + \gamma\Lambda\right\}dx_2\right)^{1/2} dx_1 \quad (18)$$

It can be verified that $\Lambda = \Lambda_0 =$ constant satisfies Eqs. (17) and (18) simultaneously. The constant Λ_0 must satisfy the following equation:

$$\gamma\Lambda_0 = \frac{(\gamma-1)\,[2-(5\Lambda_0/6)]}{1-F(\Lambda_0)} \quad (19)$$

Eq. (18) can be then evaluated as follows:

$$\eta_0 = \frac{4}{3}\left[(\gamma+1)\frac{\mu_w \Lambda_0}{\rho_1 u_1}\right]^{1/2} x^{3/2} \quad (20)$$

By Eq. (8), μ_w/μ_1 can be expressed as

$$\frac{\mu_w}{\mu_1} \simeq \left(\frac{\gamma-1}{2}M_1^2\right)^{\omega}$$

Thus, the boundary-layer growth follows the following approximate law:

$$\frac{\delta_0}{x} = \frac{2}{\sqrt{3}}(\gamma+1)^{1/4}\left(\frac{\gamma-1}{2}\right)^{\omega/4}\Lambda_0^{1/4} M_1^{\omega/2} R_{1x}^{-1/4} \quad (21)$$

It can easily be shown that

$$\frac{d\delta_0}{dx} = \frac{\sqrt{3}}{2}(\gamma+1)^{1/4}\left(\frac{\gamma-1}{2}\right)^{\omega/4}\Lambda_0^{1/4} M_1^{\omega/2} R_{1x}^{-1/4} \quad (22)$$

In Eq. (22), $d\delta_0/dx$ is the approximate slope of the shock wave, which, as assumed, forms the outer boundary of the viscous layer. The result indicates that as x increases the slope of the shock wave decreases according to $x^{-1/4}$. At $x = \hat{x}_0$, the shock wave will eventually be parallel to the local Mach wave direction such that

$$\left(\frac{d\delta_0}{dx}\right)_{\hat{x}_0} = \frac{1}{M_1} = \frac{\sqrt{3}}{2}(\gamma+1)^{1/4}\left(\frac{\gamma-1}{2}\right)^{\omega/4} \times \Lambda_0^{1/4} M_1^{\omega/2} R_1^{-1/4}\left(\frac{L}{\hat{x}_0}\right)^{1/4} \quad (23)$$

The "interaction distance" $\hat{x}_0$ can, therefore, be given as follows:

$$\frac{\hat{x}_0}{L} = \frac{9}{16}(\gamma+1)\left(\frac{\gamma-1}{2}\right)^{\omega}\Lambda_0 \frac{M_1^{2\omega+4}}{R_1} \quad (23a)$$

The approximate law of the decay of the shock wave can also be expressed in terms of p_2/p_1 as a function of x. By Eq. (11), it is seen that, for $x \leq \hat{x}_0$,

$$\left(\frac{\delta}{L}\right)^2\frac{d(p_2/p_1)}{d(x/L)} = -\left(\frac{\gamma-1}{2}\right)^{\omega}\gamma\Lambda_0\frac{M_1^{2(\omega+1)}}{R_1} = \text{constant} \quad (24)$$

Moreover, for the present approximation, Eq. (12) becomes simply

$$\frac{d}{d(x/L)}\left(\frac{p_2}{p_1}\frac{\delta^2}{L^2}\right) = \left(\frac{\gamma-1}{2}\right)^{\omega} 2\gamma\Lambda_0 \frac{M_1^{2(\omega+1)}}{R_1} \quad (25)$$

Combining Eqs. (24) and (25) yields

$$\frac{p_2}{p_1} = \frac{3\gamma}{2(\gamma+1)^{1/2}}\left(\frac{\gamma-1}{2}\right)^{\omega/2}\Lambda_0^{1/2}\frac{M_1^{\omega+2}}{R_1^{1/2}}\frac{1}{(x/L)^{1/2}} \quad (26)$$

Therefore, the shock-wave pressure jump is varying inversely to $x^{1/2}$. As the distance from the plate leading edge increases, the shock wave must become weaker. Theoretically, when $x = \hat{x}_0$, the shock-wave angle becomes the Mach-wave angle and the pressure ratio p_2/p_1 should become unity. Substitution of $\hat{x}_0/L$ from Eq. (23a) in Eq. (26) gives, however, the result

$$\left(\frac{p_2}{p_1}\right)_{\hat{x}_0} = \frac{2\gamma}{\gamma + 1} = 1.17$$

This conclusion is not surprising because our approximate equation, Eq. (15a), is strictly compatible only with the approximate shock-wave condition that

$$\frac{p_2}{p_1} = \frac{2\gamma}{\gamma + 1}\left(M_1 \frac{d\delta}{dx}\right)^2$$

(V) Correction Functions by Linearized Equations

The approximate solutions in the preceding section are based on the approximate system of equations, Eqs. (15a) and (17). It is of interest to show in what range of values of x the approximations are valid. This, indeed, can be demonstrated by the following considerations: By the approximate results of the last section, we have

$$-\frac{\gamma - 1}{\gamma + 1}\frac{\eta_0}{M_1^2} = 0\left[\left(\frac{\mu_w}{\rho_1 u_1}\Lambda_0\right)^{1/2}\frac{x^{3/2}}{M_1^2}\right]$$

$$\frac{\mu_w/\rho_1 u_1}{[1 - F(\Lambda_0)]^2}\int_0^x [1 - F(\Lambda_0)]^2 \times \left\{\frac{(\gamma - 1)\,[2 - (5\Lambda_0/6)]}{1 - F(\Lambda_0)} + \gamma\Lambda_0\right\} dx = 0\left(\frac{\mu_w}{\rho_1 u_1}\Lambda_0 x\right)$$

Therefore, the approximate equation, Eq. (15a), implies that

$$x^{1/2}/M_1^2 \ll [(\mu_w/\rho_1 u_1)\Lambda_0]^{1/2}$$

In other words, the approximate solutions are valid in such range of x's that

$$x/L \ll M_1^{2(\omega+2)}\Lambda_0/R_1 \tag{27}$$

Hence, as $x \to \hat{x}_0$ [cf. Eq. (23a)], the approximate solution will be in error. However, results in the last section do show that the error involved will not be serious. An indication of this fact is that the value of p_2/p_1 at $\hat{x}_0$ on the basis of the approximate results deviates only about 17 per cent from its theoretically true value.

To provide a remedy, we must consider the exact system of equations, Eqs. (15) and (17). As a pair of corrections to the approximate results, we may introduce the functions $\Delta\eta$ and $\Delta\Lambda$ so that they satisfy the following equations:

$$\eta = \eta_0 + \Delta\eta \tag{28}$$

$$\Lambda = \Lambda_0 + \Delta\Lambda \tag{29}$$

$$\frac{\gamma}{2(\gamma + 1)}\left(\frac{d\eta}{dx}\right)^2 - \frac{\gamma - 1}{\gamma + 1}\frac{\eta_0}{M_1^2} = \frac{\mu_w}{\rho_1 u_1}\frac{1}{[1 - F(\Lambda)]^2} \times \int_0^x [1 - F(\Lambda)]^2 \left\{\frac{(\gamma - 1)\,[2 - (5\Lambda/6)]}{1 - F(\Lambda)} + \gamma\Lambda\right\} dx \tag{30}$$

$$\Lambda = -\frac{\gamma}{\gamma + 1}\frac{M_1^2 p_1}{\mu_w u_1}\frac{d\eta}{dx}\left[\frac{d^2\eta}{dx^2} - \frac{1}{2\eta}\left(\frac{d\eta}{dx}\right)^2\right] \tag{31}$$

Assume that the correction functions are small so that the second and higher degree terms in $\Delta\eta$ and $\Delta\Lambda$ and their derivatives can be neglected. Thus, we arrive at a pair of dual relations linear in $\Delta\eta$ and $\Delta\Lambda$ as follows:

$$\frac{\gamma}{\gamma + 1}\left(\frac{d\eta_0}{dx}\right)\frac{d(\Delta\eta)}{dx} - \frac{\gamma - 1}{\gamma + 1}\frac{\eta_0}{M_1^2} = \frac{\mu_w}{\rho_1 u_1}\left(2\alpha\left[\frac{(\gamma - 1)[2 - (5\Lambda_0/6)]}{1 - F(\Lambda_0)} + \gamma\Lambda_0\right]x(\Delta\Lambda) + \left\{\gamma(1 - 2\alpha\Lambda_0) + \frac{(\alpha + \beta)\,(\gamma - 1)\,[2 - (5\Lambda_0/6)]}{1 - F(\Lambda_0)}\right\}\int_0^x \Delta\Lambda dx\right) \tag{32}$$

$$\Delta\Lambda = -\frac{\gamma}{\gamma + 1}\frac{M_1^2 p_1}{\mu_w u_1}\left\{\frac{d\eta_0}{dx}\frac{d^2(\Delta\eta)}{dx^2} + \left[\frac{d^2\eta_0}{dx^2} - \frac{3}{2\eta_0}\left(\frac{d\eta_0}{dx}\right)^2\right]\frac{d(\Delta\eta)}{dx} + \frac{1}{2\eta_0^2}\left(\frac{d\eta_0}{dx}\right)^3(\Delta\eta)\right\} \tag{33}$$

where

$$\alpha = \frac{(dF/d\Lambda)_{\Lambda_0}}{1 - F(\Lambda_0)}, \quad \beta = \frac{5}{6[2 - (5\Lambda_0/6)]} \tag{34}$$

Eqs. (32) and (33) can readily be solved. The results are

$$\Delta\eta = \frac{8(\gamma - 1)\,x^2}{3\gamma[7 - (\beta + 5\alpha)\Lambda_0]M_1^2} \tag{35}$$

$$\Delta\Lambda = \frac{2(\gamma - 1)}{\gamma + 1}\frac{p_1}{\mu_w u_1}\frac{[(\gamma + 1)\Lambda_0(\mu_w/\rho_1 u_1)]^{1/2}}{[7 - (\beta + 5\alpha)\Lambda_0]}x^{1/2} \tag{36}$$

Hence, we have

$$\eta = x^2\left\{\frac{4}{3}\left[(\gamma + 1)\left(\frac{\gamma - 1}{2}\right)^{\omega}\Lambda_0\frac{M_1^{2\omega}}{R_1}\right]^{1/2} \times \left(\frac{x}{L}\right)^{-1/2} + \frac{8(\gamma - 1)}{3\gamma[7 - (\beta + 5\alpha)\Lambda_0]M_1^2}\right\} \tag{37}$$

$$\Lambda = \Lambda_0 + \frac{2(\gamma-1)}{\gamma M_1^2}\left[7 - (\beta + 5\alpha)\Lambda_0\right]^{-1} \times \left[\frac{\Lambda_0}{\gamma+1}\frac{R_1}{\left(\frac{\gamma-1}{2}M_1^2\right)^{\omega}}\frac{x}{L}\right]^{1/2} \quad (38)$$

Evidently, for $x/L \ll M_1^{2(\omega+2)}\Lambda_0/R_1$, the second term in each of the above equations, Eqs. (37) and (38), represents a small correction as expected. The importance of the correction terms gradually increases as

$$x/L \to M_1^{2(2+\omega)}\Lambda_0/R_1$$

For

$$\frac{x}{L} \gg \frac{M_1^{2(2+\omega)}\Lambda_0}{R_1} = 0\left(\frac{\dot{x}_0}{L}\right)$$

the correction terms actually dominate; to be sure, for such cases, the above linearization process should fail. Nevertheless, it is interesting to observe that, even as $x \to \infty$, we get, from Eq. (37), $\delta/x = 0(1/M_1)$, which is consistent with the definition of the hypersonic shock régime [cf. Section (I)].

(VI) Value of Λ_0

Before we carry on the computations any further, we must first determine the value of Λ_0. In order to do this, the function $F(\Lambda)$ defined in Eq. (13) must be computed for different Λ's. Evaluation of the integral $F(\Lambda)$ has been performed analytically† with the results shown in Table 1. These values of $F(\Lambda)$ have also been independently checked by numerical integration methods. On the basis of these values of $F(\Lambda)$, the value of Λ_0 satisfying Eq. (19) is found to be

$$\Lambda_0 = 0.91 \quad (39)$$

Table 1
Values of $F(\Lambda)$

Λ	$F(\Lambda)$	Λ	$F(\Lambda)$
0.2	0.6106	0.8	0.6085
0.4	0.6101	1.00	0.6087
0.6	0.6092	...	...

(VII) Growth of the Boundary Layer and Decay of the Shock Wave

On the basis of the result in Eq. (37), the growth of the viscous layer downstream follows the following law:

$$\frac{\delta}{L} = \Sigma^{1/3}\left(\frac{x}{L}\right)^{3/4}\left[1 + \frac{\sigma}{\Sigma}\left(\frac{x}{L}\right)^{1/2}\right]^{1/2} \quad (40)$$

where, for brevity, the symbols

$$\Sigma = \frac{4}{3}\left[(\gamma+1)\left(\frac{\gamma-1}{2}\right)^{\omega}\Lambda_0\frac{M_1^{2\omega}}{R_1}\right]^{1/2} \quad (41)$$

† Analytical formula for $F(\Lambda)$ is given in reference 1.

$$\sigma = \frac{8(\gamma-1)}{3\gamma[7 - (\beta+5\alpha)\Lambda_0]\,M_1^2} \quad (42)$$

are introduced. The slope of the shock wave can then be given as follows:

$$\frac{d\delta}{dx} = \frac{3}{4}\frac{\Sigma^{1/2}}{\left(\frac{x}{L}\right)^{1/4}}\frac{\left[1 + \frac{4}{3}\frac{\sigma}{\Sigma}\left(\frac{x}{L}\right)^{1/2}\right]}{\left[1 + \frac{\sigma}{\Sigma}\left(\frac{x}{L}\right)^{1/2}\right]^{1/2}} \quad (43)$$

On taking $\sigma = 0$, Eqs. (40) and (43) become Eqs. (21) and (22), respectively. For

$$0 < (\sigma/\Sigma)\,(x/L)^{1/2} < 1$$

Eqs. (40) and (43) can be expanded as the following series:

$$\frac{\delta}{L} = \Sigma^{1/}\left(\frac{x}{L}\right)^{3/4}\left[1 + \frac{1}{2}\frac{\sigma}{\Sigma}\left(\frac{x}{L}\right)^{1/2} - \frac{1}{8}\frac{\sigma^2}{\Sigma^2}\frac{x}{L} + \ldots\right] \quad (40a)$$

$$\frac{d\delta}{dx} = \frac{3}{4}\frac{\Sigma^{1/2}}{(x/L)^{1/4}}\left[1 + \frac{5}{6}\frac{\sigma}{\Sigma}\left(\frac{x}{L}\right)^{1/2} - \frac{7}{24}\frac{\sigma^2}{\Sigma^2}\frac{x}{L} + \ldots\right] \quad (43a)$$

It is interesting to point out that in Eq. (47) of reference 5, Shen obtained a series solution rather characteristically similar to Eq. (40a). However, Shen was *not* able to sum his series and obtain a formula like Eq. (40). We also see from Eq. (43a) that Eq. (22) underestimates the slope of the shock wave. A new "interaction distance," x_0, can be found by setting $d\delta/dx$ in Eq. (43) equal to $1/M_1$.

$$\frac{x_0}{L} = \frac{81}{16}\Sigma^2 M_1^4\left[2 - 3\sigma M_1^2 + (4 - 3\sigma M_1^2)^{1/2}\right]^{-2} \quad (44)$$

When $\sigma = 0$, we have $x_0/L = \hat{x}_0/L$ as given in Eq. (23a). It can be shown that the pressure jump function p_2/p_1, obtained from substituting Eq. (43) into the oblique shock relation in Eq. (5), reduces approximately to the form of Eq. (26). To compute $(p_2/p_1)_{x_0}$ we have the simple relation

$$\left(\frac{p_2}{p_1}\right)_{x_0} = \frac{\gamma}{2(\gamma+1)}\left(2 - 3\sigma M_1^2 + (4 - 3\sigma M_1^2)^{1/2}\right) \quad (45)$$

Notice that $3\sigma M_1^2$ is, by Eq. (42), a function independent of M_1. For $\Lambda_0 = 0.91$, $\gamma = 1.4$, the numerical value of $(p_2/p_1)_{x_0}$ computed on the basis of Eq. (45) is 1.0147. Since this value deviates by only 1.5 per cent from the theoretical value of unity, the correction procedure devised in Section (V) can be considered as satisfactory. Thus, at $x = x_0$ defined in Eq. (44), the present method yields solutions that fulfill the simultaneous requirements that $(d\delta/dx)_{x_0} = 1/M_1$ and $(p_2/p_1)_{x_0} = 1.0$.

(VIII) Average Skin-Friction Coefficient on an Insulated Flat Plate

In Figs. 2 and 3, curves of $\hat{x}_0/L$ and x_0/L have been plotted, according to Eqs. (23a) and (44), respectively, against M_1 for $R_1 = 10^6$, 10^7, and 10^8. In computing these values we take $\gamma = 1.4$, $\omega = 0.768$, and $\Lambda_0 = 0.91$. It is seen from these figures that the "interaction distance" at the lower Mach Numbers are of insignificant proportion; however, as the Mach Number increases, the "interaction distance" grows rapidly. The rate of growth of the "interaction distance" depends on the Reynolds Number of the flat plate; at the lower Reynolds Number, this rate grows noticeably faster. Therefore, at a fixed Reynolds Number, the shock-wave effects are extended farther downstream as the Mach Number increases; at extremely high Mach Numbers, the shock wave, so to speak, wraps itself on the entire flat plate, $x_0/L \geq 1$. On the other hand, at a fixed Mach Number, the viscous effects on the shock wave are much more pronounced, as expected, when the Reynolds Number is low. To ensure the validity of the initial assumption of continuum flow, it is important to impose a certain restriction on the relative magnitudes of the Reynolds Number and the Mach Number such as the criterion of nonslip flow proposed by Tsien[12]—viz., $M_1/R_1^{1/2} < 1/100$.

The hypersonic viscous flow over a flat plate, according to the present theory, can then be pictured as in Fig. 4. Thus, the average skin-friction coefficient on the flat plate can be computed by the following formula:

$$C_F = (x_0/L)\, C_{F_s} + [1 - (x_0/L)]\, C_{F_t} \tag{46}$$

where

$$C_{F_s} = \frac{1}{x_0} \int_0^{x_0} C_{f_s}\, dx \tag{47}$$

$$C_{F_t} = \frac{1}{L - x_0} \int_{x_0}^{L} C_{f_t}\, dx \tag{48}$$

where C_{f_s} and C_{f_t} are, respectively, the local skin-friction coefficients in the hypersonic shock-flow region ($x \leq x_0$) and the conventional boundary-layer flow region ($x_0 < x \leq L$).† From the present results, we have

$$C_{f_s} = \left(\frac{\gamma - 1}{2} M_1^2\right)^{\omega} \frac{2}{R_1} \left[2 + \frac{\Lambda_0}{6}\left(1 + \frac{\sigma}{\Sigma}\sqrt{\frac{x}{L}}\right)\right] \times \left[\Sigma^{1/2}\left(\frac{x}{L}\right)^{3/4}\left(1 + \frac{\sigma}{\Sigma}\sqrt{\frac{x}{L}}\right)^{1/2}\right]^{-1} \tag{49}$$

By von Kármán's results,[13] we take

$$C_{f_t} = \frac{1}{2}\sqrt{8f(\theta)}\, \frac{1}{R_1^{1/2}} \left(\frac{\gamma - 1}{2}\right)^{(\omega-1)/2} M_1^{\omega-1} \left(\frac{x}{L}\right)^{-1/2} \tag{50}$$

where $\sqrt{8f(\theta)} = 1.57$. Substitution of these values in Eqs. (46)–(48) yields, after simple calculations, the following formula:

† For convenience sake, it is assumed here that C_{f_s} of the present theory applies also in the leading-edge region.

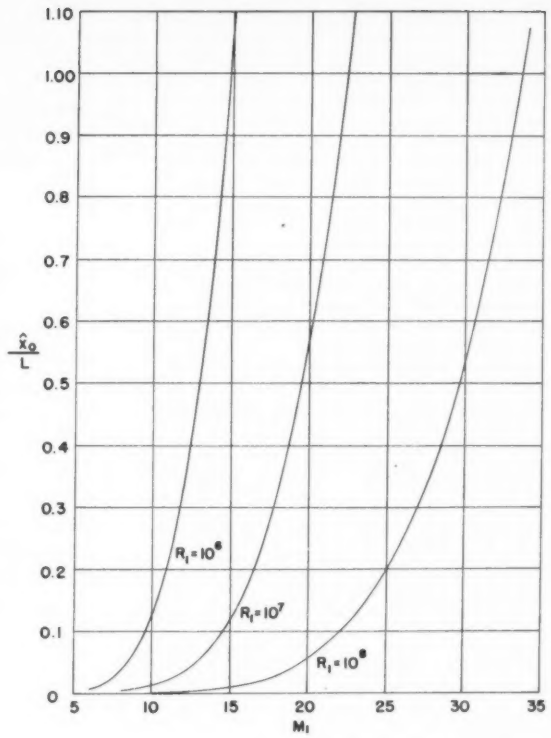

FIG. 2 — INTERACTION DISTANCE RATIO vs MACH NUMBER

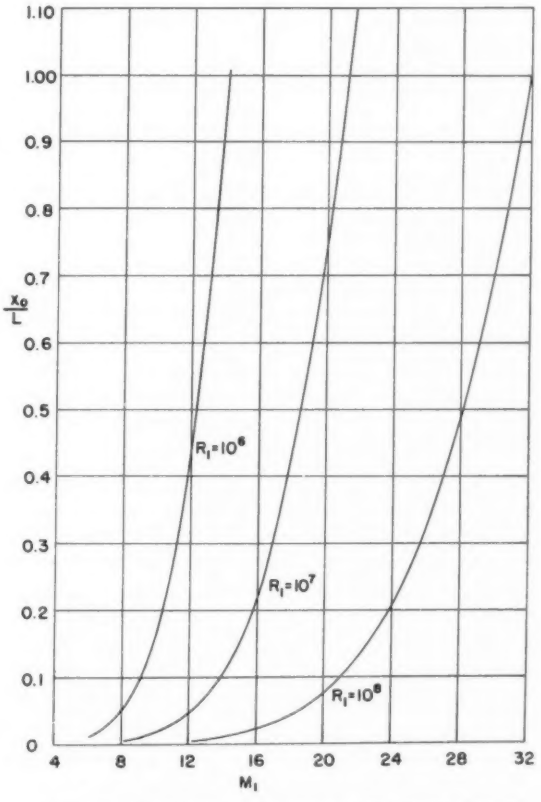

FIG. 3 — INTERACTION DISTANCE RATIO vs MACH NUMBER

$$C_F = 2\left(\frac{\gamma-1}{2}M_1^2\right)^{\omega} R_1^{-1}\Sigma^{-1/2}\left[\frac{\Lambda_0}{3}\left(\sqrt{\frac{x_0}{L}}+\frac{\sigma}{\Sigma}\frac{x_0}{L}\right)^{1/2}+\left(\frac{\sigma}{\Sigma}\right)^{-1/2}\left(4+\frac{\Lambda_0}{6}\right)\times\right.$$
$$\left.\left\{\log\left[1+2\sqrt{\frac{\sigma}{\Sigma}}\left(\sqrt{\frac{\sigma}{\Sigma}\frac{x_0}{L}}+\sqrt{\sqrt{\frac{x_0}{L}}+\frac{\sigma}{\Sigma}\frac{x_0}{L}}\right)\right]\right\}\right]+1.57\left(\frac{\gamma-1}{2}\right)^{(\omega-1)/2} M_1^{\omega-1} R_1^{-1/2}\left(1-\sqrt{\frac{x_0}{L}}\right) \quad (46a)$$

which, for $\sigma = 0$, becomes

$$C_F = 1.57\left(\frac{\gamma-1}{2}\right)^{(\omega-1)/2} R_1^{-1/2} M_1^{\omega-1}+\left[6\left(2+\frac{\Lambda_0}{6}\right)-\frac{3}{4}\times 1.57\left(\frac{\gamma+1}{\gamma-1}2\Lambda_0\right)^{1/2}\right]\left(\frac{\gamma-1}{2}\right)^{\omega} R_1^{-1} M_1^{2\omega+1} \quad (46b)$$

Without the second term on the right-hand side, Eq. (46b) simply gives von Kármán's approximate C_F formula. Therefore, the shock-wave effects on C_F are to contribute a certain correction function depending on Λ_0, M_1, and R_1 as in Eqs. (46a) and (46b). In the above calculations, it is assumed that the hypersonic shock wave is of such a strength that it becomes a Mach wave before arriving at the plate trailing edge. Therefore, Eqs. (46a) and (46b) apply, respectively, for the cases $x_0/L \leq 1$ and $\hat{x}_0/L \leq 1$.

Consider, for example, the diagram of x_0/L for the case of $R_1 = 10^7$ in Fig. 3. As M_1 increases beyond 10, x_0/L grows rapidly. Eventually, at $M_1 = 21$, we find $x_0/L = 1$. The condition of continuum flow is violated when M_1 becomes 32. In the range of hypersonic Mach Numbers, $21 \leq M_1 \leq 32$, we therefore could anticipate that $x_0/L \geq 1$—i.e., the hypersonic shock tends to wrap itself on the entire length of the flat plate (Fig. 4a). For such cases, the average skin-friction coefficient on the flat plate can be simply given as

$$C_F = \frac{1}{L}\int_0^L C_{f_x}\, dx \quad (51)$$

Substituting Eq. (49) in Eq. (51) and reducing yield the following formula:

$$C_F = 2\left(\frac{\gamma-1}{2}M_1^2\right)^{\omega} R_1^{-1}\Sigma^{-1/2}\left(\frac{\Lambda_0}{3}\left(1+\frac{\sigma}{\Sigma}\right)^{1/2}+\left(4+\frac{\Lambda_0}{6}\right)\left(\frac{\sigma}{\Sigma}\right)^{-1/2}\times\right.$$
$$\left.\left\{\log\left[1+2\sqrt{\frac{\sigma}{\Sigma}}\left(\sqrt{\frac{\sigma}{\Sigma}}+\sqrt{1+\frac{\sigma}{\Sigma}}\right)\right]\right\}\right) \quad (51a)$$

which, for $\sigma = 0$, becomes

$$C_F = 4\sqrt{3}\left(2+\frac{\Lambda_0}{6}\right)\left(\frac{\gamma-1}{2}\right)^{3\omega/4}(\gamma+1)^{-1/4}\Lambda_0^{-1/4} R_1^{-3/4} M_1^{3\omega/2} \quad (51b)$$

Eqs. (51a) and (51b) apply, respectively, for the cases $x_0/L \geq 1$ and $\hat{x}_0/L \geq 1$.

(IX) Discussions

Before we discuss the numerical results, it seems worth while to retrace the development of the present theory in order to bring out its limitations. The hypothesis has been made that the space between the flat-plate surface and the shock wave is filled up with a viscous laminar flow, which is adequately described by the compressible boundary-layer equations. Assuming, in this viscous layer, a plausible velocity distribution function that satisfies the proper boundary conditions and making use of the pressure jump relation at the oblique shock-wave front, we derive a pair of dual relations characterizing the nonlinear interactions between the shock wave and the boundary layer. A pair of approximate relations is then derived in which some important nonlinearities are preserved. Solutions are accordingly obtained on the basis of the approximate system. For a fair evaluation of the significance of the solutions thus found, the following questions must be answered: (1) Are the compressible

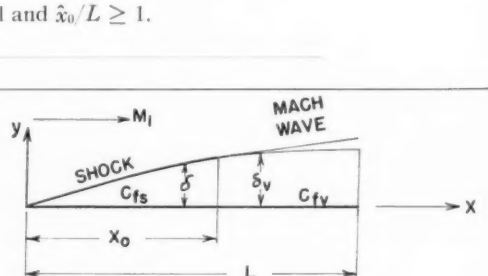

FIG. 4 – HYPERSONIC SHOCK PARTIALLY COVERS THE FLAT PLATE

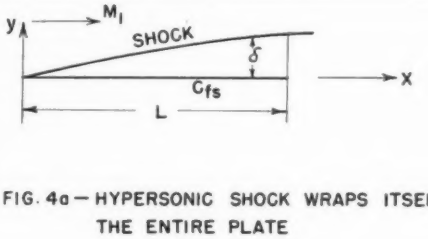

FIG. 4a – HYPERSONIC SHOCK WRAPS ITSELF ON THE ENTIRE PLATE

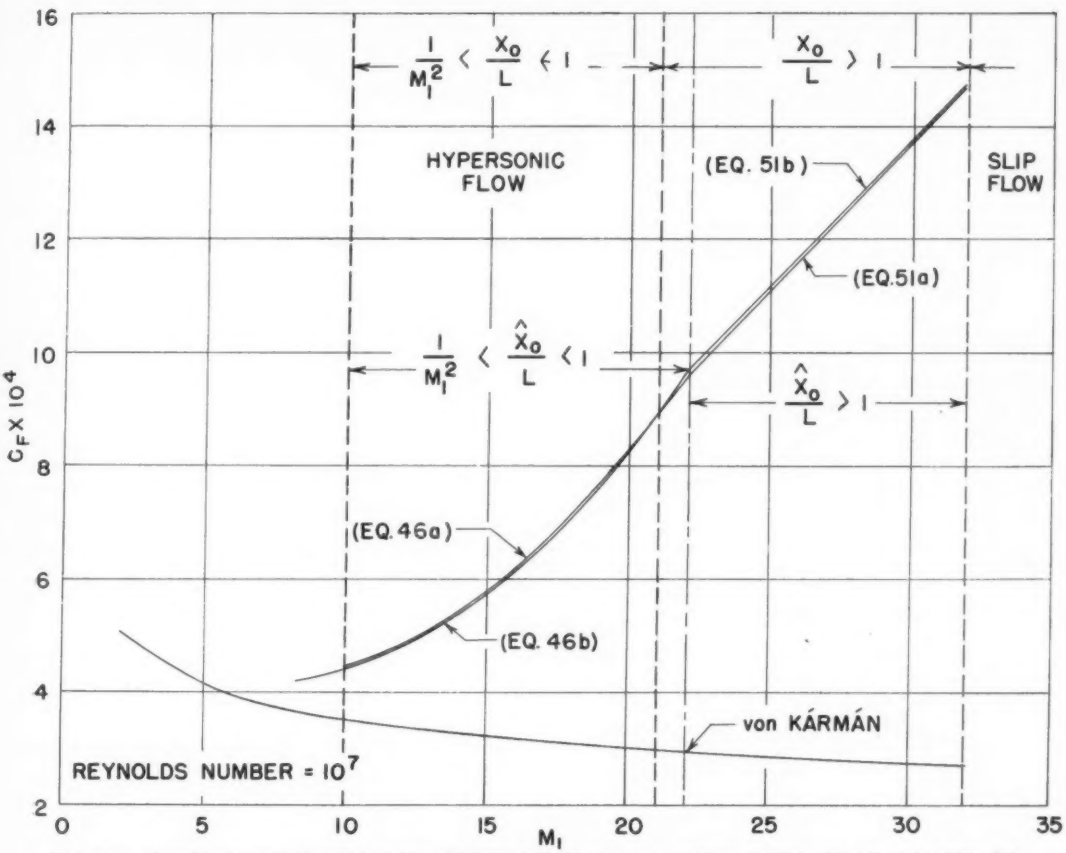

FIG. 5 — AVERAGE SKIN FRICTION COEFFICIENT ON AN INSULATED FLAT PLATE AT HYPERSONIC MACH NUMBERS

boundary-layer equations valid in the hypersonic viscous régime as postulated above? (2) How are the solutions affected by the choice of the velocity distribution function?

We have shown that the postulated hypersonic viscous régime can be defined such that $\delta/x = 0(1/M_1)$. It can be shown (Appendix of reference 1), by the familiar order of magnitude arguments, that Eqs. (1)–(3) are consistent with this definition of hypersonic régime. To be specific, we have essentially neglected terms of $0(1/M_1^2)$ in these equations. This is, indeed, consistent with the simplification introduced in Eq. (9). Hence, we may conclude that our answer to the first question above is affirmative. In an interesting paper by Lees and Probstein,[14] however, the opinion was expressed that Eqs. (1)–(3) are probably not valid in the region close to the leading edge where the shock wave coincides with the outer edge of the viscous layer. While we must admit that the present theory breaks down entirely in the leading-edge region, our results seem to indicate that the postulated type of hypersonic viscous régime may exist, at very high Mach numbers and a fixed Reynolds Number, over a large portion of the plate surface outside the leading-edge region (Figs. 2 and 3) where Eqs. (1)–(3) are expected to be valid.

The second question above is concerning the uniqueness of the solutions. We know that the values of δ, $d\delta/dx$, and p_2/p_1 obtained by the present method vary over a range with varying assumptions about the form of u/u_2. Computations using a quadratic velocity profile,† for example, yield a value of $\Lambda_0 = 0.606$, which is about two-thirds of the value used in the present paper. However, we found that the functional forms of the solutions are not affected by this choice of the quadratic (u/u_2)-function. Furthermore, we shall point out that, although the present analysis is formulated with the explicit condition $\Lambda_0 \neq 0$, nevertheless, some of our results have the same analytical forms as previously obtained by Shen.[5] Therefore, it seems appropriate to say that the analytical nature of the solutions is little affected, while their numerical values are really affected by the choice of the velocity distribution function. The quartic velocity profile has been chosen for the present calculations because it appears, from past experience with low-speed boundary-layer flow, that no

† The boundary conditions $f(1) = 1$, $f(0) = 0$ and $f''(0) = -\Lambda$ are satisfied.

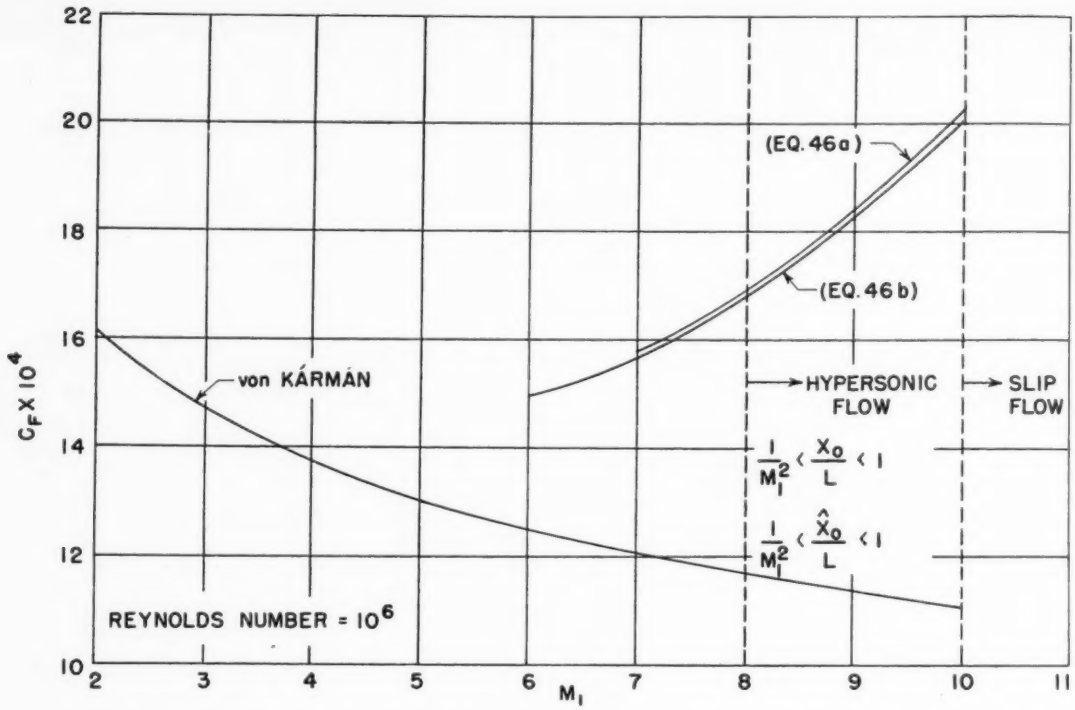

FIG. 6 — AVERAGE SKIN FRICTION COEFFICIENT ON AN INSULATED FLAT PLATE AT HYPERSONIC MACH NUMBERS

TABLE 2
Values of C_F at Various M_1 for Fixed R_1

$R_1 = 10^6$				$R_1 = 10^7$					
M_1	C_F [Eq. (46b)]	C_F [Eq. (46a)]	C_F von Kármán	M_1	C_F [Eq. (46b)]	C_F [Eq. (46a)]	C_F [Eq. (51b)]	C_F [Eq. (51a)]	C_F von Karman
6	0.00149	....	0.001249						
7	0.001569	0.001577	0.001205						
8	0.001679	0.001690	0.001168	8	0.000420	....	....	....	0.000369
9	0.001825	0.001841	0.001138	9	0.000428	....	....	....	0.000359
10	0.002009	0.002028	0.001109	10	0.000441	0.000443	....	....	0.000359
				12	0.000479	0.000482	....	....	0.000336
				16	0.000611	0.000617	....	....	0.000315
				20	0.000822	0.000831	....	....	0.000299
				22.132	0.000966	....	....	0.000957	0.000292
				26	....	....	0.001164	0.001144	0.000281
				28	....	....	0.001268	0.001261	0.000276
				30	....	....	0.001372	0.001366	0.000272
				32	....	....	0.001478	0.001473	0.000268

great improvement in accuracy was gained by considering the velocity profile as a polynomial of higher degree.

It seems, therefore, that the use of the momentum integral method in the manner outlined in the present report, which has the great merit of being comparatively easy, may be expected to give a fairly satisfactory estimate of the interaction effects between the shock wave and the boundary layer at very high Mach Numbers. The Mach Number range in which the present analysis appears reasonable must be such that (i)

$$\frac{x_0}{L} = 0\left(\frac{M_1^{2\omega+4}}{R_1}\right) > \frac{1}{M_1^2}$$

and (ii)

$$M_1/R_1^{1/2} < 1/100$$

The first criterion implies that we are only considering the effects of such hypersonic shock waves as have a persistence over a length at least of the order of $1/M_1^2$.† The second criterion is necessary to avoid the use of new boundary conditions pertaining to slip flow.

The above discussions describe the limitations of the present theory. Within the hypersonic Mach Number range defined above, we shall calculate the variation of C_F with M_1 for fixed R_1 by the formulas in Eqs. (46a),

† The ϵ-neighborhood of the leading edge mentioned on page 346 has thus been given a specific definition.

(46b), (51a), and (51b). The calculations are performed for the cases $R_1 = 10^6$ and 10^7, with $\gamma = 1.4$, $\omega = 0.768$, $\Lambda_0 = 0.91$. Figs. 5 and 6 show the results thus obtained, which are also tabulated in Table 2. In these figures, C_F data on the basis of von Kármán's approximate formula[13] are also given. It is clearly seen that, in the hypersonic speed range, the effects of the shock wave on the C_F of the plate certainly cannot be neglected. Attention should be drawn to the strong indication that, contrary to the conventional theory, which predicts a steady decrease in C_F as M_1 increases, the present results predict a steady increase of C_F with M_1.

It is tempting to draw conclusions about the percentage rise of skin-friction drag on a flat plate due to the hypersonic shock effects. However, besides the possible inherent inaccuracy due to the assumed velocity profile, our numerical answers almost certainly suffer more or less from the various simplifying assumptions such as (1) $Pr = 1$, (2) $\gamma = 1.4$, and (3) $\omega = 0.768$. In the large temperature range anticipated under free-flight conditions, none of these assumptions is expected to be true, and further complications arising from effects of dissociation and ionization may also begin to occur. But, in the test section of a hypersonic wind tunnel where the perfect gas conditions are not greatly violated, these assumptions are satisfactory. Therefore, the numerical data in Figs. 5 and 6 can be regarded as preliminary estimates of the hypersonic shock-wave effects. More realistic conclusions of a quantitative nature probably should be deferred until more experimental facts are gathered in the Mach Number range of 8 to 15 and higher.

Lees and Probstein[14] recently predicted a similar increase in the skin friction at hypersonic speeds. Their method of approach and basic assumptions are quite different. The qualitative agreement of the two theories in this respect is rather encouraging.

For $x_0/L \leq 1$, the present theory must admit the coexistence of a hypersonic shock-flow régime with an ordinary boundary-layer flow régime over the flat plate (Fig. 4). The joining together of these two régimes must be accomplished through a transitional region. The present method is not suitable for exploring this transitional phenomena. Indeed, for the Mach Number range corresponding to $x_0/L < 1$, the method of Lees and Probstein probably yields more dependable results.

For $x_0/L \geq 1$, the hypersonic shock régime takes over the entire plate surface. The interaction phenomena between the shock wave and the boundary layer are believed to be more realistically represented by the present approach. Therefore, for the Mach Number range corresponding to $x_0/L \geq 1$, the simpler method as presented in the present paper should yield satisfactory results.

Examination of the shock-wave effects on the skin friction of a noninsulated flat plate at hypersonic speeds is reserved for a later paper. The corresponding effects on the rate of heat transfer across the plate surface have been shown to be rather small.[14]

References

[1] Li, T. Y., and Nagamatsu, H. T., *Shock Wave Effects on the Laminar Skin Friction of an Insulated Flat Plate at Hypersonic Speeds*, GALCIT Hypersonic Wind Tunnel Report, Memorandum No. 9, 1952.

[2] Kuerti, G., *The Laminar Boundary Layer in Compressible Flow*, Advances in Applied Mechanics II, Academic Press Inc., 1951.

[3] Lagerstrom, P. A., Cole, J. D., and Trilling, L., *Problems in the Theory of Viscous Compressible Fluids*, GALCIT Report, 1949.

[4] Lin, C. C., Reissner, E., and Tsien, H. S., *On Two-Dimensional Non-Steady Motion of a Slender Body in a Compressible Fluid*, Jour. Math. Phys., Vol. 27, No. 3, 1948.

[5] Shen, S. F., *An Estimate of Viscosity Influence on Hypersonic Flow over an Insulated Wedge*, Jour. Math. Phys., Vol. 31, No. 3, 1952.

[6] Puckett, A. E., and Stewart, H. J., *The Thickness of a Shock Wave in Air*, Quar. Appl. Math., Vol. VII, No. 4, 1950.

[7] Bethe, H. A., and Teller, E., *Deviations from Thermal Equilibrium in Shock Waves*, Ballistic Research Laboratory Report X-117, Aberdeen Proving Ground, 1945.

[8] Shen, S. F., *On the Boundary Layer Equations in Hypersonic Flow*, Readers' Forum, Journal of the Aeronautical Sciences, Vol. 19, No. 7, p. 500, July, 1952.

[9] Liepmann, H. W., *The Interaction Between Boundary Layer and Shock Waves in Transonic Flow*, Journal of the Aeronautical Sciences, Vol. 13, No. 12, p. 623, December, 1946.

[10] Pohlhausen, E., *Zur näherungsweisen Integration der Differentialgleichungen der laminaren Grenzschicht*, Z. angew. Math. Mech., Vol. 1, 1921.

[11] Goldstein, S., *Modern Developments in Fluid Dynamics*, I; Oxford University Press, 1938.

[12] Tsien, H. S., *Superaerodynamics, Mechanics of Rarefied Gases*, Journal of the Aeronautical Sciences, Vol. 13, No. 12, p. 653, December, 1946.

[13] von Kármán, Th., *The Problem of Resistance in Compressible Fluids*, Fifth Convention of the Alexander Volta Foundation, 1935.

[14] Lees, L., and Probstein, R. F., *Hypersonic Viscous Flow over a Flat Plate*, Princeton University Aeronautical Engineering Laboratory Report 195, 1952.

[15] Lees, L., *On the Boundary-Layer Equations in Hypersonic Flow and Their Approximate Solutions*, Readers' Forum, Journal of the Aeronautical Sciences, Vol. 20, No. 2, p. 143, February, 1953.

Readers' Forum

BRIEF REPORTS of investigations in the aeronautical sciences and discussions of papers published in the JOURNAL are presented in this special department. The publication will be completed as soon as possible after receipt of the material. The Editorial Committee does not hold itself responsible for the opinions expressed by the correspondents. Contributions should not exceed 800 words in length.

Further Note on the "Dynamic Stability of a Missile in Rolling Flight"

R. E. Bolz
Professor of Aeronautical Engineering, Case Institute of Technology, Cleveland
February 24, 1953

IN BRYSON'S COMMENTS (JOURNAL OF THE AERONAUTICAL SCIENCES, Readers' Forum, January, 1953) on my paper "Dynamic Stability of a Missile in Rolling Flight" (JOURNAL OF THE AERONAUTICAL SCIENCES, June, 1952), we believe there are several errors, misinterpretations, and comments that should be corrected. I shall discuss each of Mr. Bryson's comments in the order in which he presented them.

(1) Mr. Bryson's difficulty in comment 1 can be cleared by correcting a typographical misprint in the subject paper. The sentence above Eq. (4) contains an incorrect word and should read: "In these equations, P_1 is actually the sum of the roll rate of the missile P *about* its own axis and the component of angular velocity ω_x about the X axis due to the precessional motion resulting." The meaning of Eq. (4) is easily observed by referring to Fig. 1 and Eq. (3) in the recent paper by Nicolaides.[1] Actually, the assumption made in neglecting ω_Z is only that of second-order terms in Eqs. (3b), (3c), (3e), and (3f) and was done merely to identify the important X component of angular velocity with the velocity normally called spin or roll in the *usual* gyroscopic axis system.

(2) In comment 2, Mr. Bryson has unfortunately missed an important point. Obviously, neglecting the nonhomogeneous terms cannot affect the classical linearized stability analysis; this is well known. The inclusion of the forces and moments due to misaligned surfaces and jet misalignment introduces into the analysis the possibility of an important type of instability arising from the terms in the particular solution (stability criterion III). This is termed "resonance instability" in the more recent analysis of reference 1. Mr. Bryson's inclusion of the "moment due to canted surfaces" in his statement is obviously incorrect.

(3) In comment 3, on the basis of consistency alone, Mr. Bryson has a point. However, in actuality since *nothing* is known about the magnus forces and moments due to pitching and yawing angular velocities and nothing can be said about these terms either experimentally or analytically, we felt justified in omitting them in the analysis in the interest of simplicity over consistency.

(4) The comment is correct. $K_{m\dot{\alpha}}$ is negative as defined, and, therefore, the sentence below Eq. (22) should have a minus sign preceding the term $K_{m\dot{\alpha}}$—i.e. $(-K_{m\dot{\alpha}})$.

(5) The first part of Mr. Bryson's comment corrects a typographical omission. A number 2 is missing in the denominator of the term in Table I, item 7, third column, $K_D = C_D\,(S/2d^2)$. The second part of the comment is incorrect. Eq. (22) is correct as it appears in the original paper and needs no change. Since $K_{z\alpha}$ is a *normal force coefficient*, it could be written in terms of the usual lift curve slope and drag coefficient as

$$Z = -C_D \frac{\rho V^2}{2} S\alpha - \frac{dC_L}{d\alpha} \frac{\rho V^2}{2S}$$

or

$$K_{z\alpha} = K_{L\alpha} + K_D$$

where $K_{L\alpha}$ is proportional to the lift curve slope. If this were chosen to be inserted into Eq. (22), the equation could involve the term

$$(\bar{K}_{L\alpha} - \bar{K}_D)$$

rather than the incorrect one that he suggests.

(6) Mr. Bryson's sixth comment is also incorrect. The third stability criterion arises from the particular solution and specifically from the nonhomogeneous terms included (discussed in second comment). The actual importance of this third stability criterion we had failed to notice in the analysis and is clearly emphasized in the recent reference 1.

(7) In comment 7, Mr. Bryson again failed to note an important point. It is not the transformation from time to distance along the flight path that has anything whatsoever to do with the conclusion under H on page 401 of the reference paper—namely, that dynamic stability is independent of velocity (except for variation of the coefficients with Mach Number). The point that Mr. Bryson apparently missed is that the analysis is valid for variable linear velocity V and variable roll velocity $P = P(V)$ (but small roll acceleration). The term $P_z = P/V$ in the equation is then, in general, a variable. However, according to the discussion on the bottom of page 398, the point is emphasized that, over the Mach Number range from 1.3 to 4.0, P_z has been shown to be essentially constant[2] thus rendering the equations *as written* independent of the velocity V and justifying my conclusion. The author has no data concerning the effect of velocity on P_z in the high subsonic Mach Number range, thus prohibiting the conclusion from being stated for this range.

(8) Mr. Bryson's eighth comment is one of personal preference. Using the usual reference axes system that he mentions will eliminate several terms from Eqs. (8a) and (8b). Subsequent equations, however, are of identical complexity in both cases, and the question becomes one only of preference.

(9) Mr. Bryson's comment of item 3, Tables I and II, is gratefully acknowledged. The statements were intended and should read: "Forces (moments) due to rolling combined with angles of pitch and yaw." The second part of Mr. Bryson's comment is incorrect. Items (3) and (4) in Tables I and II are not at all the same or equal. K_{zp} and the moment K_{mp} arise from wing- and fin-tip suction forces resulting from the rolling velocity. As such, they are additive to the magnus coefficients arising from the rolling fuselage. The $K_{z\dot{\alpha}}$ and $K_{m\dot{\alpha}}$ terms are damping derivatives arising from the surface potential on the lifting surfaces for accelerated motion and are essentially independent of the rolling motion of the missile.

(10) I concur with the part of Mr. Bryson's comment concerning a vagueness in conclusion (D) on page 400 of the original paper, except for his underestimation of the size and influence of magnus moment. For spin stabilized missiles, this factor appears to be of *prime* importance in its contributions to dynamic instability. Actually, referring back to Eq. (24) of the original paper, conclusion (D) should be clarified as follows:

(D) In general, a statically unstable rolling missile can be made dynamically stable by high roll rates, although this method of obtaining stability is of practical interest primarily for the wingless and tailless spinning body. For a statically stable missile, dynamic instability can be induced by high roll rates because of the important influence of the magnus moment, which from experimental indications is not at all negligible in many cases.

(11) It should be added that Mr. Bryson's analysis, first, is not free from error and, second, misses the elements intended in the original paper—namely, the influence of flight and rolling velocity variations (except on the coefficients themselves), thrust, canted fins, and assymmetry conditions.[1] The errors in Mr. Bryson's analysis are mathematical errors in the equations for b_2 and the stability condition S_2. The magnus force should not appear in any of these equations.

References

[1] Nicolaides, J. D., *On the Free Flight Motion of Missiles Having Slight Configurational Assymmetries*, Institute of the Aeronautical Sciences, Preprint No. 395, 1953.

[2] Nicolaides, J. D., and Bolz, R. E., *On the Pure Rolling Motion of Winged and/or Finned Missiles in Varying Supersonic Flight*, Journal of the Aeronautical Sciences, Vol. 20, No. 3, p. 160, March, 1953.

Turbulent Channel Flow from a Variational Principle

Stanley Corrsin
Associate Professor of Aeronautics, Department of Aeronautic The Johns Hopkins University, Baltimore
February 2, 1953

C. B. Millikan's demonstration that the steady parallel laminar flow solutions of the Navier-Stokes equations are those giving minimum total dissipation[1] can be easily modified to include corresponding steady-state turbulent flows.

Consider, for example, fully developed plane flow between parallel walls. The variational condition is

$$\delta \int_{-h/2}^{h/2} \Phi \, dy = 0 \tag{1}$$

where

$$\Phi = \tau(d\bar{U}/dy) \tag{2}$$

is the total rate of dissipation in (laminar or turbulent) steady-state flow and τ is the total mean shear stress. $\bar{U}(y)$ is mean velocity and y is spatial coordinate perpendicular to $\bar{U}$.

The "constraint" is conservation of mass flow rate,

$$\int_{-h/2}^{h/2} \bar{U} \, dy = \text{constant} \tag{3}$$

Carry out the variation with respect $\bar{U}(y)$ holding $\tau(y)$ fixed.* The Euler differential equation corresponding to Eqs. (1) and (3) is[2]

$$\lambda - (d\tau/dy) = 0 \tag{4}$$

where λ is the Lagrange multiplier.

* Holding $\tau(y)$ fixed in the variation process is the modification referred to.

Putting $\lambda = \partial\bar{P}/\partial x$, the mean longitudinal pressure gradient, we obtain the differential equation for either laminar or turbulent flow between parallel walls.

References

[1] Millikan, C. B., *On the Steady Motion of Viscous, Incompressible Fluids, with Particular Reference to a Variational Principle*, Phil. Mag., Ser. 7, Vol. 7, No. 44, pp. 641–662, April, 1929.

[2] Courant, R., *Differential and Integral Calculus II*, Chapt. VII; Blackie and Son, Ltd., 1936.

The Gas Bending Stress on a Blade in an Axial-Flow Compressor

John Mitchell Stephenson
Research Associate, Division of Engineering, Brown University, Providence, R.I.
February 16, 1953

(1) Summary and Conclusions

An approximate expression is found for the maximum bending stress imposed on a compressor blade in terms of the forces applied by the gas stream and thence in terms of the mass flow, work done, and blade geometry. For a given aerodynamic design, which implies a given solidity, the following results appear:

(a) The maximum bending stress depends on the thickness of the blade root section but is independent of the chord.

(b) The weight of the blade row is directly proportional to the blade thickness and is also independent of the chord.

(c) If the blades are hollow, the weight is reduced, but the stress may be increased. However, a figure of merit proportional to the ratio bending force/blade weight (for a given maximum stress) is improved by a factor of the order three, irrespective of the wall thickness, provided this is small.

(d) The natural bending frequency of a blade is independent of the chord and depends only slightly on the material.

Three conclusions can be drawn:

(a) For a given stage aerodynamic design, a reduction of blade weight can only be achieved by raising the allowable gas bending stress level or by using hollow blades. (However, the selection of the aerodynamic design parameters for minimum weight, assuming a given stress level, is a much more difficult problem.)

(b) Since the weight of the blades is a large fraction of the total weight of a stage, especially for small hub-tip ratios, a designer only incurs a small weight penalty by using extremely large blade chords, while two advantages accrue. First, he increases the Reynolds Number. Next, by reducing the thickness/chord ratio in this way he is able to use higher gas Mach Numbers. The chief disadvantage is the increased axial length of the shaft.

(c) The only effective ways of raising the natural bending frequency of a blade are to thicken it or to make it hollow, which increases the frequency by a factor of $\sqrt{3}$, again irrespective of the wall thickness.

It is frequently supposed that large chords—and, hence, low values of the blade height/chord ratio—imply low stage efficiencies by analogy with aircraft wings. But no proof has been given that the drag of the secondary vortices depends on the chord, and the total blade area exposed to gas friction depends only on the blade height, hub/tip ratio, and solidity. The loss of efficiency due to tip clearance is also independent of the chord. Only the wall drag certainly increases, and this accounts for less than a third of the total loss.

The presence of centrifugal loading does not alter the analysis given here but merely lowers the level of the maximum allowable bending stress for any given material.

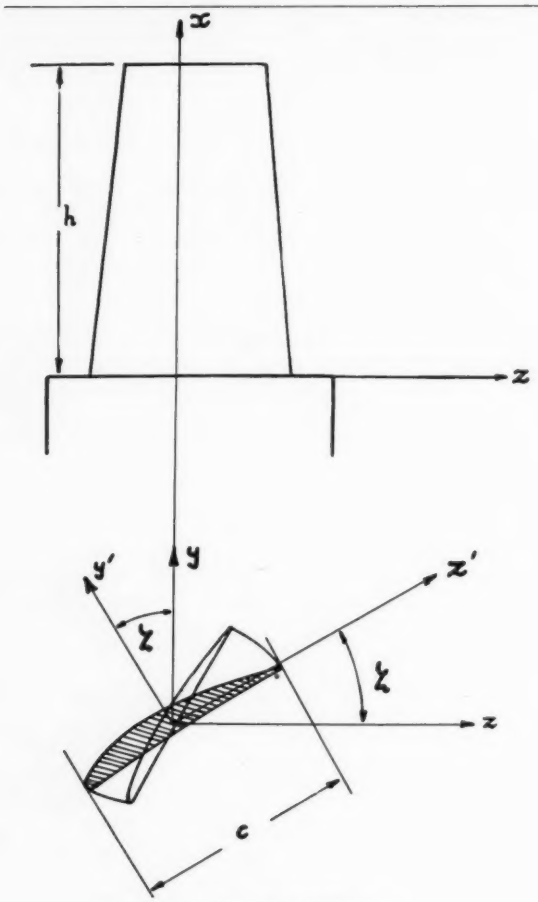

FIG. 1. System of coordinates.

(2) ANALYSIS: THE STRESS

To discuss the moments acting on a blade fixed at one end, we use the (left-hand) system of coordinates shown in Fig. 1, taking the origin at the centroid of the root section. The centroids of the other blade sections do not then necessarily lie on a radial line or even on a straight line, but the effect of this will be neglected.

The aerodynamic force components on any section of the blade are denoted as in Fig. 2. Since the principal axes of the blade sections are always nearly parallel and normal to the chord lines, we calculate the bending moments about the axes z' and y', inclined at the root section stagger angle ζ to the axial axis z and the tangential axis y; thus,

$$M_{z'} = \int_0^h Y' \cdot x \, dx$$

$$M_{y'} = \int_0^h Z' \cdot x \, dx$$

The stress at any point in the root section is, therefore,

$$\sigma = M_{y'} \cdot z'/I_{y'} - M_{z'} \cdot y'/I_{z'}$$

where the I's are the second moments of area and the positive sign in σ indicates tensile stress. Now $I_{y'}$ is of the order $100I_{z'}$, and the force Z' is usually small compared with Y'. Therefore we may write, approximately,

$$\sigma = -M_{z'}/\mu c^3$$

where $\mu c^3 = I_{z'}/y'$ is the modulus. We are only concerned here with the value of μ, corresponding to maximum stress, which is usually found near the leading and trailing edges. Thus,

$$-\sigma\mu c^3 = \int_0^h (Y \cos\zeta + Z \sin\zeta) x \, dx$$

If we write Z/Y as β and assume that, approximately, β is independent of x, we have

$$-\sigma\mu c^3 = (\cos\zeta + \beta \sin\zeta) \cdot \int_0^h Yx \, dx$$

Now if the average work done is $C_p\Delta T$ per unit mass flow, we have

$$Y \cdot Buh = Q \cdot C_p\Delta T$$

where B is the number of blades, u is the mean blade speed of rotation, and Q is the mass flow. Therefore the stress equation becomes

$$-\sigma\mu c^2 = (\cos\zeta + \beta \sin\zeta) \cdot (Q \cdot C_p\Delta T/2u) \cdot (h/Bc)$$

Note that Bc depends on the solidity of the blades, which we may assume, like all the other terms on the right side, to be fixed by the aerodynamic design of a stage. Therefore we may write

$$-\sigma c^2 = F/\mu$$

where F is a force proportional to the bending force on the blade, independent of the size or shape of the blade root profile.

(3) THE MODULUS

In general, μ can only be found by analysis of the particular profile shape used for the blade root section; but to a first approximation we may write, for a solid blade, $I_{z'} \propto ct^3$ and $y' \propto t$. Hence, $\mu c^3 \propto ct^2$, and we find that $\mu \simeq k(t/c)^2$, where k is a number of the order 0.1 and t is the maximum thickness of the section. (This formula is exactly true for an ellipse, where $k = \pi/32$, and for a rectangle, where $k = 1/6$).

Thus we have, approximately,

$$-\sigma t^2 = F/k$$

This is our first result—that the stress is independent of the chord.

For a hollow blade, made of sheet of a constant thickness d, we have approximately, if $d \ll t$, $I_{z'} \propto ct^2d$ and $y' \propto t$; and we

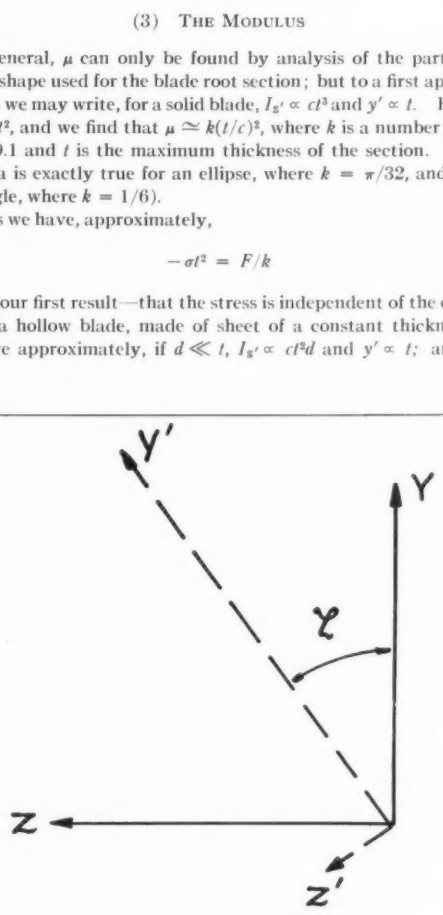

FIG. 2. The force component diagram.

find that $\mu c^2 \simeq 6ktd$, where k is the same number as for the solid blade. (Again, this formula is exact for an ellipse and for a rectangle, if $d \ll t$). Thus the stress formula for hollow blades is

$$-6\sigma td = F/k$$

Hence, if the wall thickness is less than $t/6$, the maximum stress is increased by hollowing a blade.

(4) An Example

The application of the approximate stress equation may perhaps be made clearer by a numerical example. Consider a compressor stage with the following properties: $Q = 200$ lbs. per sec.; $C_p = 10{,}900$ ft.^{2}/sec.; $\Delta T = 20°$K.; $u = 750$ ft. per sec.; $h = 10$ in.; $Bc = 80$ in.; and assume that $k = 0.1$ and

$$(\cos \zeta + \beta \sin \zeta) = 1$$

Then we have $F = 113$ lbs., so that

$$-\sigma t^2 = F/k = 1{,}130 \text{ lbs.}$$

Therefore we may draw up a table (Table 1) to show the greatest number of solid blades which can be used for a given value of the root thickness/chord ratio and of the maximum allowable bending stress. Therefore, using a smaller number of blades (of larger chord) reduces either t/c or the maximum bending stress.

Table 1

Max. σ 1,000 Lbs. per Sq.In.	Min. t, In.	t/c at Root 0.08	0.10	0.12
20	0.238	27	33	40
24	0.217	29	37	44
28	0.201	32	40	48

(5) The Weight

If blades always have the same height and taper ratios of thickness and chord, we can say that the weight W of the blades in a row is proportional to the blade root area A:

$$W \propto BA$$

Now for a solid blade, $A \simeq act$ and, for a hollow blade, $A \simeq 2acd$, where a is a number of the order 3/4. (For an ellipse, $a = \pi/4$; for a rectangle, $a = 1$). Therefore, since, again, c only occurs in the combination Bc, we have our second result that the blade weight is independent of the chord.

Now we define a dimensionless figure of merit F/W, which is proportional to the ratio of blade loading/weight; we require this to be as high as possible for any given value of the stress σ. But we have seen that

$$F = -\sigma\mu c^2$$

Thus $F/W \propto \mu c^2/BA = \Lambda$, say. Using the values of μ from paragraph (3), we have

$\Lambda = kt/aBc$ for the solid blade
$\Lambda = 3kt/aBc$ for the hollow blade

Therefore, with this criterion, a hollow blade is about three times better than one externally similar but solid.

(6) Vibration

The alternating gas forces on a blade may be assumed to produce stresses that are approximately proportional to the steady gas bending stresses, so that they are also independent of the chord. Moreover, the lowest natural frequency of a blade in bending is f, where

$$f^2 \simeq EI_{z'}/\gamma Ah^4$$

where E is Young's modulus and γ is the density of the blade material. Hence,

$$f^2 \simeq E\mu c^3 t/\gamma\, Ah^4 \cong E\Lambda Bct/\gamma h^4$$

or

$$f^2 \propto E\Lambda t/\gamma$$

which is independent of the chord (our third result).

Thus, there are three ways of raising the natural bending frequency (to avoid resonance, for example):

(a) Increasing the thickness t.

(b) Using hollow blades, with their large value of Λ [see paragraph (5)].

(c) Raising the value of E/γ by changing the blade material. However, E/γ is roughly the same for many metals, and this is rarely a useful move.

I should like to thank Prof. Max Schilhansl for his interest and for drawing my attention to his paper on this subject.[1]

Reference

[1] Schilhansl, Max, *Determination of the Lowest Natural Bending Frequency of Compressor Blades* (in German); Deutschen Akad. Luftfahrtforschung, Vol. I, May, 1942.

Additional Comments on "A Study of Transonic Gas Dynamics by the Hydraulic Analogy"

J. R. Bruman
Jet Propulsion Laboratory, California Institute of Technology, Pasadena, Calif.
January 27, 1953

That part of the subject paper[1] describing results obtained by the writer[2] and the subsequent discussion in the Readers' Forum[3, 4] appear to foster a slight misunderstanding based on ambiguous use of the term "wave."

The free-surface wave under discussion is a continuous, periodic, frictionless disturbance not related to the shock wave or its free-surface analog, the hydraulic jump. The only connection between the two phenomena is the fact that the minimum propagation velocity for the jump equals the value approached by the surface wave as its wave length increases.

Since experiments with the hydraulic analogy are usually designed to represent shock waves by hydraulic jumps, it is desirable to avoid disturbances propagated at velocities other than that of the jump being observed. It is immediately seen that spurious disturbances of sufficient wave length will at least be propagated at the velocity of the slowest hydraulic jump. The heuristic notion that this might be the most desirable test condition led the writer to propose and investigate the water depth for which the wave length required is a minimum.[2] For water, this depth is about 0.225 in. in theory—and proved, in fact, to be the optimum—for observation of hydraulic jumps. However, it seems difficult to reach this conclusion about shock waves, represented by hydraulic jumps, solely from a consideration of periodic surface waves and their velocities.

In the case of those observers[5, 6] who chose to apply the analogy with a moving stream and stationary model, the 1/4-in. depth was impractical, but this did not prevent successful work at larger depths with sufficiently large models.

References

[1] Laitone, E. V., *A Study of Transonic Gas Dynamics by the Hydraulic Analogy*, Journal of the Aeronautical Sciences, Vol. 19, No. 4, pp. 265–272, April, 1952.

[2] Bruman, J. R., *Application of the Water Channel-Compressible Gas Analogy*, North American Aviation, Inc. Report No. NA-47-87, March 3, 1947.

[3] Randels, W. C., *Comments on "A Study of Transonic Gas Dynamics by the Hydraulic Analogy,"* Readers' Forum, Journal of the Aeronautical Sciences, Vol. 19, No. 8, p. 572, August, 1952.

[4] Laitone, E. V., *A Rational Discussion of the Hydraulic Analogy*, Readers' Forum, Journal of the Aeronautical Sciences, Vol. 20, No. 1, p. 59, January, 1953.

[5] Orlin, W. J., and others, *Application of the Analogy between Water Flow with Free Surface and Two-Dimensional Compressible Gas Flow*, N.A.C.A. Report No. 875, August, 1946.

[6] Preiswerk, E., *Application of the Methods of Gas Dynamics to Water Flow with Free Surface*, N.A.C.A. T.M. Nos. 934 and 935, 1940.

Location of Detached Shock Waves Ahead of Plane Bodies

W. E. Moeckel
Lewis Flight Propulsion Laboratory, N.A.C.A., Cleveland
January 29, 1953

IN A RECENT READERS' FORUM LETTER, Professor Truitt[1] proposed what he believed to be a simple new method for predicting the location of detached shock waves ahead of wedges in transonic flow. Examination of his equations shows, however, that his method is identical to one of the methods (the "geometrical method") proposed in reference 2. Thus, in reference 2, the equation for shock location is given as (in the notation of reference 1)

$$(S + L)/l = \cot \theta' \tag{1}$$

where $(S + L)$ is the distance from the shock to the body sonic point, l is the ordinate of the sonic point, and θ' is the maximum wedge half-angle for an attached shock at the prescribed Mach Number. Eq. (1) is exactly the equation from which Professor Truitt derives his final expression.

Professor Truitt appears to have misinterpreted an assumption made in reference 2 and concludes that the misinterpreted assumption is invalid. The assumption made was that the axial distance from the *body sonic* point to the detached shock wave is independent of nose shape. This assumption is embodied in Eq. (1). Since the methods of reference 2 are based on this assumption and since Professor Truitt's method is identical to one of those methods, the good agreement between experiment and theory shown in reference 1 confirms, rather than disproves, the assumption made in reference 2. Professor Truitt's conclusion that there is an effect of nose shape on shock location results from his use of distance from wedge vertex instead of distance from wedge sonic point in plotting the data.

REFERENCES

[1] Truitt, R. W., *A Method for Location of Detached Shock Waves Ahead of Plane Bodies*, Readers' Forum, Journal of the Aeronautical Sciences, Vol. 20, No. 1, pp. 61–62, January, 1953.

[2] Moeckel, W. E., *Approximate Method for Predicting the Form and Location of Detached Shock Waves Ahead of Plane and Axially Symmetric Bodies*, N.A.C.A. T.N. No. 1921, July, 1949.

Comments on a Method for Location of Detached Shock Waves Ahead of Plane Bodies

E. V. Laitone
Associate Professor, University of California at Berkeley
January 29, 1953

IN REFERENCE 1, TRUITT ERRONEOUSLY BELIEVES that he has found a new equation for predicting the location of a detached shock, one that includes the effect of nose shape. However, all he has done is to replot Moeckel's geometric result of reference 2 to a different scale. This may be shown by writing Moeckel's Eq. (2) of reference 2 as

$$\tan \theta' = \left(\frac{t}{S + L}\right); \quad \tan \theta = \left(\frac{t}{L}\right) \tag{1}$$

corresponding to Fig. 1 of reference 1, where θ is the wedge half-angle and θ' is the corresponding maximum angle for which the shock becomes detached. Then, solving for S, the detachment distance from the nose of a wedge having total length L (see Fig. 1, reference 1), we obtain

$$S/L = (\tan \theta/\tan \theta') - 1 \tag{2}$$

which is identically Truitt's Eq. (2) in reference 1. This does not actually predict any direct effect of nose shape, as may be seen by the original form of Eq. (1), using the detachment distance measured from the sonic line $(S + L)$. These same equations are also applied by Moeckel to bodies of revolution, simply defining θ' as the cone half-angle for which the shock becomes detached. It is obvious that Eq. (1) is much more general than Eq. (2), which can only be applied to a wedge or cone.

Actually, these results are only valid for relatively blunt bodies at the higher transonic Mach Numbers as shown in reference 3. The only results valid for very slender bodies at Mach Numbers near unity are those obtained by the small perturbation method, which I originally derived in 1945 (see reference 4) and later used in references 3 and 5. This small perturbation method gives the following equation for the conditions shown in Fig. 1 of reference 1:

$$\ln\left(1 + \frac{L}{S}\right) = \frac{4\sqrt{2}\,\pi}{(\gamma + 1)\theta}\,(M_0 - 1)^{3/2} \tag{3}$$

As shown in reference 3, Eq. (3) does predict the correct effect of nose angle but only for very slender wedges ($\theta \leqq 5°$). Also note that Eq. (3) satisfies the transonic similarity relations.

REFERENCES

[1] Truitt, R. W., *A Method for Location of Detached Shock Waves Ahead of Plane Bodies*, Readers' Forum, Journal of the Aeronautical Sciences, Vol. 20, No. 1, pp. 61–62, January, 1953.

[2] Moeckel, W. E., *Approximate Method for Predicting Form and Location of Detached Shock Waves Ahead of Plane or Axially Symmetric Bodies*, N.A.C.A. T.N. No. 1921, July, 1949.

[3] Laitone, E. V., *A Study of Transonic Gas Dynamics by the Hydraulic Analogy*, Journal of the Aeronautical Sciences, Vol. 19, No. 4, pp. 265–272, April, 1952.

[4] Laitone, E. V., and Pardee, Otway O., *Location of Detached Shock Waves in Front of Bodies Moving at Supersonic Speeds*, N.A.C.A. R.M. No. A7B10, May 6, 1947.

[5] Laitone, E. V., *A Note on Detached Shock Waves*, Readers' Forum, Journal of the Aeronautical Sciences, Vol. 16, No. 7, pp. 441–442, July, 1949.

Note on Effects of Density Fluctuations on the Turbulent Skin Friction of an Insulated Flat Plate at High Supersonic Speeds

E. R. Van Driest
Aerophysics Department, North American Aviation, Inc., Downey, Calif.
February 2, 1953

IN THEIR READERS' FORUM REPORT, "Effects of Density Fluctuation on the Turbulent Skin Friction of an Insulated Flat Plate at High Supersonic Speeds" (JOURNAL OF THE AERONAUTICAL SCIENCES, October, 1951), T. Y. Li and H. T. Nagamatsu state that the density fluctuations occurring in a compressible turbulent boundary layer at high speeds are not adequately taken into account in the analyses presented by certain authors, including that of the writer.[1] The purpose of the present note is to demonstrate that the statement of Li and Nagamatsu is not justi-

fied, because the procedure followed by them appears to be physically inconsistent and, therefore, may lead to results that cannot be expected to agree with experiment.

In the writer's paper,[1] the following equations for continuity, momentum, and energy were derived to describe the mean steady flow in a thin turbulent boundary layer:

$$(\partial/\partial x)(\overline{\rho u}) + (\partial/\partial y)(\overline{\rho v}) = 0 \tag{1}$$

$$\overline{\rho u}\frac{\partial \bar{u}}{\partial x} + \overline{\rho v}\frac{\partial \bar{u}}{\partial y} = \frac{\partial}{\partial y}\left[-\overline{(\rho v)'u'}\right] \tag{2}$$

$$\overline{\rho u}\frac{\partial \bar{i}}{\partial x} + \overline{\rho v}\frac{\partial \bar{i}}{\partial y} = \frac{\partial}{\partial y}\left[-\overline{(\rho v)'i'}\right] - \overline{(\rho v)'u'}\frac{\partial \bar{u}}{\partial y} \tag{3}$$

where ρ is the density, u is the velocity component in the direction x parallel to the plate, v is the velocity component in the direction y perpendicular to the plate, and i is the enthalpy. The bars indicate temporal mean values and the primes the instantaneous fluctuation from the mean. It is seen that the momentum and enthalpy equations, Eqs. (2) and (3), are consistent with the continuity equation, Eq. (1)—i.e., the equations are consistent as far as the averaging process is concerned. The terms

$$-\overline{(\rho v)'u'} = \tau \tag{4}$$

$$-\overline{(\rho v)'i'} = q \tag{5}$$

thus may be properly called the Reynolds stress and Reynolds heat transfer, respectively. If, now, one puts

$$-\overline{(\rho v)'u'} = \epsilon(\partial \bar{u}/\partial y)$$

$$\overline{(\rho v)'i'} = \kappa(\partial \bar{i}/\partial y)$$

and assumes that $\partial \bar{i}/\partial x = 0$ and $\epsilon = \kappa$ (turbulence Prandtl Number = 1), it will immediately follow that

$$\bar{i} + (\bar{u}^2/2) = \text{constant} \tag{6}$$

for an insulated plate.

It is noted that density fluctuations are still included in Eqs. (1-6) and, in particular, in expressions (4) and (5).

Expression (4) is next expanded; whence,

$$\tau = -\overline{(\rho v)'u'} = -\bar{\rho}\,\overline{u'v'} - \bar{v}\,\overline{\rho' u'} - \overline{\rho' u' v'} \tag{7}$$

which reduces to

$$\tau = -\bar{\rho}\,\overline{u'v'} - \overline{\rho' u' v'} \tag{8}$$

when $\bar{v} = 0$ for a thin boundary layer, and to

$$\tau = -\bar{\rho}\,\overline{u'v'} \tag{9}$$

when the triple correlation $\overline{\rho' u' v'}$ is neglected. Thus the density fluctuation appears only in the triple correlation term $\overline{\rho' u' v'}$, and, therefore, if $\rho' u' v'$ is small compared to $\bar{\rho}\,\overline{u'v'}$, Eq. (9) adequately describes the compressible flow Reynolds stress. Since Eq. (9) was used to derive a friction law in reference 1, then it is true that density fluctuations were neglected by the writer in his final analysis; however, not to the extent indicated by Li and Nagamatsu.

Eq. (1) of the note by Li and Nagamatsu, on the other hand, results from adding to the above Eq. (7) various degrees of the term $\bar{u}\,\overline{\rho' v'}$, which does not even appear in the writer's analysis. In their work[2] the term $\bar{u}\,\overline{\rho' v'}$ came about as a result of using $\bar{\rho}\cdot\bar{u}$ and $\bar{\rho}\cdot\bar{v}$ for mass flux, rather than $\overline{\rho u}$ and $\overline{\rho v}$ as required by continuity [see Eq. (1) above]. If $\bar{u}\,\overline{\rho' v'}$ is added to Eq. (7), then

$$\tau = -\bar{\rho}\,\overline{u'v'} - \bar{u}\,\overline{\rho' v'} - \bar{v}\,\overline{\rho' u'} - \overline{\rho' u' v'} \tag{10}$$

Hence, when $\bar{v} = 0$,

$$\tau = -\bar{\rho}\,\overline{u'v'} - \bar{u}\,\overline{\rho' v'} - \overline{\rho' u' v'} \tag{11}$$

which is equivalent to

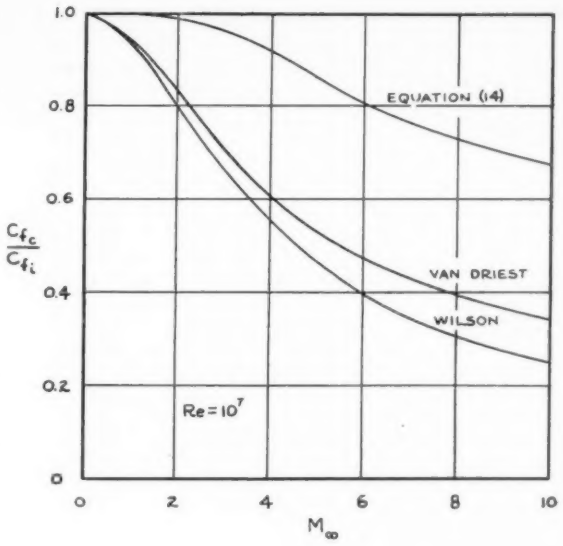

FIG. 1

$$\tau = -\overline{(\rho u)'v'} \tag{12}$$

in contrast to the writer's $-\overline{(\rho v)'u'}$.

The difference in physical interpretation of $\overline{(\rho u)'v'}$ and $\overline{(\rho v')u'}$ appears clear, the latter being consistent with the transverse momentum-transfer concept. It is because of this consistency with regard to the transport (flux) concept that the writer believes that Eqs. (1)–(3) are properly formulated.

If, now, the mixture concept be applied to both momentum and velocity gradients and if, further, $\rho' u'$ be neglected, then

$$\tau = -l^2\,[d(\bar{\rho}\cdot\bar{u})/dy]\cdot(d\bar{u}/dy) \tag{13}$$

which is the same as the Li-Nagamatsu expression for $\alpha = 1$ in their note. When it is assumed that $l = ky$ and a mean friction law is derived following the procedure in reference 1, there results, for an insulated plate,[3]

$$\frac{0.242\,(1-\lambda^2)^{1/2}}{C_f^{1/2}}\cdot\frac{\phi(\lambda)}{\lambda} = \log_{10}(Re\cdot C_f) + 0.76\log_{10}(1-\lambda^2) + \frac{1}{2}\log_{10}(1+\lambda^2) \tag{14}$$

where

$$\phi(\lambda) = \sqrt{2}\tanh^{-1}\sqrt{\frac{2\lambda^2}{1+\lambda^2}} - \tanh^{-1}\sqrt{\frac{\lambda^2}{1+\lambda^2}}$$

$$\lambda^2 = \frac{[(\gamma-1)/2]M_\infty^2}{1+[(\gamma-1)/2]M_\infty^2}$$

In Fig. 1 is plotted the ratio of the compressible-flow skin-friction coefficient to the incompressible-flow skin-friction coefficient, C_{f_c}/C_{f_i}, obtained from Eq. (14). Also plotted are the analyses of Wilson[4] and the writer,[1] both based on Eq. (9). A strong divergence of Eq. (14) from the two theories using Eq. (9) is evident. (The difference between Wilson's analysis and that of the writer is that Wilson[4] used the similarity law for mixing length, whereas the writer used the linear relation $l = ky$.) The fact that the data[4] fall near the theories of Wilson and the writer should be sufficient evidence that the use of Eq. (12) instead of Eq. (4) may lead to erroneous conclusions. To show this result was the purpose of the writer's comments in reference 3. It never was

expected by the writer that Eq. (14) would be seriously considered, because of the physical difference between $\overline{(\rho v)'u'}$ and $\overline{(\rho u)'v'}$.

It should be pointed out further that including the term $\bar{u}\,\overline{\rho'v'}$ not only brings about a definite change in the shear equation from $\tau = -\bar{\rho}l^2(d\bar{u}/dy)^2$ to Eq. (13) but also leads to difficulty in the derivation of the energy relation Eq. (6). In the opinion of the writer, either one can disregard density fluctuations altogether in accordance with Crocco,[5] or one should follow the course suggested above by the writer. Li and Nagamatsu did not derive the energy relation in their note or main report;[2] however, it is the writer's belief that, if they had attempted to derive the energy relation using their interpretation of density fluctuations, they would have encountered considerable difficulty.

Summarizing, density fluctuations have been neglected in the derivation of Eq. (9), but only to the extent of neglecting $\overline{\rho'u'v'}$ and not $\bar{u}\,\overline{\rho'v'}$, because $\bar{u}\,\overline{\rho'v'}$ does not even appear in the writer's analysis. At high Mach Numbers, $\overline{\rho'u'v'}$ may become important. However, there are many other approximations involved in the turbulence theory all the way down the line which may also become increasingly important; for example, in the derivation of friction laws, it is generally assumed that $\bar{\rho} \sim 1/\bar{T}$ to the neglect of $\overline{\rho'T'}$, where T is temperature. All in all, at least it seems clear that certain authors, including the writer, have adequately taken density fluctuations into account by use of Eq. (9) and, therefore, that the referred-to statement by Li and Nagamatsu is not justified.

References

[1] Van Driest, E. R., *Turbulent Boundary Layer in Compressible Fluids*, Journal of the Aeronautical Sciences, Vol. 18, No. 3, p. 145, March, 1951.

[2] Li, T. Y., and Nagamatsu, H. T., *Effects of Density Fluctuations on the Turbulent Skin Friction of an Insulated Flat Plate at High Supersonic Speeds*, GALCIT Hypersonic Wind Tunnel Memorandum No. 5, May, 1951.

[3] Van Driest, E. R., Proceedings of the Bureau of Ordnance Symposium on Aeroballistics (Comments on paper by R. E. Wilson, NAVORD Rep. 1651), pp. 264–267, November 16–17, 1950.

[4] Wilson, R. E., *Turbulent Boundary-Layer Characteristics at Supersonic Speeds—Theory and Experiment*, Journal of the Aeronautical Sciences, Vol. 17, No. 9, p. 585, September, 1950.

[5] Crocco, L., *Su di un valore massimo del coefficiente di transmissione del calore da una lamina piana a un fluido scorrente*, Rendiconti Della R. Accademia Nazionale Dei Lincei, Vol. 14, p. 490, December, 1931. (Translation in North American Aviation Aerophysics Lab., Rep. AL-1239, July 1, 1951.) See also L'Aerotechnical, Vol. 12, fasc. 2, pp. 181–197, February, 1932.

Further Comments on "Aerodynamic Coefficients of an Oscillating Airfoil in Two-Dimensional Subsonic Flow"

P. F. Jordan

Royal Aircraft Establishment, Farnborough, Hants, England*

February 27, 1953

IN THE SUBJECT PAPER,[1] Timman, van de Vooren, and Greidanus published numerical values; these values differ from the standard values—i.e., those published by Dietze.[2] Fettis[3] remarked that the new values[1] must be erroneous because they do not, for $M > 0$, satisfy the relation†

$$k_a = i\omega(m_a + k_b) \tag{1}$$

which is, however, satisfied by the standard coefficients.[2] In a recent letter,[4] the authors of the subject paper[1] maintain that their values must be correct; they state among other things:

(α) The relation (1) holds only for incompressible flow.

(β) The standard results[2] may well be erroneous for $M > 0$ because Dietze used an approximate method.

(γ) Dietze's iteration method does not converge if both M and ω exceed 0.7.

The writer has the following comments to make:

(a) The relation (1), taken by itself, is not new. For $M > 1$, it was stated independently by Temple and Jahn[5] and by the writer;[6] it was then observed[6] that Eq. (1) is valid for $M = 0$ but has no practical significance there.

(b) The relation (1) can be proved for any Mach Number M so that reference 1 must contain an error. Let γ_n be the (nondimensional) lift distribution due to the downwash $w_n = x^n$ at the frequency given; then Eq. (1) is easily shown to be equivalent to

$$\int_{-1}^{+1} (\gamma_1 + x\gamma_0)\,dx \equiv \int_{-1}^{+1} (w_0\gamma_1 + w_1\gamma_0)\,dx = 0 \tag{2}$$

The proof of Eq. (2) for $M \geq 1$ is elementary; it follows from the form of the basic equation

$$\gamma = w + \int_0^{1+x} w(x - \xi)k(\xi)\,d\xi \tag{3}$$

by means of partial integration. The proof for $M < 1$ is more involved but can be obtained by modern reverse-flow considerations. In fact, Eq. (2) is readily seen to be a special case of the general theorem

$$\int_S \int (w\bar{\gamma} - \bar{w}\gamma)\,dS = 0 \tag{4}$$

see Flax[7], Eq. (29). Eq. (4) is valid for any plan form S and any two downwash distributions w and $\bar{w}$; $\bar{\gamma}$ arises from $\bar{w}$ in reverse flow. [Flax[7] also states a specific relation equivalent to Eq. (1).]

(c) The argument that leads to the statement (β) in reference 4 is hard to follow. Not only Dietze but a number of other authors, notably Schade,[8] have calculated the aerodynamic coefficients in question, using approximations of essentially different forms to the exact kernel of the Possio equation. However, these different approximations are so good that they should not lead to appreciable numerical errors; in fact, the numerical values obtained by different authors agree well enough.

(d) The Possio equation is, of course, equivalent‡ to the linearized differential equation on which the theory of reference 1 is based directly. Recently, Jones[9] has recalculated (for $\omega \leq 0.5$) the coefficients in question by means of a simple method[9, 10] based on the transformed differential equation; his results confirm not only Dietze's values[2] ($M \leq 0.7$) but also Schade's values[8] for $M = 0.8$.** (The latter values had not, to the writer's knowledge, been confirmed before.)

(e) The writer is surprised by statement (γ). For $(M,\omega) = (0.7, 0.5)$ the ratio of consecutive corrections is still ~ 0.5 in Dietze's iteration. Hitherto the writer had the impression that Dietze's iteration would be convergent for any set $(M < 1, \omega)$. This impression was based on the following fact: the relation

$$\gamma_n = \sin n\varphi \quad \text{if} \quad w_n = \sqrt{1 - M^2}\cos n\varphi \tag{5}$$

which is correct for $\omega = 0$, is for $\omega \neq 0$ an approximation that becomes increasingly close as n increases for a given set (M,ω) of parameters.

(f) However that may be, the region in the M,ω-plane in which Dietze's method may be applied in practice is certainly smaller than it is for the method of reference 1. Hence, and not only for this reason, the error that has occurred in the elegant analysis of reference 1 is much to be regretted, and the usefulness of the "reverse-flow relation," as Eq. (1) should properly be called, becomes apparent in that it should enable the authors of reference 1 to trace that error.

* Acknowledgment is made to the Chief Scientist, British Ministry of Supply, for permission to publish this note.

† The notation, identical to that of reference 1, is based on the Küssner notation, but the reference point is the mid-chord. Fettis' derivation of Eq. (1) is not yet available to the writer.

‡ It can be verified for instance for $M = 1$, where the general solution of the differential equation exists, that this solution also satisfies the Possio equation.

** Jones[9] has also calculated the coefficients for $M = 0.9$, $\omega < 0.3$; these coefficients again satisfy Eq. (1).

References

[1] Timman, R., van de Vooren, A. I., and Greidanus, J. H., Journal of the Aeronautical Sciences, Vol. 18, No. 12, p. 797, December, 1951.

[2] Dietze, F., ZWB FB 1733, January, 1943; ARC 10,219.

[3] Fettis, H. E., Readers' Forum, Journal of the Aeronautical Sciences, Vol. 19, No. 5, p. 353, May, 1952.

[4] Timman, R., van de Vooren, A. I., and Greidanus, J. H., Readers' Forum, Journal of the Aeronautical Sciences, Vol. 19, No. 11, p. 790, November, 1952.

[5] Temple, G., and Jahn, H. A., R. & M. 2140, April, 1945.

[6] Jordan, P. F., AVA 46/J/1, January, 1946; ARC 10,052.

[7] Flax, F. H., CAL-42, February, 1952.

[8] Schade, Th., AVA 46/J/9, September, 1946; ARC 10,108, Addendum.

[9] Jones, W. P., ARC 15,642, March, 1953.

[10] Jones, W. P., ARC 14,336, October, 1951.

Remarks on Thermal Characteristics of Boundary Layers*

Martin Bloom

Assistant Professor of Aeronautical Engineering, Polytechnic Institute of Brooklyn

January 30, 1952

Notation

a = b/T
b = empirical constant (5,526°R. for air)
c_f = local friction coefficient (as in reference 2)
c_p, c_v = heat capacities at constant pressure and constant volume
h = enthalpy $\left(\int_0^T c_p\, dT\right)$
h_c = local heat-transfer coefficient (as in reference 2)
k = thermal conductivity
N = local Nusselt Number ($h_c x/k$)
P = Prandtl Number ($\mu c_p/k$)
R = perfect gas constant
R_x = local Reynolds Number ($\rho u x/\mu$)
r_T = temperature recovery factor $(T_e - T_1)/T_0 - T_1)$
r_h = enthalpy recovery factor $(h_e - h_1)/(h_0 - h_1)$ or $\int_{T_1}^{T_e} c_p\, dT \Big/ \int_{T_1}^{T_0} c_p\, dT$
T = absolute temperature
u = streamwise velocity
x = streamwise coordinate
ρ = mass density
μ = absolute viscosity
γ = c_p/c_v

Subscripts:

e = adiabatic surface
1 = local values at edge of boundary layer
0 = isentropic stagnation conditions
w = value at surface

Discussion

THE EXACT CALCULATIONS of laminar boundary-layer characteristics appearing in references 1–3 and the recent reports of carefully measured temperature recovery factors (e.g., references 4 and 5) prompt the following remarks:

(1) It bears restating that the variation of P with T for air has not been closely established because of uncertainty in the quantitative variation of k with T. Data used in references 1–3, based on references 6–9, indicate a *decrease* in P from about 0.74 at 500°R. to about 0.63 at 6,000°R. On the other hand, lower values of k reported in references 10–12 (shown in Fig. 19, reference 1 and Fig. 3, reference 13) would lead to higher values of P and give credence to Knuth's curve (reference 14, based on reference 15), which shows P *increasing* slightly from about 0.74 at 540°R. to about 0.78 at 5,400°R. An increasing trend is also indicated in references 16 and 17 (since γ is reliably known to decrease with increasing T). The estimated decrease in P, shown in Fig. 5, reference 2, is based upon the assumption that $k/\mu c_v$ does not vary with T. This differs from the Eucken assumption (that $k/\mu c_v \sim \sim 9\gamma - 5$), which is used in references 14 and 15, and leads to an increase in P. Young and Janssen[1] noted the uncertainty involved in evaluating P precisely but concluded that the effect of the variation was minor in their application. Thus, it seems to be most reasonable, considering the present state of the art, to *treat P as a constant*, even in accurate calculations. This gives added emphasis to the important work of Crocco[18] who used the Sutherland $\mu - T$ formula, treated c_p as an arbitrary function of T, accurately known, and maintained P constant. Furthermore, attempts to correlate data on r_T with functions of P evaluated at various temperatures, such as T_e, T_0, or T_1, must be viewed with care. This is particularly true if data are obtained from tests in which the temperatures produced are much lower than those encountered in practice.

The following commonly referred to values are given for convenient comparison:

	P	$P^{1/2}$	$P^{1/3}$
Approximate low-temperature value	0.74	0.86	0.91
Possible high-temperature values	0.63	0.79	0.86
	0.78	0.88	0.92

(2) One of Crocco's significant results, derived for laminar flow on a flat surface [Eq. (40), reference 18] is given as follows:

$$P^{1/2} = (h_e - h_1)/(h_0 - h_1) \equiv r_h \tag{1}$$

where h_0 is defined by the relation

$$h_0 - h_1 = u_1^2/2 \tag{2}$$

Values of r_T calculated from Eq. (1), by assuming $r_h = 0.85$ and $T_1 = 400$°R., differ from r_h by less than 2 per cent for $M_1 < 10$. Thus, values of T_e can be calculated closely from the expression

$$(T_e - T_1)/(T_0 - T_1) = r_T \cong r_h = P^{1/2} \tag{3}$$

where T_0 must be calculated with c_p as a function of T. In principle, however, r_T is seen to be slightly dependent upon M_1 and T_1 for laminar flow on a flat surface, assuming P is constant. Since the error incurred by neglecting this variation is probably of the same order as the uncertainty concerning the value of $P^{1/2}$, it is again seen that the value of precise correlations of measured values of r_T with functions of P is questionable at present. In fact, an experimental investigation of the validity of Eq. (1), which would require the simulation of elevated temperatures, might provide information on the variation of P with T.

From a computational standpoint, Eq. (1) can be used as readily as Eq. (3). Moreover, the accurate analytic expressions for c_p, h, and T_0 given by Donaldson[19] can be used to advantage in connection with Eq. (1). They are

$$c_p/R = (7/2) + a^2 e^a (e^a - 1)^{-2} \tag{4}$$

$$h/R = (7/2)\, T[1 + (2/7)a(e^a - 1)^{-1}] \tag{5}$$

$$T_0/T_1 = 1 + (\gamma_1/7)M_1^2 - (2/7)a_1[(e^{a_0} - 1)^{-1} - (e^{a_1} - 1)^{-1}] \tag{6}$$

Analogously, Eq. (1) yields

$$T_e/T_1 = 1 + r_h(\gamma_1/7)M_1^2 - (2/7)a_1[(e^{a_0} - 1)^{-1} - (e^{a_1} - 1)^{-1}] \tag{7}$$

For values of $T_1 < 660$°R., corresponding to altitudes less than 4×10^5 ft., Eqs. (4)–(7) give

$$c_{p_1}/R = 7/2, \quad \gamma_1 = 7/5, \quad h_1 = c_{p_1} T_1 \tag{8}$$

$$T_0/T_1 = 1 + (M_1^2/5) - (2/7)a_1(e^{a_0} - 1)^{-1} \tag{9}$$

$$T_e/T_1 = 1 + r_h(M_1^2/5) - (2/7)a_1(e^{a_e} - 1)^{-1} \tag{10}$$

It can be noted that the curve of $T_e - T_1$ shown in Fig. 13 of reference 2, for no dissociation, was calculated by using an equation identical to Eq. 1 given here, with a somewhat arbitrarily

* Done in connection with U.S.A.F. contract AF 33(616)-116, project 52-670A-86, Wright Air Development Center.

assumed constant value of $r_h = 0.85$. It is of interest to compare the values shown in Fig. 13 of reference 2 with those that were calculated precisely by the numerical procedure and given in Table 1 and in Fig. 16A of reference 2. For values of $u_1 \times 10^{-3}$ (which is close to M_1 in the case treated) less than 8, the values given by Table 1[2] agree with those shown in Fig. 13.[2] But for $u_1 \times 10^{-3} = 9.8$ and 12.5, the values given by Table 1[2] are about 1,900° and 6,100°R. higher, respectively, than those plotted in Fig. 13;[2] while, for $u_1 \times 10^{-3} = 12.4$, the value given by Fig. 16A[2] is about 900°R. lower than that of Fig. 13.[2] The value of $T_e - T_1$ determined from Table 3, reference 1, for $M_1 = 12.4$ agrees more closely with those of Figs. 13 and 16A[2] than with that of Table 1.[2] For $M_1 > 8$ the values of T_e given by Table 3[1] are not in close agreement with those of Table 1.[2] The significance of these differences is unexplained.

It should also be noted that the temperature recovery factor, as defined in reference 1, is based on T_0 determined with c_p constant. Its decrease with M_1 would be less pronounced if it were defined according to Eq. (3), here. For example, for $M_1 = 9.59$, $T_1 = 388°R.$, and $T_e = 5{,}135°R.$ (Table 3[1]), the value $r_T = 0.79$ is obtained from Eq. (3), as compared with 0.66 given in reference 1.

In connection with reference 2, it is interesting to observe that the effect of dissociation on the rate of heat transfer is small, at least for $M_1 < 13$, if the surface temperature is less than about 3,500°R. This is true because of the counterbalancing effects of dissociation on the heat-transfer coefficient and the temperature potential which, individually, are appreciably affected by dissociation. The effectiveness of the concept of a heat-transfer coefficient, therefore, appears to be reduced under these circumstances, as it is when the surface temperature is variable.

(3) Crocco also gave the following expression for the heat-transfer coefficient [Eq. (41), reference 18]:

$$(NP^{-1/3}R_x^{-1/2})_1/(0.5c_fR_x^{1/2})_1 = (h_w - h_e)h_1^{-1}/(T_w - T_e)T_1^{-1} \tag{11}$$

He noted that Eq. (11) is virtually uninfluenced by the viscosity law, despite the fact that c_f depends strongly on the viscosity law. However, c_f is not greatly affected by c_p and P. Therefore, Crocco's calculations of c_f, carried out only for $M_1 \leq 5$ and $T_w/T_1 \leq 2$, can be supplemented by values of c_f obtained with Sutherland's viscosity law, even though different values of c_p and P may have been used. Values of $(NP^{-1/3}R^{-1/2})_1$, calculated from Eq. (11) by using c_f values obtained from references 1 and 20, are shown in Fig. 1. They are compared with the values of $(NP^{-1/3}R^{-1/2})_1$ given in references 1 and 20. The difference between the curves VD and $C(YJ)$ or $C(VD)$ shows the approximate influence of the c_p variation, while the difference between curves YJ and $C(YJ)$ or $C(VD)$ shows the influence of a decreasing P.

It is of further interest to note that Crocco's values of c_f for $M_1 \leq 5$ (Fig. 20, reference 18) slightly exceed the values of reference 20, while the values based on a decreasing P[1] exceed those of reference 18. Therefore, values of $(NP^{-1/3}R^{-1/2})_1$, obtained with c_f based on a slightly increasing P, would probably correspond most closely with curves $C(VD)$. Moreover, when c_p is considered variable, $(NP^{-1/3}R^{-1/2})_1$ appears to be fairly constant over an appreciable range of M_1; this corresponds to the usual engineering approximation. Also, at the larger values of M_1, the effect of T_w diminishes.

References

[1] Young, G. B. W., and Janssen, E., *The Compressible Laminar Boundary Layer*, Journal of the Aeronautical Sciences, Vol. 19, No. 4, pp. 229-236, 288, April, 1952.

[2] Moore, L. L., *A Solution of the Laminar Boundary Layer Equations for a Compressible Fluid*, Journal of the Aeronautical Sciences, Vol. 19, No. 8, pp. 505–518, August, 1952.

[3] Klunker, E. B., and McLean, F. E., *Laminar Friction and Heat Transfer at Mach Numbers from 1 to 10*, N.A.C.A. T.N. No. 2499, October, 1951.

[4] Des Clers, B., and Sternberg, J., *On Boundary-Layer Temperature Recovery Factors*, Readers' Forum, Journal of the Aeronautical Sciences, Vol. 19, No. 9, pp. 645, 646, September, 1952.

[5] Eber, G. R., *Recent Investigation of Temperature Recovery and Heat Transmission on Cones and Cylinders in Axial Flow in the N.O.L. Aeroballistics Wind Tunnel*, Journal of the Aero Science, Vol. 19, No. 1, pp. 1–6, 14, January, 1952.

[6] Tribus, M., and Boelter, L. M. K., *An Investigation of Aircraft Heaters; II—Properties of Gases*, N.A.C.A. W-9, October, 1942.

[7] Boelter, L. M. K., and Sharp, W. H., *An Investigation of Aircraft Heaters; XXXII—Measurements of Thermal Conductivities of Air and Exhaust Gases Between 50°F. and 900°F.*, N.A.C.A. T.N. No. 1912, July, 1949.

[8] Keenan, J. H., and Kaye, J., *Gas Tables;* John Wiley & Sons, Inc., New York, 1948.

[9] Boelter, L. M. K., Martinelli, R. C., Romie, F. E., and Morrin, E. H., *An Investigation of Aircraft Heaters; XVIII—A Design Manual for Exhaust Gas and Air Heat Exchangers*, N.A.C.A. W-95, p. 133, August 1945.

[10] Stops, D. W., *Effect of Temperature upon the Thermal Conductivity of Gases*, Nature, Vol. 164, No. 4179, p. 966, December, 1949.

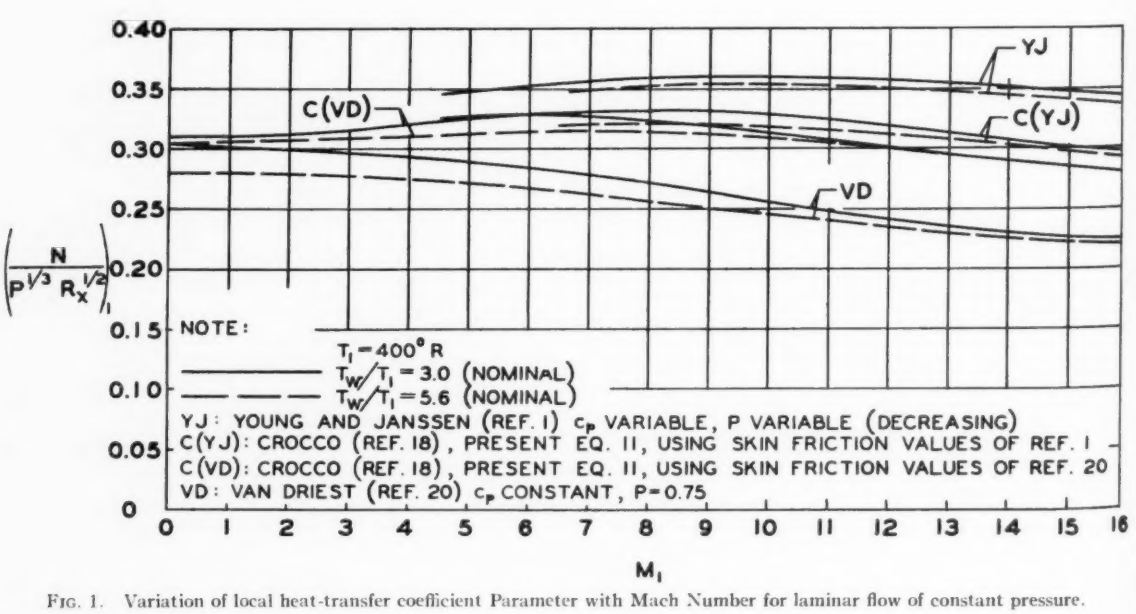
0.40
0.35
0.30
0.25
0.20
0.15
0.10
0.05
0
C(VD)
YJ
C(YJ)
VD
NOTE:
T1 = 400° R
Tw/T1 = 3.0 (NOMINAL)
Tw/T1 = 5.6 (NOMINAL)
YJ: YOUNG AND JANSSEN (REF. 1) cp VARIABLE, P VARIABLE (DECREASING)
C(YJ): CROCCO (REF. 18), PRESENT EQ. 11, USING SKIN FRICTION VALUES OF REF. 1
C(VD): CROCCO (REF. 18), PRESENT EQ. 11, USING SKIN FRICTION VALUES OF REF. 20
VD: VAN DRIEST (REF. 20) cp CONSTANT, P=0.75
0 1 2 3 4 5 6 7 8 9 10 11 12 13 14 15 16
M1

FIG. 1. Variation of local heat-transfer coefficient Parameter with Mach Number for laminar flow of constant pressure.

[11] Hirschfelder, J. O., and Curtis, C. F., *Thermodynamic Properties of Air—II, University of Wisconsin* CM-518, December 21, 1948.

[12] Groeber, H., and Erk, S., *Die Grundgesetze der Waermeuebertragung;* Julius Springer, Berlin, 1933.

[13] Humble, L. V., Lowdermilk, W. H., and Desmon, L. G., *Measurements of Average Heat Transfer and Friction Coefficients for Subsonic Flow of Air in Smooth Tubes at High Surface and Fuid Temperatures,* N.A.C.A. Report No. 1020, 1951.

[14] Knuth, E. L., *Note on the Calculation of Transport Properties of Gas Mixtures,* Readers' Forum, Journal of the Aeronautical Sciences, Vol. 19, No. 9, p. 644, September, 1952.

[15] Hirschfelder, J. O., Bird, R. B., and Spotz, E. L., *Viscosity and other Physical Properties of Gases and Gas Mixtures.* Trans. A.S.M.E., November, 1949.

[16] Boelter, L. M. K., Cherry, V. H., Johnson, H. A., and Martinelli, R. C., *Heat Transfer Notes,* p. XII-8, Table XII-b-III, University of California Press, Berkeley and Los Angeles, 1948.

[17] Jeans, J. H., *An Introduction to the Kinetic Theory of Gases;* p. 190, Cambridge University Press, 1948.

[18] Crocco, L., *The Laminar Boundary Layer in Gases,* Monografie Scientifiche di Aeronautica No. 3, December, 1946. Translation by North American Aviation, Inc., Report APL/NAA/CF-1038, July 15, 1948.

[19] Donaldson, C. duP.: *Note on the Importance of Imperfect-Gas Effects and Variation of Heat Capacities,* N.A.C.A. RM L8J14, December 10, 1948.

[20] Van Driest, E. R., *Investigation of the Laminar Boundary Layer in Compressible Fluids Using the Crocco Method,* North American Aviation, Inc., Report AL-1183, January 9, 1951.

Effect of Flapping Hinge Offset on Rotor-Blade Stall

J. P. Chawla
Hughes Aircraft Company, Culver City, Calif.
February 24, 1953

THIS NOTE IS IN REPLY to some remarks on the subject by Messrs. John R. Meyer, Jr., and G. Falabella, Jr., in the Readers' Forum Section of the February, 1953, issue of the JOURNAL. I should like only to point out the main differences between their approach and mine. Significant features of the work by Meyer and Falabella are:

(1) The rotor is simply a lifting rotor and is not inclined forward to provide a propulsive component of thrust as in a conventional helicopter. A machine at an advance ratio of 0.60 with the tip-path plane of the rotor approximately horizontal is obviously operating as a gyrodyne and not as a helicopter.

(2) The rotor is allowed to flap resulting in a hub moment that must be counterbalanced by a moment supplied by a control surface in order to trim the aircraft in flight.

I had taken the case of a conventional helicopter with normal values of Lock's Inertia Number γ. A value of $\gamma = 4$ as chosen by Meyer and Falabella is about a half to a third that of the current practice even with tip-jet units. It is recognized that with hinge offset a reduction in the value of γ is beneficial for rotor blade stall only if the blade is allowed to flap while in trimmed flight. Consequently, the reduction in angle of attack at the tip of the retreating blade shown in Fig. 1 of their note is due to a combination of (1) the reduction in γ; (2) the incorporation of flapping hinge offset; (3) the flapping of the rotor in trimmed flight; and (4) the operation of the machine as a gyrodyne with the propulsive unit being other than the rotor itself. I believe that the contribution of items (3) and (4) in reducing the stall preponderates over that of items (1) and (2); in other words, the blade mass constant and the flapping hinge offset play a secondary role.

ERRATA

I should also like to submit corrections to my original note.[1]

(1) In the expression for M_a, Eq. (5a), the term $\theta_1 C\mu$ should be preceded by a minus sign instead of a plus sign

(2) In Eqs. (5b), $B = \frac{1}{4} - \frac{1}{2}\epsilon + \frac{1}{4}\epsilon^2$

(3) In Eqs. (6a), $E = \theta_0(A + B\mu^2) - \theta_1 C\mu - \lambda C$

(4) In Eqs. (6b), $\beta_0 = \frac{\gamma}{2}\left[\frac{\theta_0}{4}(1 + \mu^2) - \frac{1}{3}(\theta_1\mu + \lambda)\right]$

(5) In the numerator of Eq. (8), $[\zeta/(1 + \zeta)]$ should be preceded by a plus sign instead of a minus sign.

The effect of these errors is to decrease slightly the beneficial effect of flapping hinge offset on stall of the retreating blade tip shown in Fig. 2 of reference 1.

REFERENCE

[1] Chawla, J. P., *Effect of Flapping Hinge Offset on Rotor Blade Stall,* Journal of the Aeronautical Sciences, Vol. 19, No. 7, p. 498, July, 1952.

Actuator Disc Theory for Compressible Flow and a Subsonic Correction for Propellers

E. V. Laitone
Associate Professor, University of California at Berkeley
January 29, 1953

THE ONE-DIMENSIONAL AXIAL-MOMENTUM THEORY can be applied to a propeller in subsonic flow if one assumes the concept of the actuator disc creating a discontinuity in pressure and density. If we are interested in only the first-order compressibility correction for small values of the free-stream Mach Number ($M_0 = V_0/A_0$) and light disc loadings, then the axial-momentum equations can easily be reduced to (e.g., using Eqs. (1) through (7) of reference 1)

$$\frac{\rho_1}{\rho_0} = (1 - M_0^2\delta_1) \tag{1}$$

$$\frac{M_1}{M_0} = 1 + \left(1 + \frac{\gamma - 1}{2} M_0^2\right)\delta_1 \tag{2}$$

$$\delta_1 = \frac{T/A}{4q_0}\left[1 - \frac{T/A}{4q_0}(1 - M_0^2)\right] \approx \frac{T/A}{2\rho_0 V_0^2} \tag{3}$$

$$m = \rho_1 V_1 A = \rho_0 V_0 A[1 + \delta_1(1 - M_0^2)] \tag{4}$$

where

$$V_1 = V_0(1 + \delta_1) \tag{5}$$

$$V_3 = V_0(1 + \delta_3) \approx V_0(1 + 2\delta_1) \tag{6}$$

using the same notation as in reference 1—namely, subscript (0) indicates free-stream conditions an infinite distance ahead of propeller (1), and subscript (3) represents the conditions far behind in the propeller wake when $p_3 = p_0$.

Now the simplest compressibility correction factor for the propeller thrust is obtained by integrating Eq. (1.3) on page 231 of reference 2, assuming a constant δ_1, constant chord, and constant angle of attack ($\alpha = \theta - \phi$) along the entire radius so

$$C_L \cos\phi \approx \frac{2\pi\alpha}{\sqrt{1 - \left(\frac{w}{a_1}\right)^2}} = \frac{\text{constant}}{\sqrt{1 - \frac{V_0^2(1 + \delta_1)^2}{a_1^2} - \left(\frac{r\omega}{a_1}\right)^2}} \tag{7}$$

$$C_D \sin\phi \approx 0 \tag{8}$$

Then for light disc loadings ($\delta_1 \to 0$), it is easily seen that

$$\frac{T_{\text{COMP.}}}{T_{\text{INC.}}} = \frac{3}{2} \times \left[\frac{\frac{1 + M_0^2}{M_R^2}\sin^{-1}\left(\frac{M_R}{\sqrt{1 - M_0^2}}\right) - \frac{\sqrt{1 - M_R^2 - M_0^2}}{M_R^2}}{1 + 3(M_0/M_R)^2}\right] \tag{9}$$

where

$$M_0 = V_0/a_0, \qquad M_R = R\omega/A_0$$

and ω is the actual rotational velocity of the propeller.

In order to apply Eq. (9) to finite disc loadings, it is easily shown that we must multiply it by Eq. (1) and replace M_0 by M_1 by means of Eq. (2) in order to get the higher order influence of the induced axial inflow ($\delta_1 V_0$), considered uniform across the disc. However, the question now arises whether this higher order term is justified in comparison with other neglected effects. For example, by using the same method as used in deriving Eq. (2.8) on page 194 of reference 2, it may be shown that for subsonic flow the first-order effect, due to the decreased enthalpy produced by the slipstream rotation, may be expressed as

$$\delta_1 = (1/2)\delta_3 [1 + \delta_1(M_0^2/M_R^2)] \tag{10}$$

Another term, also of the same order, is found to be that produced by the subsonic compressibility effect of the semi-infinite helical trailing vortex system accompanying the infinite number of propeller blades. This term may be evaluated to the first order by combining Eq. 43 of reference 3 with the procedure used in deriving Eq. (89) of reference 4 to show that

$$\delta_1 = \frac{1}{2}\delta_3\left(1 - \frac{\delta_1}{2\sqrt{1 - M_0^2}}\right) \tag{11}$$

for light disc loadings and $M_0 \to 0$.

The important fact is now seen that Eqs. (1) and (11) have exactly the opposite influence on Eq. (9) as have Eqs. (2) and (10). Consequently, Eq. (9) is probably applicable to heavier disc loads in its present simplest form. The effect of varying inflow or varying chord can be shown to be a higher order effect that tends to cancel, leaving Eq. (9) as the ratio of the compressibility effect for any propeller.

Eqs. (10) and (11) prove that the axial-momentum theory is not justified by itself alone. The question still arises, however, as to the limitations of the actuator disc concept in subsonic flow. For example, it is easily shown that the so-called isentropic "ideal propeller" used in reference 1 is not a valid assumption for larger disc loadings. For Eq. (8) of reference 1 it is stated that the term due to $\rho_3 < \rho_0$ exists because of the propeller profile drag and such additional losses. This, however, is not the case, since Eq. (8) of reference 1 corresponds to the required increase of entropy that *must* coexist with the discontinuous pressure rise assumed for the actuator disc. Therefore, one cannot assume both the thin actuator disc and $\rho_3 = \rho_0$ as in reference 1. Actually, Eqs. (1) through (6), the first-order effect, should provide a better approximation than reference 1. It is interesting to note that Eq. (4) approaches the correct limit for the mass-rate of flow for sonic conditions ($M_0 \to 1$)—namely,

$$m_* = \rho_0 V_0 A = \rho_0 V_0 \pi R^2 \tag{12}$$

The first-order effect of $\rho_3 < \rho_0$ may be easily obtained from the energy equation and the first-order approximation for power required (TV_1) as

$$\delta_1 = \frac{1}{2}\delta_3\left(1 + \frac{[(\rho_0/\rho_3) - 1]}{\left(\frac{\gamma - 1}{2}\right) M_0^2\, \delta_3^2}\right) \tag{13}$$

showing that the effect of $\rho_3 < \rho_0$ cannot be neglected unless

$$[(\rho_0/\rho_3) - 1] << (\delta_3)^2 \approx (2\delta_1)^2$$

REFERENCES

[1] Vogeley, Arthur W., *Axial-Momentum Theory for Propellers in Compressible Flow*, N.A.C.A. T.N. No. 2164, July, 1951.

[2] Durand, W. F., *Aerodynamic Theory*, Vol. IV, pp. 169–360.

[3] Theodorsen, Theodore, *Theory of Propellers*, McGraw-Hill Book Company, Inc., New York, 1948.

[4] Tsien, Hsue-Shen, and Lees, L., *The Glauert-Prandtl Approximation for Subsonic Flows of a Compressible Fluid*, Journal of the Aeronautical Sciences, Vol. 12, No. 2, pp. 186–187, April, 1945.

Theory of Heat Transfer Through a Laminar Boundary Layer

Myron Tribus

Director of Icing Research, Engineering Research Institute, University of Michigan, Ann Arbor, Mich.

February 13, 1953

THE Readers' Forum note by H. Schuh (JOURNAL OF THE AERONAUTICAL SCIENCES, Vol. 20, No. 2, p. 146, February, 1953) appears to cover the same ground as the paper by M. J. Lighthill on "Contributions to the Theory of Heat Transfer Through a Laminar Boundary Layer" (*Proc. Roy. Soc. London*, Series A, Vol. 202, pp. 359–377, 1950).

The Lighthill results are somewhat more general than those given by Schuh.

Errata—"Diffuser Efficiency of Free-Jet Supersonic Wind Tunnels at Variable Test Chamber Pressure"†

Rudolf Hermann

Professor, Department of Aeronautical Engineering, University of Minnesota, Minneapolis

March 9, 1953

IN THE REFERENCE ARTICLE,† the following errors were made:

(1) Eq. (29) should read

$$M_{2\alpha,\,2\beta}{}^* = \frac{\left(\frac{2\gamma}{\gamma+1} - \frac{1}{f'}\frac{\gamma-1}{\gamma+1}\right) M_1{}^{*2} + \frac{1}{f'}}{2M_1{}^*} \pm \sqrt{\left[\frac{\left(\frac{2\gamma}{\gamma+1} - \frac{1}{f'}\frac{\gamma-1}{\gamma+1}\right) M_1{}^{*2} + \frac{1}{f'}}{2\,M_1{}^*}\right]^2 - 1}$$

(2) On page 379, the fifth line following Eq. (42), η_α must read η_β.

† JOURNAL OF THE AERONAUTICAL SCIENCES, Vol. 19, No. 6, June, 1952.

INSTITUTE *of the* AERONAUTICAL SCIENCES

1932–1953

Since its incorporation in October, 1932, as a scientific membership society to advance the art and science of aeronautics, the Institute of the Aeronautical Sciences, in over twenty years of service to aviation, has become the representative technical society for the aviation industry and profession. It is the only organization in the United States which brings together all of the sciences and branches of engineering and technology which are applied to aeronautics.

Publications

Papers presented at meetings or submitted to the Editorial Board are published in the JOURNAL OF THE AERONAUTICAL SCIENCES or the AERONAUTICAL ENGINEERING REVIEW. The JOURNAL prints in each issue full-length scientific papers on new research and developments in various fields applied to aviation. The REVIEW keeps members and subscribers up to date on aeronautical news and literature through reviews of new books and periodical articles, government publications and trade literature and publishes papers on applied engineering and aircraft production.

The AERONAUTICAL ENGINEERING CATALOG, published yearly, is a guide to sources and specifications of materials, parts, and accessories used in the design and production of aircraft, aircraft engines, and parts.

Research Facilities

Through the Aeronautical Archives of the Institute, members have for their use the most complete aeronautical library and reference research facilities maintained by any technical society. At the New York building of the Institute, The W. A. M. Burden Library of books, reports and periodicals, the Aeronautical Index of subject files, biographic files and bibliography, and the historical and art collections in the Archives are available for study. The Pacific Aeronautical Library at 7660 Beverly Boulevard, Los Angeles, maintains a reference collection and reading room for members and loans books to company libraries in the area. Through the Paul Kollsman Lending Library, aeronautical books are lent by mail without charge to members anywhere in the continental United States. In addition to a complete collection of standard aeronautical reference works, the Kollsman Lending Library has available for loan new aviation books as they are reviewed in the AERONAUTICAL ENGINEERING REVIEW.

Membership

In addition to membership in professional societies representing their particular fields, specialists applying their knowledge and experience to aeronautics find membership in the Institute of great value in the contacts made with others engaged in aeronautical work and in the broad coverage of all aeronautical problems furnished through its meetings and publications. All applications for membership are carefully reviewed by the Membership Committee, which recommends the grade of membership for which the applicant is found eligible. There are advanced grades of membership—Fellow and Honorary Fellow—to which members may be elected as their experience warrants. Thus, a member receives due recognition—more valuable because it is given by his colleagues—for his contributions to the progress of aeronautics. New applicants may be elected by the Membership Committee to the grade of Associate Fellow if they have been engaged for not less than ten years in the practice of the aeronautical sciences and shall have been in responsible charge of important scientific or engineering work, or shall have otherwise made outstanding contributions to the aeronautical sciences; to the grade of MEMBER if they have been engaged in professional work for at least eight years and have acquired a recognized standing in engineering, design, or other special work applied to aeronautics; to the grade of Associate Member if they have acquired a recognized standing in an administrative capacity in the aviation industry; to the grade of Technical Member if they are recent engineering school graduates or are engaged in technical aeronautical work. Student Members are admitted by application through Student Branches organized at their schools. Aeronautical companies, as well as individuals, are affiliated with, and participate in, the support of the Institute through Corporate Membership.

Dues

An entrance fee of $10 is required of all new members who apply for admission to a grade of membership to be specified by the Membership Committee (Corporate Members, Foreign Members, and Student Members being excepted).

Annual membership dues include a subscription to the AERONAUTICAL ENGINEERING REVIEW. Dues for the various grades of membership are as follows: Fellows—$16.50; Associate Fellows—$16.50; MEMBERS—$13.50; Associate Members—$13.50; Technical Members—(26 years of age and over) $13.50, (under 26) $6.50.

The regular subscription price for the JOURNAL OF THE AERONAUTICAL SCIENCES and the AERONAUTICAL ENGINEERING REVIEW is $12 and $3.00 per year, respectively. Members may subscribe to the JOURNAL at $4.00 per year.

Those who are engaged in aeronautical work or who have an interest in any technical phase of aviation will find the services of the Institute to be a necessary aid in keeping abreast of developments in these times of such rapid progress. An application form and further information about membership can be obtained from an Institute member or by writing to the Secretary.

INSTITUTE OF THE AERONAUTICAL SCIENCES, INC.

2 EAST 64TH STREET

NEW YORK 21, N.Y.

SUGGESTIONS *for* CONTRIBUTORS *to the Publications of the* INSTITUTE *of the* AERONAUTICAL SCIENCES

The Institute of the Aeronautical Sciences invites both members and nonmembers from any country to submit papers for publication in the JOURNAL OF THE AERONAUTICAL SCIENCES and the AERONAUTICAL ENGINEERING REVIEW. The Institute, following the practice of other societies, does not pay for contributions.

The following directions for the preparation of papers, if followed by authors, will save correspondence, avoid the return of papers for changes, minimize the work of preparation for the printer, and save the expense due to the charges made for "author's corrections."

MANUSCRIPTS: The original typewritten copy of the paper is desired, double or triple spaced on one side of white paper sheets, consecutively numbered. There should be wide margins to allow for the marking of directions to the printer. Correcting, changing, or adding to papers after they are in type is costly. It is, therefore, imperative that papers submitted be in final form. Typographical errors may be corrected on proofs, but if authors wish to add material, they may do so at their own expense. In mailing, drawings may be rolled but manuscripts should be sent flat. Send by first-class mail (register if you wish for your own protection) to the Editorial Office, Institute of the Aeronautical Sciences, 2 East 64th Street, New York 21, N.Y. All manuscripts will be examined by the Editorial Committee and by the Editor. Authors will be advised as promptly as possible whether the paper is acceptable for publication.

TITLES: The title of the paper should be brief. The name and initials of the author should be written as he prefers. The use of the full name of an author is advocated because of the frequent duplication of initials and surnames which sometimes makes it difficult to establish the identity of the author. This is particularly important for large annual indexing and abstracting services. All titles and degrees or honors are omitted. The name of the organization with which the author is associated should be placed after his name on a separate line. The date on which the paper is received will be inserted by the Editor. The author's title should be indicated in a footnote.

SUMMARIES OR ABSTRACTS: An abstract to be printed at the beginning should accompany each article. It should be adequate as an *index* and as a *summary*. It should contain a statement of major conclusions reached, since summaries in many cases constitute the only source of information used in compiling scientific reference indexes. Abstracts printed in other journals, especially foreign, in most cases, consist of summaries from printed papers. The summary should explain as adequately as possible the major conclusions to a nonspecialist in the subject and should contain from 100 to 300 words, depending on the length of the paper.

SUBHEADINGS: Subheadings should be inserted by the author at frequent intervals. The work of editorial preparation will be simplified by the author providing many subheadings.

MATTER USUALLY DELETED: Photographs or illustrations of little technical interest and not showing advances in general practice. Too detailed tabular matter (general results of such tables may be included in the text). Lengthy descriptions of materials or processes or of preliminary experiments or theories that preceded final results; salient features only are of interest.

REFERENCES AND FOOTNOTES: References should appear as footnotes only, numbered consecutively and grouped together at the end of the manuscript. The arrangement should be as follows: (For books)—[1] Durand, W. F. *Aerodynamic Theory*, 1st Ed., Vol. 1, p. 23; Julius Springer, Berlin, 1934. (For Magazines)—[1] England, C. R., Crawford, A. B., and Mumford, W. W., *Some Results of a Study of Ultra-Short-Wave Transmission Phenomenon*, Proc. I.R.E., Vol. 20, No. 12, pp. 481–482, March, 1933. Please give author, title, edition, volume, page, publisher, and date of publication as indicated. Omission of one required fact causes much extra editorial work and possible inaccuracies.

ILLUSTRATIONS: Illustrations should accompany manuscripts, and each should always be referred to in the text, by number. Drawings or graphs should not be larger than 12 × 16 inches, and must be made with jet black India ink on white paper or tracing cloth, the latter being preferred. *Do not use typewriter for lettering.* The smallest lettering on 8- × 10-inch figures should be no less than 1/4 inch high. Cross-section paper (white with black lines) may be used but it should not have more than 4 lines per inch. If finer ruled paper is used, the major division lines should be drawn in with black ink, omitting the finer divisions. In the case of finely ruled paper, only blue-lined paper can be accepted. *Tracing paper and blueprints* are not acceptable. Lettering and all markings must be large enough to be readable after reduction. Mail rolled or flat; never fold. Drawings that cannot be reproduced (including pencil drawings) will be returned to the author for redrawing thus delaying publication of the paper. Photographs should be distinct and show clear black and white contrasts. They must be on glossy white paper. Avoid round and oval photographs.

CAPTIONS AND LEGENDS: Legends or captions must accompany each drawing or photograph submitted. If written on the drawing or photograph, they should be placed below and well outside the part to be reproduced. Each table should have a caption such as Table 1, Table 2, Table 3, etc. Captions should be complete in themselves so as to make the data intelligible to the reader without reference to the text. A duplicate list of captions for figures should be included as the last page of the manuscript. Use "Fig. 1" (not Figure 1), Figs. 3 and 4, etc., in both the text and the numbering of illustrations. In the text, "Eq. (1)" or "Eqs. (1) and (2)" is used, not "Equation (1)." In captions and legends, except for "Fig." and "Eq.," and in table headings write all words in full; do not abbreviate.

MATHEMATICAL WORK: Only the simplest formulas should be typewritten; all others should be carefully written in pen and ink, the writing to be large enough so that ample room is provided to mark mathematical matter for the printer. A considerable spacing for marking should be allowed above and below all equations. All complicated equations should be repeated on separate sheets with plenty of space left for marking. The solidus should be used for simple fractions appearing within the text. Make all expressions clear to the typesetter. Greek letters used in formulas should be clearly designated by name on the margin of the manuscript. All symbols should be clearly written and carefully checked. The difference between capital and lower-case letters should be clearly distinguished and care taken to avoid confusion between zero (0) and the letter (o), between the numeral (one) and the letter (ell) and the prime (′), between alpha and a, kappa and k, u and mu, v and nu, n and eta. All subscripts and exponents should be clearly marked, and dots and bars over letters or mathematical expressions should be avoided. Avoid complicated exponents and subscripts. When it is necessary to repeat a complicated expression, it should be represented by some convenient symbol.

NOMENCLATURE AND ABBREVIATIONS: Standard abbreviations should be used, and it should be noted that most abbreviations are lower case such as m.p.h., b.m.e.p., i.hp., b.hp., hp., . . . etc.